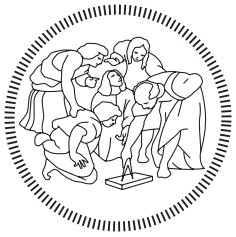

Politecnico di Milano

SCHOOL OF INDUSTRIAL AND INFORMATION ENGINEERING
Department of Aerospace Science and Technology (DAER)
Master of Science in SPACE ENGINEERING

Analytical design of end-of-life disposal manoeuvres for Highly Elliptical Orbits under the influence of the third body's attraction and planet's oblateness.

Master Thesis

Student:
Francesca Scala
Matricola 874013

Supervisor:
Prof. Camilla Colombo

Co-supervisor:
PhD Ioannis Gkolias

Academic Year 2017–2018

When referring to this work, full bibliographic details must be given, i.e.

Scala Francesca, "Semi-analytical design of end-of-life disposal manoeuvres for Highly Elliptical Orbits under the influence of the third body's attraction and planet's oblateness". 2018, Politecnico di Milano, Faculty of Industrial Engineering, Department of Aerospace Science and Technologies, Master in Space Engineering, Supervisor: Camilla Colombo, Co-supervisor: Ioannis Gkolias

Printed in Italy

To my parents, Teresa e Giordano

Acknowledgments

Remember to look up at the stars and not down at your feet.
Try to make sense of what you see, and wonder about
what makes the universe exist. Be curious.

— Stephen Hawking

First, I would like to acknowledge and to express my gratitude to my thesis supervisor Professor Camilla Colombo, of Aerospace Science and Technology Department at Politecnico di Milano, for giving me the opportunity to work on such stimulating topics and for giving me very professional guidance. I'm also sincerely grateful to my correlator Dr Ioannis Gkolias for the precious advice and support he gave me. I want to thank them for sharing invaluable scientific guidance and innovative ideas, helping me to choose the right direction for completing the work, until the last day.

I want also to acknowledge Professor Michèle Lavagna for giving me the opportunity to participate in many events at Politecnico for the Aerospace department, as the MeetMeTonight and many others. It was exciting and stimulating to work with her team.

I would like to thank all my colleagues, they taught me how to work in a team, sharing their knowledge and expertise. A special thanks to my colleagues and friends Marzia Z., Margherita P. and Laura P, you were the light for my days in Bovisa. Thank you for making me feel at home and for all your valuable advice. Thank you for all the conversations and the experiences we shared together. I want to thank Paolo V., Lorenzo T. and Giovanni B. for supporting and encouraging me during these months of thesis. And finally thank-you to Marco G., Cristiano C., Matteo Q., Luca M., Sebastiano A., Claudio F., Emanuele B., Marco M., Hermes S., Alessandro S., Francesco A., Francesco R., Andrea P., Andrea G. and Andrea S.. With each of you, I shared unforgettable and precious moments of my university experience. I own you all my achievements, work and live together is the best experience I could have ever imagined.

I want to thank my friends from the high school, Federica V., Francesca P, Matteo M., Roberto G., Luca C and Martina T., you were always by my side and you always support me, no matters what.

A big thank-you to my best friend Erica C., you were always my polar star. Thank you for your wonderful and splendid friendship.

A special thank goes to my parents, they always support me during my study, encouraging me in front of difficulties and success. Without you, none of this would have been possible.

Finally, I wish to tank my boyfriend Mattia, you share with me more than any other. These years were not simple, but all our experiences made us even closer. Thank you for your patience, presence and love in any moment of my life. I'm nothing without you and you make me happy as nobody else can do.

Milano, December 2018 Francesca Scala

Abstract

The increasing number of satellites orbiting the Earth gives rise to the need for investigating disposal strategies for space vehicles, to keep operative orbits safe for future space missions. In the last years, several studies have been conducted focused on designing end-of-life trajectories. The aim of this thesis is the feasibility analysis for a fully-analytical method for end-of-life de-orbit strategy of spacecraft in Highly Elliptical Orbits. The main perturbations to the Keplerian motion are planet's oblateness and third bodies' gravitational attraction. Following the classical theory, the analytical expression of the double-averaged potential due to a third body's perturbations and zonal J_2 effect is derived in the planet Centred Equatorial frame. This allows for a simplified formulation of the system's long-term dynamics. This thesis aims to introduce an innovative approach for the manoeuvre design, relying on a fully-analytical method to reduce the computational cost. Some studies were already developed but using a semi-analytical approach: the resulting algorithm is time consuming for manoeuvres' optimisation. The analysis is done considering the third body and J_2 contributions and the re-entry is modelled using the two-dimensional Hamiltonian phase space. The model is used to estimate the eccentricity variations of the large set of orbits required during the optimisation process. The disposal manoeuvre is selected through a multi-criteria optimisation. As real cases scenarios, the disposal manoeuvre for Earth's and Venus' satellite missions are designed, considering the limitation upon the available propellant onboard. It is demonstrated that the third-body gravitational perturbation provides a suitable environment for manoeuvres design. These results could serve as initial conditions for more accurate analysis with a high-fidelity model and confirm the potential efficiency of exploiting the use of orbital perturbations for satellite navigation. This thesis was part of the COMPASS project: "Control for orbit manoeuvring by surfing through orbit perturbations"(Grant agreement No 679086). This project is European Research Council (ERC) funded project under the European Unions Horizon 2020 research.

Keywords: Orbital perturbations; Long-term Evolution; End-of-life disposal; Optimal manoeuvres

Sommario

L'incremento del numero di satelliti in orbita terrestre fa nascere la necessità di studiare metodi di rimozione dei veicoli spaziali, per mantenere gli standard di sicurezza necessari in orbita per le missioni future. Nel corso degli anni, diversi studi hanno analizzato strategie di rimozione passiva. Lo scopo di questa tesi è lo studio e la determinazione di metodi analitici per il rientro e la rimozione di satelliti in orbite fortemente ellittiche. Seguendo la teoria classica, è stata sviluppata una formulazione analitica del potenziale dovuto al disturbo del terzo corpo e di J_2, nel sistema di riferimento equatoriale, eliminando i contributi ad alta frequenza. Lo scopo di questa tesi è l'introduzione di un approccio innovativo, basato su algoritmi analitici, con lo scopo di ridurre il costo computazionale. In passato, diversi studi si sono basati su un approccio semi analitico: l'agoritmo risulta computazionalmente inefficiente per l'ottimizzazione delle manovre. Si è sviluppata quindi un'analisi semplificata, considerando l'effetto della perturbazione del terzo corpo e di J_2, sviluppando una descrizione dell'Hamiltoniana bidimensionale. La manovra è stata modellata tramite un processo di ottimizzazione su diversi parametri, e il risultato è stato ottenuto tramite le equazioni di Gauss per una variazione dei parametri orbitali. Come casi studio, le possibili traiettorie a fine vita sono state valutate sia per missioni terrestri che intorno a Venere, considerando anche il limite dovuto alla quantità di combustibile disponibile a bordo. Dai risultati, è stato dimostrato che la perturbazione orbitale dovuta all'attrazione del terzo corpo può essere sfruttato per il design di manovre nello spazio delle fasi, e questo può essere considerato come il punto di partenza per ulteriori analisi, che comprendano modelli più accurati, dimostrando la potenziale efficienza dell'utilizzo di codici analitici che sfruttino le perturbazioni orbitali per il controllo dei satelliti. Questa tesi è parte del progetto COMPASS: "Control for orbit manoeuvring by surfing through orbit perturbations"(Grant agreement No 679086). Questo progetto è un progetto finanziato dall'European Research Council (ERC) nell'ambito della ricerca European Unions Horizon 2020.

Parole chiave: Perturbazioni orbitali; effetto secolare; rientro a fine vita; manovra ottima

Contents

List of Figures

List of Tables

List of symbols and data

G	$6.67 \times 10^{-20}\,\mathrm{km^3/kg/s^2}$	Universal gravitational constant
μ	$398\,600\,\mathrm{km^3/s^2}$	Earth's gravitational parameter
$R_\oplus$	$6378.16\,\mathrm{km}$	Earth's mean equatorial radius
J_2	1082.628×10^{-6}	Coefficient of the Earth's oblateness
a	(km)	Semi-major axis
h_p	(km)	Altitude of perigee
e	(-)	Eccentricity
i	(rad) or (deg)	Inclination
ω	(rad) or (deg)	Argument of perigee
Ω	(rad) or (eg)	Right ascension of the ascending node
f	(rad) or (deg)	True anomaly
E	(rad) or (deg)	Eccentric anomaly
M	(rad) or (deg)	Mean anomaly
δ	(rad) or (deg)	Geocentric latitude
$\mathbf{r}$	(km)	Satellite position vector
$\mathbf{v}$	(km/s)	Satellite velocity vector
$\mathcal{R}$	$(\mathrm{km^2/s^2})$	Disturbing function
$\mathcal{H}$	$(\mathrm{km^2/s^2})$	Hamiltonian Function
Θ_{kozai}	(-)	Kozai parameter
Δv	(km/s)	Velocity variation of a manoeuvre
α	(rad)	In-plane Δv angle
β	(rad)	Out-of-plane Δv angle
☾	-	Symbol for Moon parameters
☉	-	Symbol for Sun parameters
♀	-	Symbol for Venus parameters

Chapter 1

Introduction

You sort of start thinking anything's possible if you've got enough nerve.

—J. K. Rowling, Harry Potter and the Half-Blood Prince

Since the first Earth's artificial satellite Sputnik 1 was launched in October 1957[1], the number of space vehicles per year increased exponentially. An average of 143 spacecraft per years was launched between 1957 and 2017, for a total of 8'593 satellites. Figure 1.1 shows the number of launches since 1972[2], grouped by proprietary country and mission scope. In the last decade, the overall number of private satellites grew up significantly, reaching over 350 satellites in orbit in 2017. As a matter of fact, the continuously increasing space activity results in a systematic congestion of particular orbital regions about the Earth. Any spacecraft that remains in orbit uncontrolled after the end of the operations is considered a space debris.

During the first few decades of humans' space exploration, no strategy for the end-of-life was studied or planned, resulting in an increasing amount of dead satellites still on orbit. Despite space vehicles in Low Earth Orbit (LEO) achieving a natural re-entry in short time period due to the atmospheric drag, in Geostationary Earth Orbit (GEO), Medium Earth Orbit (MEO) or Highly Elliptical Orbit (HEO) they could stay on their orbits even for centuries, becoming for all practical purposes space debris. Moreover, the proliferation of debris is triggered by collisions between dead satellite still in orbits or explosions of malfunctioning spacecraft at the end of mission. As Kessler and Cour-Palais described in

[1] `https://www.nasa.gov/multimedia/imagegallery/image_feature_924.html`, last visited 24/10/2018
[2] `http://claudelafleur.qc.ca/Spacecrafts-index.html`, retrieved on 24/10/2018

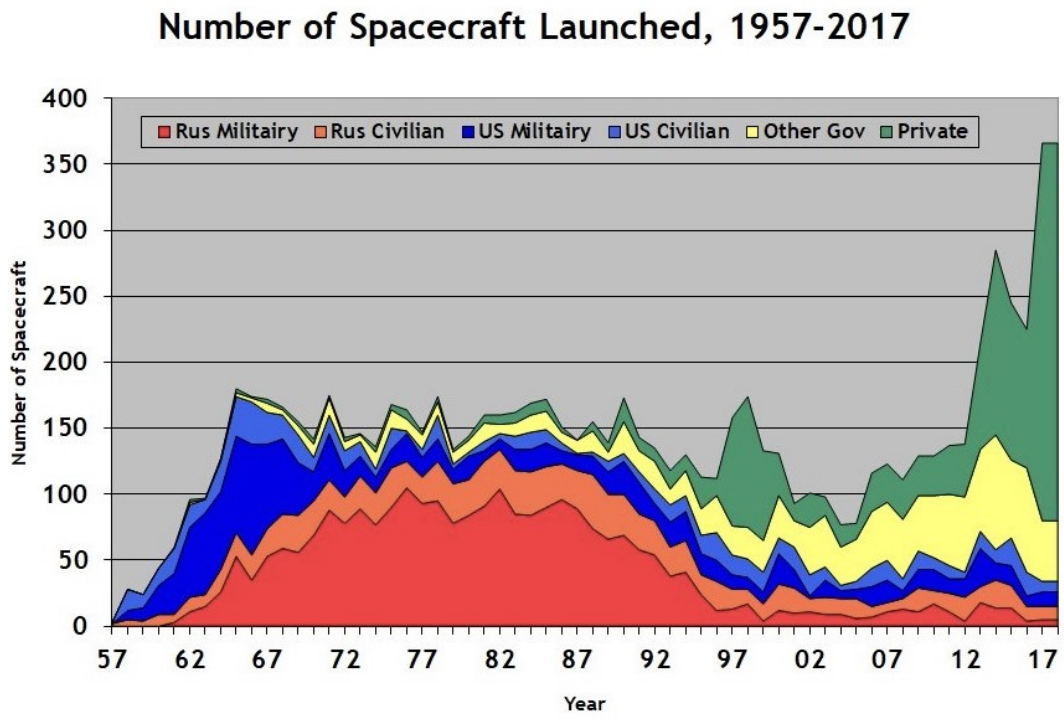

Figure 1.1 No. of launched object per year, in the period 1957-2017 from *Spacecraft Encyclopedia*[3].

Table 1.1 Number of space objects of different size from ESA website[4]

Diameter	no. of objects
$>$ 10 cm	29'000
1 cm to 10 cm	750'000
1 mm to 1 cm	166 million

1978, the rising number of artificial satellites would increase further the impact probability. In particular, they point out that, in the absence of any additional measure, the debris flux could overcome the natural meteoroid one. They studied mathematical model to predict the rate of formation of such a belt (Kessler and Cour-Palais, [1]). This problem is commonly addressed as the "Kessler Syndrome": in an uncontrolled environment, the debris flux will increase exponentially in time (Kessler et al., [2]). The main danger revealed by Kessler's work is reaching a critical debris population density, such that a collisional cascade process is triggered. To prevent such a scenario, the need of introducing a severe normative for future mission rises: both post-mission disposal and active debris removal should be introduced to reduce the effective number of objects in orbit.

[3]Spacecraft Encyclopedia - C. Lafleur - `http://claudelafleur.qc.ca/Spacecrafts-index.html`, retrieved on 24/10/2018

From the latest report provided by ESA's Space Debris Office[4], the number of debris objects regularly tracked by Space Surveillance Networks is about 21'000. In particular, if space debris of smaller size are also considered, as in Table 1.1, then the situation looks way more alarming and action should be taken. Since its foundation in 1993, the Inter-Agency Space Debris Coordination Committee (IADC)[5] defines the recommended guidelines for the mitigation of space debris. There are two protected regions around the Earth, one for low-Earth orbits and one at geosynchronous altitude. The removal of any object in LEO is required within 25 years after the end-of-mission, while for GEO the guideline is to move to a graveyard orbit 250 km above (IADC Space Debris Mitigation Guidelines, [3]). For the Highly Elliptical Orbit (HEO) there is no regulation yet, but, since many current and future missions target that region (e.g. Proba-3, INTEGRAL, XMM-Newton, Cluster II, Image, Themis, Chandra, IBEX), the implementation of a strategy is highly recommended. In this work the end-of-life is considered subject to the same regulation as for the LEO region: the residence time in LEO must be within 25 years in case of atmospheric re-entry, but the total de-orbit trajectory could last longer.

The dynamics of HEO, with high apogee altitude, is much affected by the influence of the Moon's gravitational attraction, which is more important than the second degree of the zonal harmonic J_2 term. A correct approximation of the orbit evolution in time requires a model including at least the J_2 and the third body disturbing function, the latter expanded up to the fourth order in the parallax factor (Colombo et al., [4]). To model the end-of-life disposal, the short-period effects are negligible, and they are removed by using a double-averaged model of the potential function. In fact, the third-body attraction causes secular and long-term variation in all the orbital parameters, except for the semi-major axis. Especially important for the understanding of the problem is the secular evolution in the eccentricity-argument of perigee plane.

In this work, the natural evolution of satellites' orbital elements is exploited for lowering the perigee altitude. In particular, taking an approach different from previous works (see Section 1.1), the aim is to design manoeuvres with a fully-analytical approach and subsequently reduce the computational time. The disposal manoeuvres are designed for satellites in HEO, by studying the long-term and secular variation in eccentricity and inclination caused by the third-body attraction. The end-of-life strategy could be either an atmospheric re-entry or a graveyard orbit.

[4]ESA website, *Space Debris by the numbers:* `https://www.esa.int/Our_Activities/Operations/Space_Debris/Space_debris_by_the_numbers`, last visited on 24/10/2018

[5]`https://www.iadc-online.org/`, last visited 24/10/2018

1.1 State of the Art

This section provides a historical overview of the model used to describe the orbital dynamics under the influence of a third-body external perturbation to the classical Keplerian description. In addition, it presents the current state of the art for HEO disposal design.

1.1.1 Analytical modelling of orbit perturbations

The study of secular perturbations caused by a third body was widely studied in the past. The third body effect was first addressed in the '60s by Lidov (1926-1993), a Russian scientist and expert in physical and mathematical sciences, who was also part of the Soviet orbital design team during the space race. He made a fundamental contribution in the determination of mathematical models to describe the three body environment for the Earth-Moon and the Sun-Moon system. In one of his most important works (Lidov, [5]), he described the mathematical model for the orbital evolution of satellites under the effect of a third body, either the Moon or the Sun. The resulting oscillation of the orbital parameters was computed for Earth's satellites for a wide class of orbits, in terms of eccentricity values, with a semi-major axis of the order of 30-40 $\times 10^3$ km.

In the same years, also Kozai (1925-2018), a Japanese scientist and astronomer at Tokyo Astronomical Observatory, developed a model to describe the dynamics of the orbit of an asteroid in the Jupiter-Sun system (Kozai, [6]). The model was developed in the Delaunay's variables, by exploiting the Hamiltonian perturbation theory, and he was able to assess the secular variation under the assumption of circular Jupiter orbit. For the first time, the results were expressed in the Hamiltonian phase space to study the stationary and libration points for the orbit.

The results of these studies are today addressed as the Lidov-Kozai effect. The long-term evolution was produced using an averaging technique on the Hamiltonian system, under the assumptions that the characteristic time of variation of the orbital parameter is much higher than the characteristic period of the third body. Both Kozai and Lidov found out that the orbiting particle oscillations are dependent on the initial eccentricity and inclination of the orbit (Shevchenko, [7]). In particular, the effect is more evident for highly inclined orbits: the Highly Elliptical Orbits have a typical inclination of about 60°. Basically, this was an unexpected behaviour, since classical theories were applied to low inclination solar system bodies, for which this effect was not present.

In the '70s, Kaufman developed the expressions for the orbital disturbing potential. In his works (Kaufman, [8]; Kaufman and Dasenbrock, [9]), he expanded the third body

potential using Legendre polynomials, following the classical approach of Laplace-Lagrange. On the other hand, the single averaged was done in close form by considering that the period of the satellite is much lower than the secular characteristic time. He also described the analytical expressions of orbital variation in terms of Earth's oblateness J_2 and J_2^2, starting from the works of Kozai, [10] and Kaula, [11].

In more recent years, many studies arise upon the Lidov-Kozai mechanism for different astrophysical applications. The most interesting results were produced by studying the application to highly inclined orbit. Recently, some studies (Folta and Quinn, [12]; Abad et al., [13]) used the Hamiltonian formulation to describe the natural evolution of Lunar orbiter under the third body influence. These works relied on the development of the Earth perturbation as a third body disturbance and the potential was expanded up to the second order term in the Hamiltonian formulation to study the frozen conditions for the orbit.

All the previous works considered the third body perturbation only. Nevertheless, especially for Earth's satellites, other external effects are present: the J_2 zonal contribution is very important to describe the actual long-term evolution of a space probe. In particular, for HEOs, the coupling between the Moon and J_2 contribution generates a particular behaviour in the orbital dynamics. Delsate et al. used the Hamiltonian system to describe the time evolution of a Mercury orbiter [14]. They developed a simplified model combining the zonal effect of J_2 together with the third body disturbance of the Sun. They discovered that the coupling effect due to the J_2 coefficient acts against the increasing of eccentricity predicted by the Lidov-Kozai effect. Moreover, in his model, it was assumed that the perturbing body orbit lies on the planet equatorial plane. This is a good assumption when the angle between the equator and the ecliptic is relatively small (for Mercury, the obliquity of the orbit is 0.034°).

In 2005, due to the increasing interest of exploring Europa, Lara and San Juan studied the possible implication of Jupiter's attraction on the dynamical behaviour of an orbiter around Europa. They studied the stability regions for different inclined and eccentric family of orbits. Their model considers the perturbing effect of both J_2 and the third body attraction of Jupiter, [15]. A similar study was done by Carvalho et al. in 2012. He studied the stationary condition for space vehicle orbiting Europa [16]. In particular, he developed a model considering the most relevant term of the gravitational attraction: J_2, J_3, J_{22}, together with the third body effect expanded up to the second order. But still, the perturbing body is considered on the same orbital plane of the parent body. An important contribution was given by Tremaine et al., [17]. They described and studied the satellites dynamics in the Laplace plane. They focused on the stability and instability condition of

the classical Laplace surface, for highly inclined orbits. In his studies, he considered the potential of an oblate planet in the quadrupole approximation, considering the coupling with the third body influence. Depending on the obliquity with respect to the equator, he defined stable, coplanar Laplace equilibria for both circular and eccentric solutions.

In 2012, Colombo et al. [18] develop a model to study the orbital dynamics of spacecraft with a high area-to-mass ratio. Their model considers the influence of the zonal harmonic J_2 and the Solar Radiation Pressure (SRP). They develop an analytical and a numerical model to investigate the feasibility of using SRP for passive de-orbit for MEO satellites. Similarly, Tresaco et al. developed a complete analytical model to study the feasibility of solar sails for orbit navigation around Mercury ([19], [20]), in addition, they considered the third body in case of elliptical orbit approximation. They explored the effect of SRP upon satellite to enhance different future mission concept using Solar Sails: deep space exploration, space debris removal and long-term mission in the solar system. The dynamical model was developed in the Mercury equatorial frame rotating with the Sun node, considering the Sun orbiting on an elliptic inclined orbit. They considered the influence of J_2 and J_3 zonal harmonics terms, the third body perturbation of the Sun expanded up to the second order and the SRP. The resulting Hamiltonian system was used to study the frozen orbit conditions for probes around Mercury: they focused their study on frozen conditions for low eccentric orbits (less than 0.1). Recently, Naoz [21] studied the hierarchical three body approximation applied to astronomical systems, such as planetary or stellar scales and supermassive black holes. He recovered the dominant behaviour of a system under the elliptical Lidov-Kozai effect, studying both the chaos regime and the frozen condition for a particle in the perturbed environment.

In all these works, the perturbation model was averaged to study the secular and the long-term dynamics; in addition, the averaging procedure reduces the degree of freedom of the system, resulting in a Hamiltonian representation dependent only on eccentricity and argument of perigee, while the semi-major axis and inclination are treated as parameters. The approximation was found out to be suitable for the description of frozen condition and the secular evolution. Some two-dimensional maps were provided to describe the oscillation of eccentricity and inclination as a function of the perigee anomaly. Moreover, in all those works the simplification that the third body is on the equatorial plane of the main attractor or on the same plane of the satellite was considered. This simplification was necessary to drop in the Hamiltonian the dependence on the argument of the node, resulting in a one degree of freedom expression, suitable to describe analytically the phase space in terms of eccentricity and perigee anomaly. This description is not suitable in the case a second

disturbing body is considered: the model becomes very complex and the argument of the node is no more cancelled out.

In successive works (Colombo et al. [4]; Breiter, [22]; Rosengren et al., [23]) the single and the double-averaged potential was used to describe the resonance effects of a third body for Earth's satellites. The Hamiltonian description was carried out in the perturbing body plane (Moon) centred at the Earth. In particular, the results were used to describe the two-dimensional Hamiltonian phase space for HEOs under the effect of the third body perturbation only. From those maps, a strategy for the end-of-life condition was designed, targeting the disposal trajectory in the phase space. In 2014, Colombo et al., [24], [25], increased the precision of the model, by including numerically the SRP, the zonal and the Sun effect, dropping the simplification that the Sun and the Moon lie on the same plane. In addition, they determined that a description of the third body potential is essential for a correct prediction of HEOs evolution, using the dual averaged expression to develop the long-term evolution through the Lagrangian equations. Nevertheless, in the analytical Hamiltonian derivation, the third body orbit was approximated to a circular one, to simplify the expressions, in fact, the Moon is on a low eccentric orbit (Colombo, [25]; Colombo et al., [26]).

These works developed for the first time the single and the double-averaged method to compute orbital manoeuvre for disposal purposes. They exploited the manoeuvre to navigate in the phase space, computing the optimal manoeuvre through an optimisation procedure. The delta-v was computed using the Gauss equations in finite difference (Colombo, [27]), then the dynamic of the final orbit was computed by integrating the semi-analytical model, with single or double-averaged dynamic. The optimisation was based on a global optimiser to evaluate the best direction of the manoeuvre in the phase space. In addition, the manoeuvre optimisation was done numerically, integrating the equations of motions at each time step: this results in a very expensive code in terms of computational time, as it needed to be integrated over a period of 20 to 30 years for each function evaluation, even if benefiting of the speed of the semi-analytical technique.

In this thesis, the analytical expression of the disturbing potential function is computed for the third body effect in case of an elliptical inclined orbit of the disturbing body (both for the Sun and the Moon) and for the zonal harmonic expression. The former is expanded up to the fourth order to have a high fidelity model, while for the latter, only the J_2 term was considered since the other terms are negligible for Highly Elliptical Orbits due to their big semi-major axis (in the order of $10^4 - 10^5$ km).

Analytical theories with Hamiltonian formulation

The Hamiltonian formalism was widely used in past dissertations. Classically, the dynamic of a system can be described by the energy approach developed by Lagrange (1736-1813) [28]. This formulation is based on the knowledge of the kinetic T and potential V energy of the system. Hamilton (1805-1865) [29] then developed the Hamiltonian principle to describe the behaviour of a system in time, in an equivalent way to the Lagrangian representation.

The orbital evolution of solar system bodies was one of the main driving forces for the advancements of the Hamiltonian system theory. Many techniques were developed particularly to address orbital mechanics problems (Shevchenko, [7]). In recent years, Valtonen and Karttunen applied those principles to orbital mechanics. Moreover, the Hamiltonian function for the two-body problem is a time-invariant relation and it is typically described in Delaunay's variables (see Valtonen and Karttunen, [30]). They showed that the Hamiltonian function for the perturbed two-body problem is a time-invariant relation.

The Hamiltonian formulation is very effective for describing satellite dynamics in the phase space representation. In many works, it was used to try to develop an analytical approximation to the real dynamics of the system (Colombo et al. [24]; Colombo et al. [26]; Delsate et al. [14]; Tresaco et al. [20]). The complete reduction of the orbital dynamics in a particular body configuration is not always feasible but the strength of this approach resides in the possibility to describe the evolution of the real system using one single equation. Maps in terms of the argument of perigee were used to understand and analyse the natural libration in inclination and eccentricity. This kind of representation allows stressing the natural oscillation of an orbit in a perturbed environment, identifying also stable and unstable conditions for the space probes.

In this work, the Hamiltonian formulation was used to try to find one degree of freedom representation. This approach has the potential of describing the orbit dynamics using two-dimensional maps for the design of disposal manoeuvres. The two-dimensional maps are recovered from the analytical Hamiltonian, which in the case of no dependence of the node argument, can be expressed through the Lidov-Kozai parameter. The latter is a constant of motion for the system, defined by the initial conditions, and allows to describe the oscillation in inclination as a function of the eccentricity. In this way, since the semi-major axis is constant in the double average representation, the Hamiltonian of the system has only one-degree of freedom: the solutions can be represented as level curves in the eccentricity-argument perigee plane. This model can be used to produce the eccentricity-argument of perigee maps (Colombo et al. [24]; Colombo [25]).

End-of-life strategies

As already explained, the need for mitigation and disposal strategy for Earth's satellites is becoming more and more important. For HEO no guidelines currently exist, but the implementation of removal manoeuvres and the mitigation of risk collision is highly recommended for current and future missions (Ailor [31]; Colombo et al. [26]). For the Highly Elliptical Orbit very few studies were performed in the past since the major interests were on the LEO, MEO and GEO spacecraft. Current and future space missions target the HEO for scientific purposes, like INTErnational Gamma-Ray Astrophysics Laboratory (INTEGRAL), the first space observatory that can simultaneously observe objects in gamma rays, X-rays and visible light, X-ray Multi-Mirror Mission-Newton (XMM-Newton), the biggest European satellite with a telescope for X-ray detection. Typically, the end-of-life removal could consist of an active removal of the satellite from the protected region, or a passive approach exploiting the orbit energy. The former can be done after mission completes and the satellites become a space debris, while the latter is required before the operative life of the space vehicle ends.

Active space debris removal The European Space Agency (ESA) defines that Active Debris Removal (ADR) is essential to stabilise the growth of space debris. In fact, the removal of the current dead space vehicle still in orbit is mandatory to reduce the probability of an orbit impact, which could cause even the duplication of space debris. This approach is the only feasible solution to compensate for the non-compliance satellite to disposal normative. ADR is very efficient to reduce the probability of future on-orbit collision. ESA Clean Space[6] is studying an active debris removal mission called e.deorbit to tackle with such a problem. There are two concepts under consideration: one using a net and the other a robotic arm.

An overview of ADR options is given in Shan et al., [32]. Net debris capture was studied also in other works at Politecnico of Milan (Benvenuto et al., [33]), while the robotic arm is mainly developed by Airbus and OHB (Airbus, [34]; Forshaw et al., [35]). These methods can be very effective for the removal of already existing debris but do not exploit any prevention or mitigation strategy for avoiding the creation of more future dead satellites in orbit. To face the problem of preventing more space debris in orbit, the passivation technique can be studied. Some studies were already done in this field.

[6]ESA Clean Space website: `http://www.esa.int/Our_Activities/Space_Engineering_Technology/Clean_Space`, latest visited on 11/2018

Passive space debris removal From ESA statistics[7], only a few very large objects, such as heavy scientific satellites, re-enter Earth's atmosphere in a year. In total, about 75% of all the largest objects ever launched have already re-entered. Objects of moderate size, i.e. 1 m or above, re-enter about once a week, while on average two small tracked debris objects re-enter per day. The controlled or uncontrolled re-entry of spacecraft and space systems is, however, associated with several legal and safety aspects that must be considered.

Passive de-orbiting systems, such as drag augmentation devices and tethers, can be used for de-orbiting and re-entry (uncontrolled) of small satellites in LEO. In the same way, for space vehicles in orbits affected by the SRP, solar sails can be used for orbit navigation. The SRP was investigated for changing the operative orbit at the end-of-life of the satellite by exploiting the effect of the cross-sectional area. In particular solar sails were already studied for navigation purposes, by enhancing the SRP effect. On the other hand, this contribution was considered for the de-orbiting by increasing the area-to-mass ratio at the end of mission so that the re-entry in the atmosphere is feasible (Lücking et al. [36]; Lücking et al., [37]). It was used by Colombo et al. [38] to study the orbit evolution and maintenance of a constellation of very small satellites, the Space Chips. The Hamiltonian approach was used to study the possible frozen orbits in the phase space representation. In a following work, Tresaco et al. [20] explored the effect of SRP upon satellite to enhance different future mission concept using Solar Sails: deep space exploration, space debris removal and long-term mission in the solar system. For the HEOs, the effect due to the attraction of the Moon was defined by Kozai and Lidov, as reported previously. Colombo et al. in [24] investigated how those long-term effects can be used to identify stability and instability conditions. The former, quasi-frozen orbits, are addressed for graveyard orbit determination, while the latter was used to target an Earth re-entry. This approach was developed also in subsequent works (Colombo et al., [26]; Colombo, [25]), and all of them study the orbital evolution in the phase space. The model here developed was used to optimise the manoeuvre to achieve the re-entry or the graveyard condition. Global optimisation methods were used to find the best manoeuvre direction, evaluating the dynamics with a semi-analytical approach at each step. The Hamiltonian formulation for the phase space determination was computed analytically in terms of the third-body disturbing function only. The consideration of other perturbations effect, as the coupled luni-solar perturbation and J_2 effect, was done by numerically integrating the single-averaged equation of motions to simplify the Hamiltonian formulation and the phase space representation.

[7]ESA Clean Space website: `http://www.esa.int/Our_Activities/Space_Engineering_Technology/Clean_Space`

1.2 Aim of the thesis

The aim of the present thesis is to investigate the feasibility of producing a fully analytical approach for optimal disposal manoeuvre computation. An analytical model for orbital perturbations of both Earth's and Venus' satellite was developed, including the potential due to the J_2 zonal harmonics and the third body disturbance: the Sun for Venus' orbiter and Moon and Sun for Earth's case. Since the study focuses on the secular and long-term prediction, the single and double averaged expression of each contribution is analytically evaluated and then substituted in the Hamiltonian system. From the latter, the two-dimensional phase space representation is recovered in terms of eccentricity and argument of perigee values, once the dependence on the Right Ascension of the Ascending Node (RAAN) is dropped. The analytical representation of the reduced Hamiltonian system has two advantages:

- the two-dimensional phase space describing the time evolution and oscillation of orbital elements is derived algebraically and not through a numerical integration.
- the Hamiltonian can be solved for the initial condition of the satellite to recover the maximum or the target eccentricity condition: this brings the knowledge of the minimum perigee that the orbit under study can reach in time due to natural evolution. This operation in previous works (Colombo et al [24], Colombo [25]) was done by numerically integrating the single-averaged dynamics until the maximum eccentricity, corresponding to the minimum perigee, was reached.

Hence, computing analytically the natural evolution of the satellite orbit can reduce the computational time and costs for the selection of the disposal manoeuvre. In fact, contrary to previous analysis, the optimal manoeuvre is not evaluated performing the integration of the Lagrange planetary equations in time but working completely in the reduced phase space. The aim of the thesis is to study the Hamiltonian phase space for developing the optimal manoeuvre for the end-of-life strategy. The dissertation develops the argument of perigee ω-eccentricity e maps in the Hamiltonian formalism. The study presents how the phase space changes depending on the orbital elements. Only the secular dynamics is represented: the double averaging technique is quite effective for describing the long-term evolution of satellite orbit since it reduces significantly the computational time for orbit propagation. In this work, the two-dimensional maps are obtained by eliminating the node effect, hence this model would be addressed as a triple averaged one. It results that the third body effect is essential for HEO time evolution, in combination with planet gravitational

field: J_2 tends to reduce the beneficial effect of the third body attraction, for the re-entry purpose: as the satellite is closer to the planet surface (lower altitude), it will feel a smaller influence of the third body. For this reason, only highly elliptical orbits are considered in this thesis.

The 'surfing'[8] among the natural orbital perturbations (Colombo, [25]) results in the minimisation of the velocity required for different missions, and its feasibility was already demonstrated by former studies (Colombo et al., [24]). This is a revolutionary concept and can reduce the cost and the mass of a spacecraft: it can simply navigate in the space around a planet following the natural evolution of the orbit.

In addition, the novelty of this work is the feasibility study to develop a very light analytical code capable of computing the best manoeuvre condition starting from the current ephemeris of the satellite. The model used could be further improved in the subsequent works, with the aim of producing a new generation of onboard software for the disposal strategy design, since it requires very low computational effort.

1.3 Thesis outline

This thesis provides an in-depth presentation, of the end-of-life strategy design. The work is organised to provide the reader with the knowledge necessary to understand how the perturbations can be modelled and which methods can be used to perform optimal manoeuvre for satellite removal in HEOs.

Chapter 2 is an outline of the perturbed two-body problem, introducing the classical equations of the two body system in the planetocentric Inertial Reference Frame. Then the Gauss and Lagrange planetary equations are reported in order to introduce the long-term dynamics in orbital elements. Finally, a brief overview of the Hamiltonian formulation is provided.

Chapter 3 covers the analytical recovery of the disturbing function. The double-averaged Hamiltonian expression for the description of the secular effects. Only the J_2 term of the zonal harmonic contribution will be considered, while for the Luni-Solar perturbation, the potential is expanded up to the fourth order and then it is averaged twice, both over the satellite's mean anomaly and the perturbing body's mean anomaly.

Chapter 4 shows the procedure used to reduce the Hamiltonian formulation obtained with the second average potentials, to one degree of freedom. It describes the triple averaging technique used for the node elimination and discusses the level of accuracy of the new

[8]COMPASS website: `www.compass.polimi.it`

reduced model.

Chapter 5 describes the disposal manoeuvre strategy, focusing on the optimisation procedure using an analytical or semi-analytical orbital propagation to recover the best delta-v solution. The disposal algorithm scheme is reported for a better understanding of the approach.

Chapter 6 presents the numerical results for the cases of study missions: Venus' orbiter, INTEGRAL and XMM-Newton. The optimal manoeuvre considering different levels of approximation is reported, first without considering the Sun influence and then adding it. Moreover, different approaches are compared in terms of orbital evolution and the cost of the manoeuvre.

Chapter 7 concludes the thesis work, describing the main achievements and possible future developments of semi-analytical approaches for disposal manoeuvre design.

Chapter 2

Review of the perturbed two body problem

2.1 Historical Background

SINCE ancient times, the motion of celestial bodies is of great interest for humanity. Copernicus (1473-1543) was the first to develop a model of the Solar System, which considers the Sun as the centre and the planets orbiting on trajectories around the Sun. This model was the starting point to all the subsequent theories.

Galileo Galilei (1564-1642) picked up the work done by Copernicus. His work was fundamental for the work of Johann Kepler and Isaac Newton.

Kepler's Laws Johannes Kepler (1571-1630), based on astronomical observations, developed the three fundamentals laws of the orbital mechanics, to describe the kinematics of planetary motion.

1. the orbit of each planet is an ellipse with the Sun at one focus,
2. the line joining the planet to the Sun sweeps out equal areas in equal times,
3. the square of the period of a planet is proportional to the cube of its mean distance to the Sun.

Newton's Laws Isaac Newton (1642-1727), was able to describe the dynamics of the planetary motion. In his book *Philosophiae Naturalis Principia Mathematica* he introduced the three laws of motion:

1. each body continues its state of rest, or uniform motion in a straight line unless it is compelled to change that state by forces exerted on it.

2. The change of motion is proportional to the force and is made in the direction in which the force is exerted.

3. To each action, there is always opposed an equal reaction.

Classically, the motion of a satellite was simply characterised with Newton's gravitational law, proportional to the inverse of the square distance between the two bodies. It was derived by the second law of motion, describing the equations of motion of a space object under the influence of the central main attractor only.

2.2 Earth Centred Inertial Frame

The first important requirement is to define a suitable reference system for describing the orbit of the satellite. For Earth's satellites, an Earth-based system is typically used (Vallado, [39]). This system uses as reference plane the equatorial plane. It originates at the centre of the Earth, and it is defined by three orthogonal unit vectors: IJK. The I axis point towards the vernal equinox, the K axis is in the North Pole direction, and the J axis completes the orthogonal tern. It is an inertial frame fixed with the vernal equinox direction.

This Earth centred equatorial frame is typically referred to the Earth-Centred-Inertial (ECI) frame, as represented in Figure 2.1a.

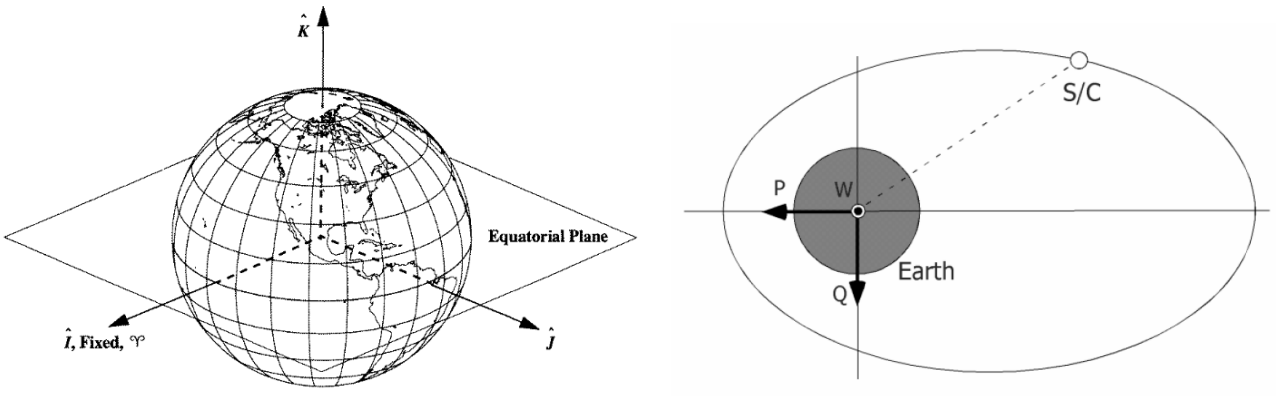

(a) Earth Centred Inertial Frame (IJK) (Vallado, [39]). **(b)** Perifocal reference system (Narumi and Hanada, [40]).

Figure 2.1 Earth centred inertial frame and perifocal reference system.

2.3 Perifocal Reference Frame

A second important reference system is the Perifocal frame, which is commonly used for processing satellite observation. It is defined in the spacecraft orbit plane centred at the main attractor. The x-axis is defined in the direction of the orbit perigee, described by the eccentricity direction vector. The z-axis is in the direction of the a-dimensional orbital angular momentum unit vector $\hat{\mathbf{h}}$, and finally, the y-axis is defined to complete the tern in the direction of the semi-latus rectum.

The resulting orthogonal unit vector tern is called $\hat{\mathbf{Q}}$, $\hat{\mathbf{P}}$, $\hat{\mathbf{h}}$, as reported in Figure 2.1b.

2.4 The two-body problem dynamics

As shown in several texts, Curtis [41], Vallado [39], Chao [42] and many others, starting from the Newton's Law of gravitation and the second law of motion, the spacecraft equations of motion can be derived under the influence of a central force field.

The ideal two-body problem, with no external perturbation at all, consists of:

- One main attractor: a central planet with mass m_0,
- Orbiting object: Satellite/Asteroid/Moon with mass m_1 under the following assumptions:
  - $m_1 \ll m_0$ (its mass is negligible),
  - orbital parameters: semi-major axis a, eccentricity e, inclination i, argument of perigee ω, Right Ascension of the Ascending Node Ω,
  - position vector $\mathbf{r}$ and velocity vector $\mathbf{v}$.

The equations of motion are written in terms of relative vector $\mathbf{r}$, the position vector from the centre of the main attractor to the satellite:

$$\frac{d^2\mathbf{r}}{dt^2} = -\frac{\mu \mathbf{r}}{r^3}. \tag{2.1}$$

The gravitational attraction of the main body was considered through the planetary constant μ, related to the mass of the main attractor m_0 and of the orbiting object m_1 and to the universal gravitational constant $G = 6.67 \times 10^{-20}\,\mathrm{km}^3/\mathrm{kg\,s}^2$:

$$\mu = G(m_0 + m_1) \overset{m_1 \ll m_0}{\longrightarrow} \mu = G m_0. \tag{2.2}$$

On the other hand, it is typically convenient to pass to the orbital elements $\{a, e, i, \omega, \Omega, f\}$: the semi-major axis a, the eccentricity e, the inclination i, the argument of perigee ω, the right ascension of the ascending node Ω, the true anomaly f. In this new representation, the celestial body trajectory can be described by the following relation:

$$r = \frac{a(1-e^2)}{1+e\cos f}, \tag{2.3}$$

where the true anomaly f along the orbit varies in time in the interval $[0, 2\pi]$ through the eccentric and mean anomaly relations, as better explained in Appendix A. In fact, the mean anomaly is directly connected with the time t passed from the perigee passage through the mean motion n.

$$\tan\left(\frac{f}{2}\right) = \sqrt{\frac{1+e}{1-e}}\tan\left(\frac{E}{2}\right), \tag{2.4}$$

$$M = E - e\sin E, \tag{2.5}$$

$$M = M_0 + n(t - t_0), \tag{2.6}$$

where M_0 and t_0 are the mean anomaly and the time at the perigee passage, $n = \sqrt{\mu/a^3}$ is the mean motion, E the eccentric anomaly and e the eccentricity.

2.5 Perturbed Equations of Motion

In the real world, the Keplerian equations of motion in Equation (2.1) are an ideal representation of the actual motion of a space object. In fact, several external sources of perturbation to the ideal motion are present. In the following sections, a detailed formulation and derivation are reported for the most relevant sources for planetary orbiters: planet gravitational harmonics, in particular, the zonal ones and the third body attraction: for the Earth due to both Sun and Moon, for Venus due to the Sun only.

All the external sources of disturbance act on the orbiting object as a perturbing acceleration, which affects the ideal Keplerian motion as follow:

$$\frac{d^2\mathbf{r}}{dt^2} = -\frac{\mu\mathbf{r}}{r^3} + \mathbf{a}_{perturbing}. \tag{2.7}$$

Although this approach is very simple to derive, to better understand the effect of disturbances on the real motion, it is better to describe the orbit in terms of Keplerian elements: $a, e, i, \Omega, \omega, f$. This is a more intuitive approach. In this way, the variation from

the ideal motion is presented in terms of variation of orbital elements instead of position vector components, making more understandable the overall behaviour.

2.5.1 Lagrange Planetary Equations

If only conservative forces due to external perturbations are considered, the equations of variations of the Keplerian elements in terms of the disturbing function, $\mathcal{R}$, can be written in the Lagrangian form (see Valtonen and Karttunen [30]; Vallado, [39]; El'iasberg, [43] for theoretical reference):

$$\begin{aligned}
\frac{da}{dt} &= \frac{2}{na}\frac{\partial \mathcal{R}}{\partial M} \\
\frac{de}{dt} &= \frac{1}{na^2 e}\left((1-e^2)\frac{\partial \mathcal{R}}{\partial M} - \sqrt{1-e^2}\frac{\partial \mathcal{R}}{\partial \omega}\right) \\
\frac{di}{dt} &= \frac{1}{na^2 \sin i\sqrt{1-e^2}}\left(\cos i\frac{\partial \mathcal{R}}{\partial \omega} - \frac{\partial \mathcal{R}}{\partial \Omega}\right) \\
\frac{d\Omega}{dt} &= \frac{1}{na^2 \sin i\sqrt{1-e^2}}\frac{\partial \mathcal{R}}{\partial i} \\
\frac{d\omega}{d} &= -\frac{1}{na^2 \sin i\sqrt{1-e^2}}\cos i\frac{\partial \mathcal{R}}{\partial i} + \frac{\sqrt{1-e^2}}{na^2 e}\frac{\partial \mathcal{R}}{\partial e} \\
\frac{dM}{dt} &= n - \frac{1-e^2}{na^2 e}\frac{\partial \mathcal{R}}{\partial e} - \frac{2}{na}\frac{\partial \mathcal{R}}{\partial a},
\end{aligned} \tag{2.8}$$

where M is the mean anomaly and n is the mean motion of the satellite. The disturbing function $\mathcal{R}$ is defined as the opposite of the force potential function V: $\mathcal{R} = -V$, and it is represented by the sum of the contribution of each external source. For an Earth's satellite it is defined as:

$$\mathcal{R} = \mathcal{R}_{gravity} + \mathcal{R}_{Moon} + \mathcal{R}_{Sun}, \tag{2.9}$$

where $\mathcal{R}_{gravity}$ is due to the gravitational attraction of the main body, $\mathcal{R}_{Moon}$ is due to the third body gravitational attraction of the Moon, and $\mathcal{R}_{Sun}$ due to the Sun disturbance.On the other hand for a Venus' probe it depends only on planet's oblateness and Sun attraction:

$$\mathcal{R} = \mathcal{R}_{gravity} + \mathcal{R}_{Sun}. \tag{2.10}$$

2.5.2 Long-Term Lagrange Planetary Equations

A common practice to study the long-term behaviour of the equation of motion is to average the disturbing potential function. Through the averaging technique, see for details Chao [42], the short-period terms averages out, retaining only secular and long-periodic effects.

The averaging technique consists of a first integration over one period (one revolution) of the orbiting object, and after that, a second averaging is performed over one period of the third disturbing body. The single and the double-averaged potential must be replaced in Lagrangian equations of motion (Equation (2.8)). The general expression is described by:

$$\frac{d\bar{\alpha}}{dt} = \frac{d\bar{\alpha}}{dt}\left(\alpha, \bar{\mathcal{R}}\right), \tag{2.11}$$

$$\frac{d\bar{\bar{\alpha}}}{dt} = \frac{d\bar{\bar{\alpha}}}{dt}\left(\alpha, \bar{\bar{\mathcal{R}}}\right), \tag{2.12}$$

where α is the vector of the orbital elements, $\bar{\mathcal{R}}$ is the single-averaged potential and $\bar{\bar{\mathcal{R}}}$ is the double-averaged potential. This approach is very useful for the case of study since it allows to reduce a lot the computational time of integration. Furthermore, it is a correct approach to describe the long-term behaviour of a satellite, as it is required for the design of end-of-life strategy.

2.5.3 Gauss planetary equation

When not only conservative forces are present, but also non-conservative ones, the Lagrange's planetary equations (Equation (2.8)) cannot be used any more. This happens, for example, when the satellite's dynamic is subjected to drag disturbance or impulsive firings. In this case, the equations of variations of Keplerian elements are expressed in terms of the disturbing acceleration, $\mathbf{a_{perturbing}}$, in the velocity frame $\hat{\mathbf{t}}, \hat{\mathbf{n}}, \hat{\mathbf{h}}$, with $\hat{\mathbf{t}}$ aligned with the direction of motion, $\hat{\mathbf{h}}$ is in the direction of the adimensional angular momentum and $\hat{\mathbf{n}}$ completes the orthogonal tern.

$$\begin{aligned} \hat{\mathbf{t}} &= \frac{\mathbf{v}}{||\mathbf{v}||} \\ \hat{\mathbf{h}} &= \frac{\mathbf{r} \times \mathbf{v}}{||\mathbf{r} \times \mathbf{v}||} \\ \hat{\mathbf{n}} &= \hat{h} \times \hat{t}, \end{aligned} \tag{2.13}$$

where $\mathbf{v}$ is the velocity vector, $\mathbf{r}$ is the position vector. The acceleration can be written in terms of variation of velocity in $\hat{\mathbf{t}}, \hat{\mathbf{n}}, \hat{\mathbf{h}}$ direction:

$$\mathbf{a_{perturbing}} = [a_t, a_n, a_h] = \left[\frac{dv_t}{dt}, \frac{dv_n}{dt}, \frac{dv_h}{dt}\right]. \tag{2.14}$$

In case an impulsive manoeuvre is given, the Gauss planetary equations can be written, in first approximation, in terms of impulsive variation of the velocity vector $\delta\mathbf{v} = [\delta v_t, \delta v_n, \delta v_h]^T$ (Colombo, [27]), where r_d and v_d are respectively the radius and the velocity at the point where the instantaneous change is provided, h is the angular momentum, p is the semi-latus rectum, $u_d = \omega + f$ is the argument of latitude, b is the semi-minor axis, and dM takes into account only the instantaneous change in the mean anomaly.

$$\begin{aligned}
\delta a &= \frac{2a^2 v_d}{\mu}\,\delta v_t \\
\delta e &= \frac{1}{v_d}\left[2\,(e+\cos f)\;\delta v_t - \frac{r_d}{a}\sin f\;\delta v_n\right] \\
\delta i &= \frac{r_d \cos u_d}{h}\,\delta v_h \\
\delta\omega &= \frac{1}{e v_d}\left[2\sin f\;\delta v_t + \left(2\,e + \frac{r_d}{a}\cos f\right)\;\delta v_n\right] - \frac{r_d \sin u_d \cos i}{h \sin i}\,\delta v_h \\
\delta\Omega &= \frac{r_d \sin u_d}{h \sin i}\,\delta v_h \\
\delta M &= -\frac{b}{e\,a\,v_d}\left[2\left(1 + \frac{e^2 r_d}{p}\right)\sin f \delta\, v_t + \frac{r_d}{a}\cos f\,\delta v_n\right].
\end{aligned} \tag{2.15}$$

2.6 Hamiltonian formulation

The Hamiltonian formulation is now introduced for a later derivation of the planar phase space since it is essential for the study of the disposal manoeuvre at the end-of-life of a mission. In particular, the Hamiltonian formalism can fully describe the dynamical properties of the system. In this section, the Hamiltonian is derived for a two-body system, starting from the general problem. The formulation here presented is based on Valtonen and Karttunen [30].

2.6.1 Hamiltonian principle

In general, any dynamical system can be described by means of the Lagrangian function $\mathcal{L}$. This function is written in terms of generalised coordinates q_i, their derivatives $\dot{q}_i$ and time t. From the formulation in Lagrange [28], the Lagrangian Function is defined as:

$$\mathcal{L} = \mathcal{L}(q_1, ..., q_m, \dot{q}_1, ..., \dot{q}_m, t) = T - V, \tag{2.16}$$

where T and V are respectively the kinetic and the potential energy of the system, assumed to have m degrees of freedom. In addition to the generalised coordinates q_i, it is possible to

define the generalised momenta p_i:

$$p_i = \frac{\partial \mathcal{L}}{\partial \dot{q}_i}. \tag{2.17}$$

Therefore, the Lagrangian function becomes: $\mathcal{L}(p_i, q_i, t)$. Similarly, using a Legendre transformation, the Hamiltonian $\mathcal{H}$ of the system can be recovered from $\mathcal{L}$:

$$\mathcal{H} = \mathcal{H}(q_i, p_i, t) = \sum_{i=1}^{m} \dot{q}_i p_i - \mathcal{L}(q, \dot{q}, t), \tag{2.18}$$

leading to the following equations of motion:

$$\frac{dq_i}{dt} = \frac{\partial \mathcal{H}}{\partial p_i}, \qquad \frac{dp_i}{dt} = -\frac{\partial \mathcal{H}}{\partial q_i}, \qquad (i = 1, 2, ..., m). \tag{2.19}$$

At this point, it is possible to demonstrate that the Hamiltonian does not depend explicitly on time, hence it is a constant of motion of the system and it will not vary in time (see Valtonen and Karttunen [30]). Furthermore, this yield to demonstrate that the Hamiltonian is equal to the total energy of the system and thus, using the Euler's theorem for the two-body problem:

$$\mathcal{H} = \sum_{i=1}^{m} \dot{q}_i \frac{\partial T}{\partial \dot{q}_i} - \mathcal{L} = 2\,T - \mathcal{L} = T + V. \tag{2.20}$$

Now, using canonical coordinates, the Hamiltonian of the two-body system vanishes, and the variables become constants of motion. The new Hamiltonian is reported in Equation (2.22), while the orbit of the satellite is described using the simplified canonical elements, also called Delaunay's elements in Equation (2.21). This representation allows to write the Hamiltonian formulation in terms of the semi-major axis of the orbit, a.

$$\begin{aligned} l &= M, & g &= \omega, \\ h &= \Omega, & L &= \sqrt{a\mu}, \\ G &= L\sqrt{1-e^2}, & H &= G\cos i. \end{aligned} \tag{2.21}$$

$$\mathcal{H}_{new} = \mathcal{K} = -\frac{\mu^2}{2L^2} = -\frac{\mu}{2\,a}. \tag{2.22}$$

From now on, the new Hamiltonian will be simply referred to $\mathcal{H}$ and it is expressed in the Keplerian orbital elements, rather then Delaunay variable, due to their more physical meaning.

2.6.2 Hamiltonian of the perturbed two-body problem

The representation in Equation (2.22) is valid only for the ideal two-body problem, with no perturbation at all. Therefore, to consider all the external sources that are present in the real motion, a perturbing potential must be introduced in the Hamiltonian. This is simply the one recovered in Equation (2.11), which considers all the possible external disturbances. The perturbed Hamiltonian of the Earth-satellite system is reported in Equation (2.23). But the relation is general and can be written for any planet-satellite system.

$$\mathcal{H} = -\frac{\mu}{2\,a} - \mathcal{R} = -\frac{\mu}{2\,a} - \mathcal{R}_{zonal} - \mathcal{R}_{Moon} - \mathcal{R}_{Sun} - \mathcal{R}_{SRP}. \tag{2.23}$$

In this dissertation, the influence of the Sun will be considered only as a second approximation, while Solar Radiation Pressure effect will not be considered. This approximation is valid under the assumption that for HEO orbit, the most significant perturbations are the Lunar and the J_2 effect.

Sensitivity analysis for Earth's satellite disturbing function In this thesis, only HEOs are investigated. As an example case, an orbit like the INTEGRAL one can be considered. In addition, the satellite is assumed to have a small area-to-mass ratio. This is a reasonable assumption for most of the Earth' satellites since typically they do not have solar sails on board or very big cross-sectional area. Obviously, if the mission under study has a significant area exposed to the Sun, the contribution of the SRP must be retained in the analysis.

The magnitude of different perturbations acting on a HEO is reported in Table 2.1.

Table 2.1 Magnitude of forces for an INTEGRAL like mission, (with area-to-mass ratio $\ll 1$, and a semi-major axis of 8.7×10^4 km)

Source	Disturbing force $\mathcal{R}$
Earth Oblateness (J_2)	10^{-5}
Moon Attraction	10^{-4}
Sun Attraction	10^{-6}
SRP	10^{-10}

Chapter 3

Orbital perturbations

THE classical two-body problem is an ideal representation of the actual dynamics of a satellite. The perturbations to this ideal motion are introduced in terms of disturbing potential or disturbing acceleration. In this chapter, the potentials for a planet natural satellite (as the Moon for the Earth), the Sun perturbation and the planet gravitational field are recovered, since those are the most important terms for Highly Elliptical Orbit (HEO) satellite.

In this work, the third body is treated as a perturbing mass to the ideal two body problem (planet-satellite system), and this is valid under the assumptions that the semi-major axis of the satellite is much smaller than the third body semi-major axis (at least of one order of magnitude). This consideration is valid for both the cases under study. In the Earth-satellite system, the perturbations due to Moon, Sun and J_2 are considered, while for the Venus' probe only Sun and J_2 effect is present.

The development of the third body potential is essential to recover the equation of motion from the Hamiltonian. Then to study the long-term behaviour, the contribution of the third body was firstly expanded in the semi-major axis ratio, and then averaged over the orbital frequencies.

In addition, the zonal harmonic potential is recovered as well, to model in a more accurate way the gravitational field for the vehicle. During the expansion with the Legendre polynomials, the terms related to the coefficient J_2, for the planet oblateness, is the most significant.

The procedure followed during the computation of each term of the Hamiltonian is described in Figure 3.1.

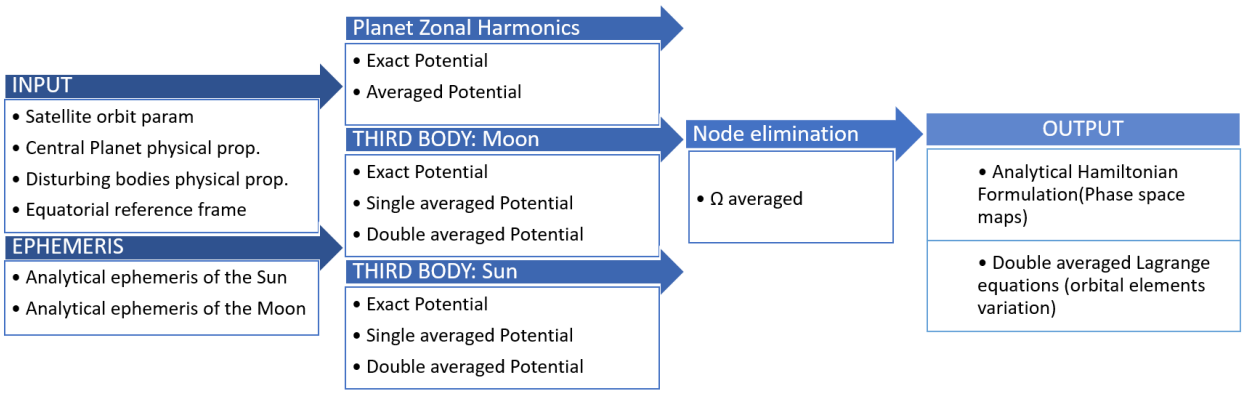

Figure 3.1 Schematic procedure for the analytical recovery.

3.1 Historical Background

The influence of an external third body was widely studied in the past. The three-body problem naturally follows the classical two-body problem. Newton (1642-1737) considers the problem of the three-body system to study the behaviour of the Moon under the influence of the Earth and the Sun. In more recent years, this approach was applied to many different cases of study. Kozai (1928-2018) studied the motion of an Asteroid under the influence of both Jupiter and the Sun (Kozai, [6]). He described the third body disturbing potential for the secular effect, eliminating the short-periodic term by the Hamiltonian of the system. His work was based on the assumptions that the orbit of the third body, in this case, Jupiter, was circular. In the same period, also another scientist developed a model to describe the evolution of an orbit under the effect of the gravitational perturbation of a third body. Lidov (1926-1993) applied the problem to Earth's artificial satellites, considering as external perturbing body the Moon and the Sun (Lidov, [5]).

3.2 Inertial Equatorial Reference Frame

In this thesis, differently from most of past works (Kozai [6]; Lidov, [5]; Tresaco et al., [20]; El'iasberg, [43]), the potential function due to external source of disturbances is not described in the perturbing body plane or in the invariable plane. The planet equator was taken as the reference plane for all the dissertation, as was done in Colombo, [25]. This decision was driven by three main fundamental aspects in the Earth's system:

1. the simplification that the Sun and the Moon orbit on the same plane can be dropped,

2. the zonal harmonics potential can be introduced with no effort, without the need to transform the formulation in the perturbing body plane,

3. typically, the satellite ephemeris are evaluated in the equatorial plane, not in the perturbing body one, hence it is more straightforward to derive the overall effect on an Earth satellite.

In fact, introducing the Sun effect in a model derived in the Earth-Moon plane can create many troubles, mainly if the Sun is considered orbiting on another plane. In addition, rotating the contribution of the zonal harmonic to an inclined plane drop the advantage of having a spherically symmetric potential, which is instead retained in the equatorial frame. Despite this, the assumption has some drawbacks:

1. the potential expression including the influence of Moon, Sun and J_2 is more complex than the classical one (El'iasberg, [43]),

2. the final expression depends on the satellite RAAN, yielding to the need of introducing the elimination of the node to access the two-dimensional Hamiltonian phase space.

3.3 Zonal Harmonic Potential

In this section, the effect of the Earth's gravitational field is analysed to recover the long-term behaviour. In this thesis, only the influence of the J_2 term is considered. This is valid for satellite on orbits where the influence of the gravitational field is not the principal one (i.e. for HEO). Note that for close Earth satellite LEO the low altitude requires a precise computation of the higher order gravitational terms.

3.3.1 Analytical expression

The potential function describing the gravitational field of the central body is reported in Vallado [39] and Blitzer [44]. In particular they described the external Geopotential at any point $P(r, \lambda, \delta)$ in terms of Legendre Polynomials, and separated the contribute independent of the longitude, the Zonal Harmonics, to the one related to it, the Tesseral Harmonics:

$$V = -\frac{\mu}{r}\left[1 - \sum_{l=2}^{\infty} J_l \left(\frac{R_\alpha}{r}\right)^l P_l(\sin\delta) + \sum_{l=2}^{\infty}\sum_{m=1}^{l} J_{lm}\left(\frac{R_\alpha}{r}\right)^l P_l(\sin\delta)\cos m(\lambda - \lambda_{lm})\right] \quad (3.1)$$

where μ is the planet's gravitational parameter, r is the orbital radius, $J_l = -C_{l,0}$ are the zonal gravitational coefficient, R_α is the main attractor equatorial radius, $P_l(\sin\delta)$ are the

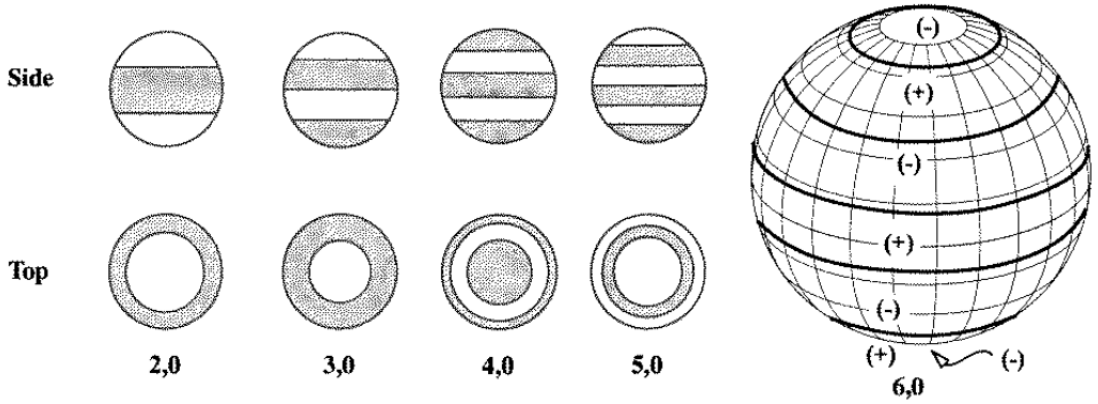

Figure 3.2 Spherical Harmonics bands of latitude for J_2 to J_6 term in the Zonal contribution (Vallado, [39])

Table 3.1 Earth's Zonal Harmonics coefficients (from EGM-2008 [45]) and Venus' Zonal Harmonics coefficient (from Mottinger et al. [46])

	J_2	J_3	J_4	J_5	J_6
Earth	1082.626×10^{-6}	-2.532×10^{-6}	-1.619×10^{-6}	-2.277×10^{-6}	5.406×10^{-6}
Venus	4.458×10^{-6}	1.34×10^{-6}	2.41×10^{-6}	0.259×10^{-6}	0.336×10^{-6}

Legendre polynomials as function of the geocentric latitude δ, $J_{lm} = -C_{l,m}$ are the Tesseral harmonics coefficients and λ is the geocentric longitude. In particular, the zonal gravitational coefficients for the Earth and Venus are reported in Table 3.1. These coefficients describe the difference of the planet's shape from a perfect sphere. The Figure 3.2 represents the contribution of each term on the planet shape approximation. In this thesis, only the zonal harmonic would be considered, and therefore the disturbing function, $\mathcal{R} = -V$ is the following:

$$\mathcal{R}_{zonal} = -\frac{\mu}{r} \sum_{l=2}^{\infty} J_l \left(\frac{R_\alpha}{r} \right)^l P_l(\sin \delta). \tag{3.2}$$

In addition, only the first term of the zonal harmonic is retained in this approximation since it is the dominant term:

$$\mathcal{R}_{zonal,J2} = -\frac{\mu J_2}{2\,r} \left(\frac{R_\alpha}{r} \right)^2 (3 \sin \delta^2 - 1). \tag{3.3}$$

3.3.2 Long term effect via closed-form single-averaging

Since this work focuses on the study of the long-term dynamics of the satellites, the first step is to cancel out the short-term effects due to the true anomaly variation along the orbit. This procedure acts as a low pass filter to cancel out the high-frequency variations. Therefore, before substituting the Equation (3.3) in Equation (2.9) and Equation (2.8), the averaging procedure is done over one orbital period of the orbiting object. During the averaging, all the orbital elements are considered constant, apart from the true anomaly. The complete procedure for the averaging is now reported, where all the computation were done in an analytical way with Mathematica® software. At first, the potential shall be written in terms of orbital elements, hence the relations in Equation (3.4) for the orbit radius r and the geocentric latitude δ are used. The position along the orbit is written in terms of the true anomaly, while the latitude is a function of inclination, argument of perigee and true anomaly (see Appendix A).

$$\begin{aligned} r &= \frac{a(1-e^2)}{1+\cos f} \\ \sin\delta &= \sin(\omega+f)\sin i, \end{aligned} \tag{3.4}$$

where e is the eccentricity, ω the satellite argument of perigee, f is the satellite true anomaly and i is the inclination of the orbit. Hence, the Equation (3.3) becomes:

$$\begin{aligned} \mathcal{R}_{J2} &= -\frac{\mu\, J_2\, R_\alpha^2}{2}\frac{3\sin^2 i\sin^2(\omega+f)}{r^3} \\ &= -\frac{\mu\, J_2\, R_\alpha^2}{2}\frac{3\sin^2 i(\sin\omega\cos f+\cos\omega\sin f)}{r^3} \\ &= -\frac{\mu\, J_2\, R_\alpha^2}{4}\frac{2-3\sin^2 i+3\sin^2 i(\cos 2\omega\cos 2f-\sin 2\omega\sin 2f)}{((a(1-e^2))/(1+\cos f))^3}. \end{aligned} \tag{3.5}$$

Since the averaging is done over the mean anomaly M, as reported in Chao, [42]:

$$\bar{\mathcal{R}}_{zonal} = \frac{1}{2\pi}\int_0^{2\pi} \mathcal{R}_{zonal} dM. \tag{3.6}$$

An efficient way to perform the integral is to write the radius and the mean anomaly (r, M) in terms of the true anomaly: f. The relations used are shown in Appendix A:

$$dM = \frac{r^2}{a^2(1-e^2)^{1/2}}\,df = \frac{(1-e)^{3/2}}{(e\cos f+1)^2}\,df, \tag{3.7}$$

$$r = \frac{a(1-e^2)}{1+e\cos f}, \tag{3.8}$$

This new representation is very good for integral computation, since is provides terms with no angles on the denominator, yielding to trivially solvable expressions. Therefore, the terms to be integrated are:

$$\frac{1}{2\pi}\int_0^{2\pi}\frac{1+e\cos f}{(1-e^2)^3}(1-e^2)^{3/2}\,df = (1-e^2)^{-3/2} \tag{3.9}$$

$$\frac{1}{2\pi}\int_0^{2\pi}\frac{(1+e\cos f)\sin 2f}{(1-e^2)^3}(1-e^2)^{3/2}\,df = 0 \tag{3.10}$$

$$\frac{1}{2\pi}\int_0^{2\pi}\frac{(1+e\cos f)\cos 2f}{(1-e^2)^3}(1-e^2)^{3/2}\,df = 0. \tag{3.11}$$

By substituting the results of the integrals in Equation (3.5), the final expression for the single averaged zonal harmonics potential, re-arranging the sin term though trigonometric relations, is:

$$\begin{aligned}\bar{\mathcal{R}}_{zonal,J2} =& \frac{\mu\, J_2\, R_\alpha^2}{4\,a^3}\frac{2-3\sin^2 i}{(1-e^2)^{3/2}} \\ =& \frac{\mu J_2 R_\alpha^2}{8\,a^3(1-e^2)^{3/2}}(1+3\cos 2i).\end{aligned} \tag{3.12}$$

Therefore, the disturbing potential due to J_2 depends only on three orbital parameters: the semi-major axis a, the eccentricity e and the orbit inclination i. Hence, after evaluating the derivative of the disturbing potential respect to the orbital elements, the time variation due to J_2 can be recovered. The disturbing function enters the Lagrange planetary equation through its partial derivatives respect to the orbital elements. At first, note that the only non null partial derivatives of $\bar{\mathcal{R}}_{zonal,J_2}$ are with respect to a, e, i:

$$\frac{\partial\bar{\mathcal{R}}_{zonal,J_2}}{\partial a} = -\frac{3\,\mu\, J_2\, R_\alpha^2(3\cos 2i+1)}{8\,a^4\,(1-e^2)^{3/2}} \tag{3.13}$$

$$\frac{\partial\bar{\mathcal{R}}_{zonal,J_2}}{\partial e} = \frac{3\,\mu\, J_2\, R_\alpha^2\, e(3\cos 2i+1)}{8\,a^3\,(1-e^2)^{5/2}} \tag{3.14}$$

$$\frac{\partial\bar{\mathcal{R}}_{zonal,J_2}}{\partial i} = -\frac{3\,\mu\, J_2\, R_\alpha^2\sin 2i}{4\,a^3\,(1-e^2)^{3/2}} \tag{3.15}$$

$$\frac{\partial\bar{\mathcal{R}}_{zonal,J_2}}{\partial \omega} = \frac{\partial\bar{\mathcal{R}}_{zonal,J_2}}{\partial\Omega} = \frac{\partial\bar{\mathcal{R}}_{zonal,J_2}}{\partial M} = 0. \tag{3.16}$$

By substituting the relations recovered in the Lagrangian Equation, Equation (2.8), it can be observed that J_2 causes variations in the argument of perigee ω and in the right ascension of the ascending node Ω only, see also Vallado [39]. Also a variation in the mean

anomaly is present, as reported in the following equations:

$$\frac{d\bar{a}_{zonal,J_2}}{dt} = \frac{d\bar{e}_{zonal,J_2}}{dt} = \frac{d\bar{i}_{zonal,J_2}}{dt} = 0 \tag{3.17}$$

$$\frac{d\bar{\omega}_{zonal,J_2}}{dt} = \frac{3\,\mu\,J_2\,R_\alpha^2(5\cos 2i + 3)}{8\,n\,a^5\,(e^2-1)^2} \tag{3.18}$$

$$\frac{d\bar{\Omega}_{zonal,J_2}}{dt} = -\frac{3\,\mu\,J_2\,R_\alpha^2\sin 2i}{4\,n\,a^5\cos i\,(1-e^2)^2} \tag{3.19}$$

$$\frac{d\bar{M}_{zonal,J_2}}{dt} = n + \frac{3\,\mu\,J_2\,R_\alpha^2(3\cos 2i) + 1)}{8\,n\,a^5\,(1-e^2)^{3/2}}. \tag{3.20}$$

The secular variation of the semi-major axis, the eccentricity and the inclination are null since J_2 affects only the short-term period with periodic oscillations along one orbit revolution, which has been averaged out during the process. On the other hand, there is a secular drift in both ω and Ω in time. This variation is commonly referred to as the secular nodal precession and the secular apsidal rotation: $d\bar{\omega}_{zonal,J_2}/dt$ and $d\bar{\Omega}_{zonal,J_2}/dt$. For the Earth's case, the time evolution of Ω and ω for a different type of orbits, from circular to highly elliptical and for different semi-major axes, is reported in Figure 3.3a and Figure 3.3b respectively. In particular, the results were reported for different orbit type, from circular to highly elliptical, with a different semi-major axis.

It is important to make some considerations: the nodal regression is near to zero for polar orbits, at that point, the secular effect of J_2 is zero; on the other hand, perigee remains fixed at the critical inclinations, 63.4° and 116.6°. Therefore, depending on the application, different inclinations can be exploited to minimise or maximise the secular effect of J_2.

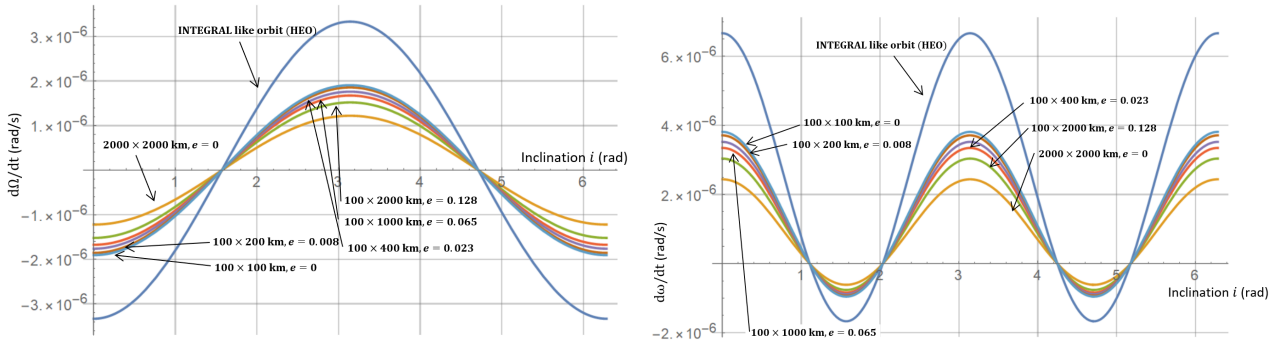

(a) Nodal regression due to J_2 for different orbit types. **(b)** Apsidal rotation due to J_2 for different orbit types.

Figure 3.3 J_2 effect on Ω and ω: rate of change in time.

3.4 The third body disturbing function

The three-body system here considered consists of an inner binary system, made by the main attractor (Earth or Venus) and the orbiting body (Satellite), and an outer perturbing third body (either the Moon or the Sun). In this study, the influence of the third body is threatened as a perturbation of the ideal two body problem, as in the works of Vallado [39] and Kaufman [8], and it is based on the following assumptions:

- the third body m_3 orbits on a much wider and distant orbit than the satellite,
- the perturbing body could be a planet natural satellite, the Sun or another planet,
- the distance of the third body m_3 from the main attractor m_0 is much higher than the orbiting object m_2 semimajor axis, i.e. the semi-major axis of the satellite shall be at least one order of magnitude less than the perturbing one,
- the mass of the orbiting object m_2 is much smaller than the main attractor mass m_0 and the perturbing body mass m_3,
- the orbital parameters in the equatorial frame are:
  - third body: a_{3b}, e_{3b}, i_{3b}, ω_{3b}, Ω_{3b}, f_{3b},
  - orbiting body: a, e, i, ω, Ω, f.

The geometry of the three-body system is shown in Figure 3.4. The Earth-Moon-Satellite system is taken as a case of study, but the dissertation is general and therefore can be applied to any three-body system. Hence, it is valid also for the Sun effect and the Venus-Sun system.

In Figure 3.4b, $\mathbf{r}$ is the satellite position vector, $\mathbf{r_{3b}}$ is the Moon position vector and ρ is the relative position vector between the satellite and the Moon. Those vectors are expressed in the Earth Centred reference system, while the angle between $\mathbf{r}$ and $\mathbf{r_{3b}}$ is called S. This angle is expressed through the scalar product of the two vector $\mathbf{r}$ and $\mathbf{r}_{3b}$ (Kaufman, [8]):

$$\cos S = \frac{\mathbf{r} \cdot \mathbf{r}_{3b}}{r\, r_{3b}} = \hat{\mathbf{r}} \cdot \hat{\mathbf{r}}_{3b} \tag{3.21}$$

3.4.1 Analytical expression of the disturbing potential

Starting from the Earth-Satellite-perturbing body system, the disturbing acceleration experienced by the satellite due to the third body can be recovered. In particular, the

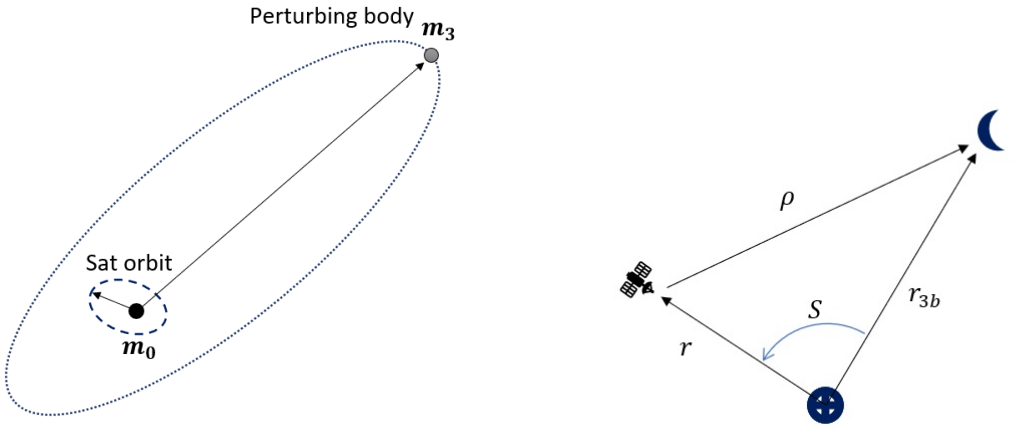

(a) Graphical representation of the three body system. **(b)** Third body system: Earth-Moon-Sat

Figure 3.4 Three body system geometry.

acceleration experienced by a satellite under the effect of a point mass third body is due to the gravity of the main attractor and to the disturbing function $\mathcal{R}_{3b}$:

$$\ddot{r} = -\frac{\mu \mathbf{r}}{r^3} + \mu_{3b}\nabla\left(\frac{1}{\rho} - \frac{\mathbf{r}_{3b}\cdot\mathbf{r}}{r_{3b}^3}\right) = -\frac{\mu \mathbf{r}}{r^3} + \nabla\mathcal{R}_{3b}, \tag{3.22}$$

where μ_{3b} is the gravitational coefficient of the third body, $\mathbf{r}$ is the satellite position vector, $\mathbf{r}_{3b}$ is the third body position vector, ρ is the norm of the relative position vector between the satellite and the third body: $\rho = |\mathbf{r} - \mathbf{r}_{3b}|$. In particular the first term of right hand side of Equation (3.22) is simply the two body gravitational attraction, while the second one is due to the disturbance of the third body. The disturbing potential due to the third body is (from Murray and Dermott [47]):

$$\mathcal{R} = \frac{\mu_{3b}}{|\mathbf{r} - \mathbf{r_{3b}}|} - \mu_{3b}\frac{\mathbf{r}\cdot\mathbf{r_{3b}}}{r_{3b}^3}, \tag{3.23}$$

where $\mu_{3b} = \mathcal{G}m_3 = \frac{m_3}{m_0+m_3}\mathcal{G}(m_0+m_3) = \mu'\mathcal{G}(m_0+m_3)$, with μ' the reduced mass of the system and $\mathcal{G}$ =6.6740 $\times 10^{-20}\,\mathrm{km}^3/\mathrm{kg}/\mathrm{s}^2$ is the universal gravitational constant.

At this point it is possible to expand the potential in Equation (3.23) using Legendre Polynomials. From the cosine law, by considering the geometry in Figure 3.4b, the term $|\mathbf{r} - \mathbf{r_{3b}}|^2$ is:

$$|\mathbf{r} - \mathbf{r_{3b}}|^2 = r^2 + r_{3b}^2 - 2\,r\,r_{3b}\,\cos S \tag{3.24}$$

Table 3.2 Legendre Polynomials $P_{l,m}[\cos S]$ for $m = 0$

l	$P_l[\cos S]$
1	$\cos S$
2	$\frac{1}{2}\left(3\cos^2 S - 1\right)$
3	$\frac{1}{2}\left(5\cos^3 S - 3\cos S\right)$
4	$\frac{1}{8}\left(35\cos^4 S - 30\cos^2 S + 3\right)$

Hence, the term in Equation (3.23) becomes:

$$\frac{1}{|\mathbf{r} - \mathbf{r_{3b}}|} = \frac{1}{r_{3b}}\left(1 - 2\,\frac{r}{r_{3b}}\cos S + \left(\frac{r}{r_{3b}}\right)^2\right)^{-1/2} \tag{3.25}$$

which can be expanded as:

$$\frac{1}{|\mathbf{r} - \mathbf{r_{3b}}|} = \frac{1}{r_{3b}}\sum_{l=0}^{\infty}\left(\frac{r}{r_{3b}}\right)^l P_l[\cos S], \tag{3.26}$$

where $P_l[\cos S]$ are the Legendre Polynomials, as reported in Table 3.2. On the other hand, the second term can be written as:

$$\frac{\mathbf{r}\cdot\mathbf{r_{3b}}}{r^3} = \frac{r\,r_{3b}\cos S}{r_{3b}^3} = \frac{1}{r_{3b}}\frac{r}{r_{3b}}\cos S = \frac{1}{r_{3b}}\frac{r}{r_{3b}}P_1[\cos S]. \tag{3.27}$$

Therefore, by substituting Equation (3.26) and Equation (3.27) into Equation (3.23), the overall disturbing function is:

$$\begin{aligned}\mathcal{R} =& \frac{\mu_{3b}}{r_{3b}}\sum_{l=0}^{\infty}\left(\frac{r}{r_{3b}}\right)^l P_l[\cos S] - \frac{\mu_{3b}}{r_{3b}}\frac{r}{r_{3b}}P_1[\cos S] \\ =& \frac{\mu_{3b}}{r_{3b}}\sum_{l=2}^{\infty}\left(\frac{r}{r_{3b}}\right)^l P_l[\cos S],\end{aligned} \tag{3.28}$$

where the term related to $P_0[\cos S]$ does not depend on r and therefore was eliminated. In fact, the potential $\mathcal{R}$ enters in the equation of motion through the gradient with respect to the position coordinates (see Lagrange Equations in Equation (2.8)).

At this point, the ratio between the inner orbit semi-major axis and the distance of the third body is set equal to the parameter δ (Kaufman, [8]; Colombo, [48]):

$$\delta = \frac{a}{r_{3b}}, \tag{3.29}$$

and the final expression of the disturbing potential is:

$$\begin{aligned}\mathcal{R} =& \frac{\mu_{3b}}{r_{3b}} \sum_{l=2}^{\infty} \left(\frac{a}{r_{3b}}\right)^l \left(\frac{r}{a}\right)^l P_l[\cos S] \\ =& \frac{\mu_{3b}}{r_{3b}} \sum_{l=2}^{\infty} \delta^l \left(\frac{r}{a}\right)^l P_l[\cos S].\end{aligned} \tag{3.30}$$

Note that, from Lidov, [5], the approximation of the third body potential with Legendre polynomials can be truncated to the second order term (i.e. $l = 2$) only under certain conditions. In particular, he considered orbits with semimajor axis in the order of 30-40 $\times 10^3$ km and the Moon as the perturbing body. The results from the polynomial approximation were accurate if the ratio δ remain relatively small, and he defined the maximum threshold to have the correct approximation as:

$$\delta \sim 10^{-2} \tag{3.31}$$

Hence, for the Earth-Moon system, considering the HEO class of orbits, with semi-major axis in the order of 40-80 $\times 10^3$ km, the δ parameter is slightly higher, $\sim 10^{-1}$. For this reason, to provide a better approximation of the real trajectory, terms up to the fourth order were retained in the polynomial expansion. This requirement is compliant with the assumptions made in Section 3.4: the Moon semi-major axis is 0.3844×10^6 km and the Sun distance is 1 AU $\sim 1.496 \times 10^8$ km. Both are at least one order of magnitude higher than the satellite semi-major axis, even if the critical case is for the lunar attraction.

Therefore, in this work the potential is expanded up to the fourth order as following, as suggested in Colombo et al., [24]:

$$\mathcal{R} = \frac{\mu_{3b}}{r_{3b}} \sum_{l=2}^{4} \delta^l F_l(\cos S, e, f), \tag{3.32}$$

where second, third and fourth order terms from the polynomial expansion are

$$F_2 = \left(\frac{r}{a}\right)^2 P_2[\cos S] = \frac{1}{2}\left(\frac{r}{a}\right)^2 \left(3\cos^2 S - 1\right) \tag{3.33}$$

$$F_3 = \left(\frac{r}{a}\right)^3 P_3[\cos S] = \frac{1}{2}\left(\frac{r}{a}\right)^3 \left(5\cos^3 S - 3\cos S\right) \tag{3.34}$$

$$F_4 = \left(\frac{r}{a}\right)^4 P_4[\cos S] = \frac{1}{8}\left(\frac{r}{a}\right)^4 \left(35\cos^4 S - 30\cos^2 S + 3\right) \tag{3.35}$$

Yielding to the final expression of the disturbing function due to a third body:

$$\begin{aligned}\mathcal{R} = \frac{\mu_{3b}}{r_{3b}}\Big(\frac{1}{2}\delta^2\left(\frac{r}{a}\right)^2\left(3\cos^2 S - 1\right) + \frac{1}{2}\delta^3\left(\frac{r}{a}\right)^3\left(5\cos^3 S - 3\cos S\right) + \\ \frac{1}{8}\delta^4\left(\frac{r}{a}\right)^4\left(35\cos^4 S - 30\cos^2 S + 3\right)\Big)\end{aligned} \tag{3.36}$$

The $\cos S$ term was defined in Equation (3.21), in terms of satellite and a perturbing body position vector. To continue the derivation, it is necessary to express it in terms of orbital elements. The spacecraft position vector is expressed in the perifocal frame (see Section 2.3):

$$\mathbf{r} = r\,\cos f\,\hat{\mathbf{P}} + \sin f\,\hat{\mathbf{Q}}. \tag{3.37}$$

Since only the unit vector enters in the $\cos S$ relation, the expression is recovered by dividing the position vector by its magnitude:

$$\mathbf{r}^0 = \hat{\mathbf{P}}\cos f + \hat{\mathbf{Q}}\sin f, \tag{3.38}$$

with $\hat{\mathbf{P}}$ and $\hat{\mathbf{Q}}$ are respectively the unit vector in the eccentricity vector direction and the one orthogonal to the previous one in the orbital plane. They can be expressed following the approach of Kaufman, [8]), through a series of rotation described by matrix multiplication:

$$\hat{\mathbf{P}} = R_3(\Omega)R_1(i)R_3(\omega)\hat{I} \qquad \hat{\mathbf{Q}} = R_3(\Omega)R_1(i)R_3\left(\omega + \frac{\pi}{2}\right)\hat{I}, \tag{3.39}$$

where $\hat{I}$ is the unit vector in direction of γ point. The rotation matrices are 3D rotation matrices for rotating counter-clockwise a vector about the origin, here reported for a generic angle θ:

$$\begin{aligned}R_3(\theta) &= \begin{pmatrix}\cos(\theta) & -\sin(\theta) & 0\\ \sin(\theta) & \cos(\theta) & 0\\ 0 & 0 & 1\end{pmatrix}\\ R_1(\theta) &= \begin{pmatrix}1 & 0 & 0\\ 0 & \cos(\theta) & -\sin(\theta)\\ 0 & \sin(\theta) & \cos(\theta)\end{pmatrix}.\end{aligned} \tag{3.40}$$

Starting from the Equation (3.38) and considering the unit vector in the direction of the third body as $\hat{\mathbf{r}}_{\mathbf{3b}}$, the $\cos S$ term, in the disturbing function Equation (3.36), can be written

as an explicit relation of the true anomaly of the satellite:

$$\begin{aligned}\cos S =& \hat{\mathbf{r}} \cdot \hat{\mathbf{r}}_{\mathbf{3b}} = \left(\hat{\mathbf{P}} \cos f + \hat{\mathbf{Q}} \sin f\right) \cdot \hat{\mathbf{r}}_{\mathbf{3b}} \\ =& \left(\hat{\mathbf{P}} \cdot \hat{\mathbf{r}}_{\mathbf{3b}}\right) \cos f + \left(\hat{\mathbf{Q}} \cdot \hat{\mathbf{r}}_{\mathbf{3b}}\right) \sin f \\ =& A_{3b} \cos f + B_{3b} \sin f.\end{aligned} \tag{3.41}$$

Reducing the generic expression of the third body potential to a function of A, B, f and e only, as in Colombo et al. [24]:

$$\mathcal{R} = \frac{\mu_{3b}}{r_{3b}} \sum_{l=2}^{4} \delta^l F_l(A_{3b}, B_{3b}, e, f). \tag{3.42}$$

3.5 Third body secular effect via double averaging technique

The secular effect of the third body on a satellite is studied in this section by averaging out the short-term effects. This approach consists of a double analytical averaging of the disturbing function. The first averaging is done over the satellite orbital period, and to do so, the disturbing function is written in terms of the eccentric anomaly and the other orbital elements of the space vehicle (see Appendix A).

$$\bar{\mathcal{R}} = \frac{1}{2\pi} \int_0^{2\pi} \mathcal{R} dM = \frac{1}{2\pi} \int_0^{2\pi} \mathcal{R} \left(1 - e \cos E\right) dE \tag{3.43}$$

The second averaging is done over the third body orbital period. In this case the averaging is done re-conducing the terms to the true anomaly, in order not to have cos or sin terms in the denominator, yielding to an easier computation:

$$\bar{\bar{\mathcal{R}}} = \frac{1}{2\pi} \int_0^{2\pi} \bar{\mathcal{R}} dM_{3b} = \frac{1}{2\pi} \int_0^{2\pi} \bar{\mathcal{R}} \frac{(1 - e_{3b})^{3/2}}{(e_{3b} \cos f_{3b} + 1)^2} df_{3b} \tag{3.44}$$

Note that the procedure for the averaging is the same either for the Moon or the Sun case. In particular, the single averaged expression resulting from the procedure is exactly the same apart from A_{3b} and B_{3b} coefficients. On the other hand, the double averaging is reported for both cases, since A_{3b} and B_{3b} coefficients changes in each case. For the Sun, it is not necessary to switch to the true anomaly, since the potential is already a function of the sun longitude λ_{ecl} and therefore, of the Mean anomaly $M_\odot$. All the computations were done analytically with the Mathematica® software. The analytical expression of the double-averaged of the potential was cross-checked with literature results (Colombo, [25]).

3.5.1 Single-averaged third-body disturbing function

As just explained, the dissertation in this section is valid for both the Sun and the Moon effect. The procedure consists in cancelling out the contribution due to the variation of the true anomaly along the orbit. At this level in order to remove the short-term effect, a first averaging upon one satellite orbital period is performed. Therefore, it's better to express the Equation (3.36) by exploiting the orbital elements. For either the Sun and the Moon, the general expression of the potential can be expressed as follows, without loosing generality:

$$\mathcal{R}_{3b} = \frac{\mu_{3b}}{r_{3b}} \sum_{l=2}^{4} \delta_{3b}^{l} \, F_l(A_{3b}, B_{3b}, r, f, e) \tag{3.45}$$

The terms to be averaged are r and f, since they are the only terms in Equation (3.45) that vary over the orbital period. A fundamental assumption is considered: the orbital parameters of the satellite are constant over one revolution. This means that after this averaging, the orbital elements of the satellites are no more the osculating one, but they are average orbital elements. They can describe only the long-term variation and cannot predict any oscillation that could occur over one orbit revolution.

To perform the integration, both r and f, as well as the mean anomaly M are expressed in terms of the eccentric anomaly E to have a simple term to integrate, just as the procedure followed for the Zonal Harmonic disturbing function. The relations used are reported in Appendix A, so that the averaging results:

$$\bar{\mathcal{R}}_{3b} = \frac{1}{2\pi} \int_0^{2\pi} \mathcal{R}_{3b}(E) \, (1 - e \cos E) dE \tag{3.46}$$

The integral was computed analytically, by solving different order terms one per time. For each F_i $(i = 2 : 4)$ function the computations are reported. The dissertation starts with the second order term (F_2), then passes to the third order term (F_3) and finally, the fourth order (F_4) is computed.

Second order term The second order term is obtained considering the coefficient $l = 2$ in the Equation (3.45):

$$\mathcal{R}_{3b,2} = \frac{\mu_{3b}}{r_{3b}} \delta_{3b}^{2} \, F_2(A_{3b}, B_{3b}, e, f) \tag{3.47}$$

Where the term $F_2(A_{3b}, B_{3b}, e, f)$ is:

$$F_2 = \frac{1}{2} \left(\frac{r}{a} \right)^2 \left(3 \cos^2 S - 1 \right) \tag{3.48}$$

The potential is now expressed using the trigonometric relations of sine and cosine and introducing the Equation (3.72) of $\cos S$.

$$\begin{aligned}\mathcal{R}_{3b,2} =& \frac{\mu_{3b}}{r_{3b}}\left(\frac{1}{2}\delta_{3b}^2\left(\frac{r}{a}\right)^2\left(3\cos^2 S - 1\right)\right) \qquad \text{with} \qquad \cos S = A_{3b}\cos f + B_{3b}\sin f \\ =& \frac{1}{4}\frac{\mu_{3b}}{r_{3b}}\delta^2\left(\frac{r}{a}\right)^2\left(3\left(A_{3b}^2 - B_{3b}^2\right)\cos 2f + 6A_{3b}B_{3b}\sin 2f + 3(A_{3b}^2 + B_{3b}^2) - 2\right)\end{aligned} \tag{3.49}$$

In this expression three terms can be identified to be averaged. The integration is performed once the true anomaly f and the radius r are substituted in terms of the eccentric anomaly E, as well as the mean anomaly M (see Appendix A):

$$\frac{1}{2\pi}\int_0^{2\pi} r^2(E)\, dM = \frac{1}{2}\left(3\mathrm{e}^2 + 2\right) \tag{3.50}$$

$$\frac{1}{2\pi}\int_0^{2\pi} r^2(E)\cos\left(2f(E)\right)\, dM = \frac{5\mathrm{e}^2}{2} \tag{3.51}$$

$$\frac{1}{2\pi}\int_0^{2\pi} r^2(E)\sin\left(2f(E)\right)\, dM = 0 \tag{3.52}$$

By substituting these relations in the second order term of Equation (3.49), the first average disturbing function for the second order becomes:

$$\bar{\mathcal{R}}_{3b,2} = \frac{\mu_{3b}}{4r_{3b}}\delta^2\left(3A_{3b}^2\left(4e^2 + 1\right) - 3B_{3b}^2\left(e^2 - 1\right) - 3e^2 - 2\right) \tag{3.53}$$

Third order term The third order term is obtained with coefficient $l = 3$.

$$\mathcal{R}_{3b,3} = \frac{\mu_{3b}}{r_{3b}}\delta^3\, F_3(A_{3b}, B_{3b}, e, f) \tag{3.54}$$

As before the Equation (3.72) is introduced, considering the same relation for the $\cos S$ term as in the second order case:

$$\begin{aligned}\mathcal{R}_{3b,3} =& \frac{\mu_{3b}}{r_{3b}}\left(\frac{1}{2}\delta^3\left(\frac{r}{a}\right)^3\left(5\cos^3 S - 3\cos S\right)\right) \\ =& \frac{\mu_{3b}}{8r_{3b}}\delta^3\frac{r^3}{a^3}\Big(3A_{3b}(5A_{3b}^2 + 5B_{3b}^2 - 4)\cos f - 2B_{3b}\sin f\big(5(B_{3b}^2 - 3A_{3b}^2)\cos 2f \\ & - 15A_{3b}^2 - 5B^2 + 6) + 5A_{3b}(A_{3b}^2 - 3B_{3b}^2)(\cos f\cos 2f - \sin f\sin 2f)\Big)\end{aligned} \tag{3.55}$$

Also in this case the integration is done by substituting the true anomaly with the eccentric one: $f \to E$. Different terms to be integrated can be identified by re-arranging the expression, which depends on the true anomaly and on the radius r. Then the integration

is performed for each term:

$$\frac{1}{2\pi}\int_0^{2\pi} r^3(E)\ (\cos f(E)+\sin f(E))\ dM = -\frac{5}{8}\,A_{3b}\,a^3\,e\,(4+3\,e^2) \tag{3.56}$$

$$\frac{1}{2\pi}\int_0^{2\pi} r^3(E)\ (\cos f(E)+\sin f(E))\cos 2f(E)\,dM = -\frac{5}{8}\,A_{3b}\,a^3\,e\,(2+5\,e^2) \tag{3.57}$$

$$\frac{1}{2\pi}\int_0^{2\pi} r^3(E)\ (\cos f(E)+\sin f(E))\sin 2f(E)\,dM = \frac{5}{4}\,B_{3b}\,a^3\,e\,(-1+\ e^2) \tag{3.58}$$

And performing the integration, the third order term single averaged is:

$$\bar{\mathcal{R}}_{3b,3} = \frac{5\mu_{3b}}{16 r_{3b}}\delta^3 A_{3b} e\left(-5A_{3b}^2\left(4e^2+3\right)+15B_{3b}^2\left(e^2-1\right)+9e^2+12\right) \tag{3.59}$$

Fourth order term The fourth order term is obtained with coefficient $l = 4$.

$$\mathcal{R}_{3b,4} = \frac{\mu_{3b}}{r_{3b}}\delta^4\,F_4(A_{3b}, B_{3b}, e, f) \tag{3.60}$$

As before the Equation (3.72) is introduced:

$$\begin{aligned}
\mathcal{R}_{3b,4} =& \frac{\mu_{3b}}{r_{3b}}\left(\frac{1}{8}\delta^4\left(\frac{r}{a}\right)^4\left(35\cos^4 S - 30\cos^2 S + 3\right)\right)\\
=& \frac{\mu_{3b}}{64 r_{3b}}\delta^4\left(\frac{r}{a}\right)^4\Big(105A_{3b}^4 + 280A_{3b}^3 B\sin 2f + 280A_{3b}^3 B_{3b}\sin 2f\cos 2f\\
&- 120A_{3b}^2 + 210A_{3b}^2 B_{3b}^2 + 280A_{3b}B_{3b}^3\sin 2f - 280A_{3b}B_{3b}^3\sin 2f\cos 2f\\
&+ 35\left(A_{3b}^4 - 6A_{3b}^2 B_{3b}^2 + B_{3b}^4\right)\left(2\cos^2 2f - 1\right) + 105B_{3b}^4 - 120B_{3b}^2\\
&+ 20\left(7A_{3b}^4 - 6A_{3b}^2 - 7B_{3b}^4 + 6B_{3b}^2\right)\cos 2f - 240A_{3b}B_{3b}\sin 2f + 24\Big)
\end{aligned} \tag{3.61}$$

Five different terms can be identified to be integrated:

$$\frac{1}{2\pi}\int_0^{2\pi} r^4\,dM = \frac{1}{8}\,a^4\,\left(8+40\,e^2+15\,e^4\right) \tag{3.62}$$

$$\frac{1}{2\pi}\int_0^{2\pi} r^4\,\cos 2f\sin 2f\,dM = \frac{1}{2\pi}\int_0^{2\pi} r^4\,\sin 2f\,dM = 0 \tag{3.63}$$

$$\frac{1}{2\pi}\int_0^{2\pi} r^4\,\left(2\cos^2 2f - 1\right)\,dM = \frac{63}{8}\,a^4\,e^4 \tag{3.64}$$

$$\frac{1}{2\pi}\int_0^{2\pi} r^4\,\cos 2f\,dM = \frac{21}{8}\,a^4\,e^2(2+e^2) \tag{3.65}$$

The fourth order single averaged after the integrals have been substituted in the initial

expression, becomes:

$$\begin{aligned}\bar{\mathcal{R}}_{3b,4} =&\frac{3\mu_{3b}}{64r_{3b}}\delta^4\Big(35A_{3b}^4\left(8e^4+12e^2+1\right)-10A_{3b}^2(7B_{3b}^2\left(6e^4-5e^2-1\right)+18e^4+\\&+41e^2+4)+35B_{3b}^4\left(e^2-1\right)^2+10B_{3b}^2\left(3e^4+e^2-4\right)+15e^4+40e^2+8\Big)\end{aligned} \tag{3.66}$$

Single-averaged third body disturbing function The single averaged third body disturbing function is recovered from the previous expressions: Equation (3.53), (3.59) and (3.66). It does not depend any more on the satellite position along the orbit: f.

$$\begin{aligned}\bar{\mathcal{R}} =&\frac{\mu_{3b}}{4r_{3b}}\delta^2\left(3A_{3b}^2\left(4e^2+1\right)-3B_{3b}^2\left(e^2-1\right)-3e^2-2\right)+\\&+\frac{5\mu_{3b}}{16r_{3b}}\delta^3A_{3b}e\left(-5A_{3b}^2\left(4e^2+3\right)+15B_{3b}^2\left(e^2-1\right)+9e^2+12\right)+\\&+\frac{3\mu_{3b}}{64r_{3b}}\delta^4\Big(35A_{3b}^4\left(8e^4+12e^2+1\right)-10A_{3b}^2\Big(7B_{3b}^2\left(6e^4-5e^2-1\right)+18e^4+\\&+41e^2+4\Big)+35B_{3b}^4\left(e^2-1\right)^2+10B_{3b}^2\left(3e^4+e^2-4\right)+15e^4+40e^2+8\Big)\end{aligned} \tag{3.67}$$

This expression has the advantage of cancelling out the short-term variation in the orbital elements, and from now on, the Keplerian parameters are free from short period oscillation: they are the average Keplerian parameters. The disturbing function depends on the parameters A_{3b} and B_{3b} as well as on the third body position vector r_{3b}. Moreover, these contributions contain yet the variations caused by the motion of the third body on its orbit. For the Moon the orbital period is 27.3 d, for the Sun it is of 365.2 d, finally, if a different system is considered, for example, the Sun-Venus one, the orbital period of the Sun is 224.7 d.

Recalling the expression for $\delta = \frac{a}{r_{3b}}$, the contribution due to the third body attraction is proportional to

$$\frac{\mu_{3b}}{r_{3b}^l} \qquad \text{with} \qquad l = \text{order of approximation} \tag{3.68}$$

This consideration is very important, since, as the third body is far from the main attractor, the perturbation is smaller. In the Earth-Moon-Sun system this yield to have a bigger effect due to the Moon attraction than for the Sun. The distance in this case ($r_\odot$ =149.6 $\times 10^6$ km, $r_\leftmoon = 0.3844 \times 10^6$ km) is dominant with respect to the mass of the two body ($M_\odot$ =1 988 500 $\times 10^{24}$ kg, $M_\leftmoon$ =0.073 $\times 10^{24}$ kg)[1].

[1]Data retrieved from NASA Planetary Fact Sheet: `https://nssdc.gsfc.nasa.gov/planetary/planetfact.html`

3.5.2 Double averaged disturbing function

The double averaged technique consists now in averaging another time, this time over the period of the perturbing body. During the averaging, the orbital elements of the perturbing body are considered constant. The parameters that vary during the procedure are r_{3b} and both A_{3b} and B_{3b} terms. The analytical expression of these two terms is dependent on the third body considered. For both the Sun and the Moon is done in the following sections. Hence, the final results are dependent on the perturbing body. This section separates the derivation of the double averaged potential for the Moon and the Sun.

3.5.3 Moon Disturbing Function

The Moon acts as a disturbing body to all Earth orbits, and in particular its effect is predominant for HEOs. The perturbation depends on the position of the Moon in the Equatorial frame and its orbit can be described by Keplerian parameters:

$$\{a_{\leftmoon} \, , \, e_{\leftmoon} \, , \, i_{\leftmoon} \, , \, \omega_{\leftmoon} \, , \, \Omega_{\leftmoon} \, , \, M_{\leftmoon} \, \} \tag{3.69}$$

The Moon position vector $\mathbf{r}_{\leftmoon}$ shall be expressed in the equatorial frame with the Moon orbital elements through a coordinate transformation (see Figure 3.5b). This transformation consists of a series of rotation around the axis of the equatorial tern. At first, $\mathbf{r}_{\leftmoon}$ is rotated about the z axis (R_3) in the north pole direction counter-clockwise of the angle $\Omega_{\leftmoon}$, then, a rotation around the γ point direction (R_1) is done to align with the perturbing body plane and finally, a rotation about the angular momentum of the orbit (R_3) is done to align with the actual position of the Moon, using the argument of latitude.

The overall rotation can be written in terms of successive rotations about the $\hat{K}$, $\hat{I}$, and finally again $\hat{K}$ axes using the matrix multiplication, as shown below:

$$\mathbf{r}_{\leftmoon} \; = r_{\leftmoon} \, R_3 \, (\Omega_{\leftmoon} \,) \, R_1 \, (i_{\leftmoon} \,) \, R_3 \, (u_{\leftmoon} \,) \, \hat{I} \tag{3.70}$$

$$\hat{\mathbf{r}}_{\leftmoon} \; = R_3 \, (\Omega_{\leftmoon} \,) \, R_1 \, (i_{\leftmoon} \,) \, R_3 \, (u_{\leftmoon} \,) \, \hat{I} \tag{3.71}$$

Where $r_{\leftmoon}$ is the distance magnitude and $u_{\leftmoon} \; = \omega_{\leftmoon} \; + f_{\leftmoon}$ is the argument of latitude. At this point, substituting Equation (3.70) and (3.38) in Equation (3.21), the relation becomes:

$$\cos S = (\hat{\mathbf{P}} \cdot \hat{\mathbf{r}}_{\leftmoon} \,) \cos f + (\hat{\mathbf{Q}} \cdot \hat{\mathbf{r}}_{\leftmoon} \,) \sin f = A_{\leftmoon} \; \cos f + B_{\leftmoon} \; \sin f, \tag{3.72}$$

where the complete expression of $A_{\leftmoon}$ and $B_{\leftmoon}$ is reported in Appendix C.

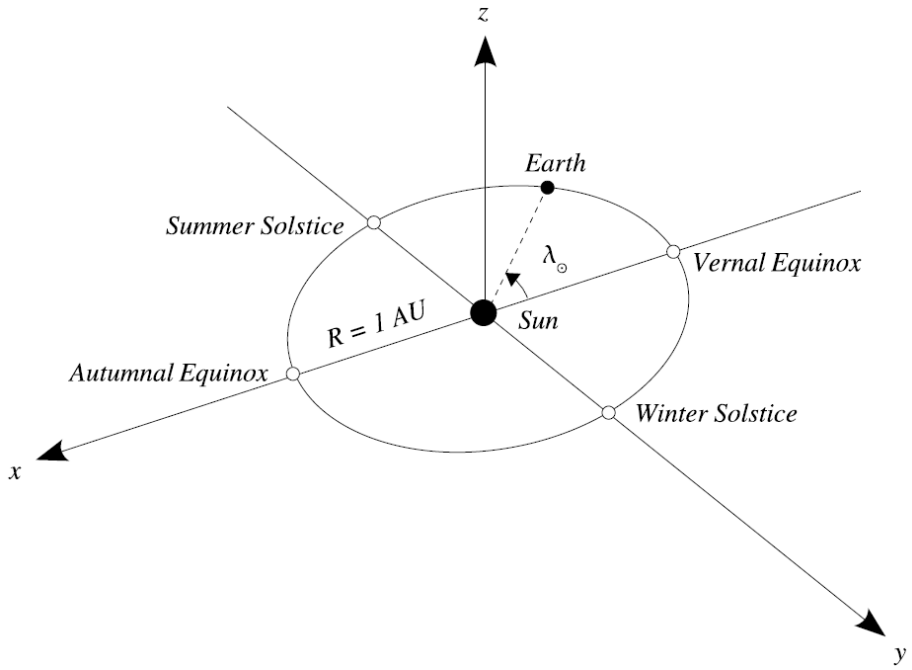

(a) Sun position vector in the ecliptic frame (Alenazi and Gondolo, [49]).

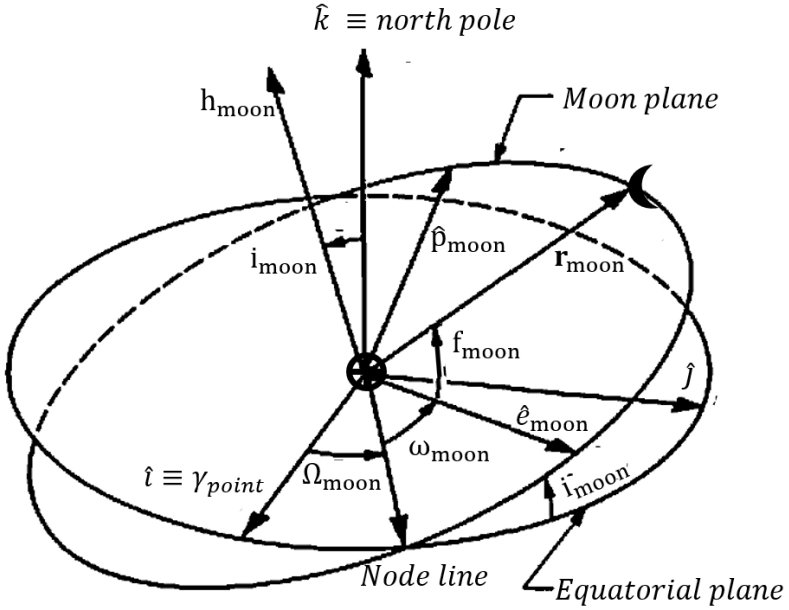

(b) Moon position vector in the Eaquatorial frame (Battin, [50]).

Figure 3.5 Third body position geometry.

The Moon disturbing function, with $\delta_{\leftmoon} = \frac{a}{r_{\leftmoon}}$, is a function of the moon position, true anomaly and orbit eccentricity. In particular, recovering the compact description in Equation (3.32), it can be written as:

$$\mathcal{R}_{\leftmoon} = \frac{\mu_{\leftmoon}}{r_{\leftmoon}} \sum_{l=2}^{4} \delta_{\leftmoon}^{l} \; F_l(A_{\leftmoon}, B_{\leftmoon}, f, e) \tag{3.73}$$

This representation is valid for any Planet-Moon system, not only for the Earth-Moon case. When a different double system is considered, the orbital elements and the gravitational parameters should be changed accordingly.

3.5.4 Sun disturbing Function

The Sun has an effect like the lunar influence. Its perturbation depends on the Sun distance and on the Sun position vector. The latter is expressed in the equatorial frame thanks to the ecliptic longitude of the Sun λ_{ecl} and the planet's obliquity of the ecliptic ϵ. In case of Earth-Sun system, the position of the Sun is described as reported in (Vallado, [39]). The Sun position vector in the ecliptic frame is shown in Figure 3.5a. The passage to the equatorial frame requires a rotation around the z-axis of the obliquity angle ϵ. In the figure, the system under study is the Sun-Earth, but the representation is valid for any other planet of the solar system.

Here the case of Earth-Sun is studied, but the procedure followed is general and can be used for any other system, such as Venus-Sun system, or Sun-Jupiter-Europa system (in this case Europa is considered the central planet). The Sun position vector is computed remembering that the ecliptic latitude of the Sun is zero:

$$\mathbf{r}_{\odot} = r_{\odot} \cos\lambda_{ecl} \hat{I} + r_{\odot} \cos\epsilon \sin\lambda_{ecl} \hat{J} + r_{\odot} \sin\epsilon \sin\lambda_{ecl} \hat{K} \qquad (AU) \tag{3.74}$$

Where the longitude and equator inclination on the ecliptic for the Earth are:

$$r_{\odot} = 1.000140612 - 0.016708 \cos M_{\odot} - 0.000139589 \cos(2M_{\odot}) \qquad (AU) \tag{3.75}$$

$$\lambda_{ecl} = \lambda_{mean,\odot} + 1.914\,666^{\circ} \sin M_{\odot} + 0.019\,994^{\circ} \sin(2M_{\odot}) \tag{3.76}$$

$$\epsilon = 23.439^{\circ} \tag{3.77}$$

Moreover, a first preliminary approximation could be to consider the Sun apparently orbiting on a circular orbit and, therefore, considering $r_{\odot}$ simply constant in time. This is a good approximation for planets of the solar system where the eccentricity of the orbit is

quite small. This is valid for Earth with an orbit eccentricity of 0.017. It is even a more accurate approximation when the Venus-Sun system is under study: the eccentricity of Venus orbit is 0.007.

Now, the $\cos S$ term is computed using the representation in Equation (3.74) for the Sun position vector. As in the case of the Moon disturbance, it depends on the unit vector: the satellite position unit vector is the same of Equation (3.38), while $\mathbf{r}^0_\odot = \mathbf{r}_\odot / r_\odot$. Hence, the $\cos S$ term is recovered as:

$$\cos S = \left(\hat{P} \cdot \mathbf{r}^0_\odot\right) \cos f + \left(\hat{Q} \cdot \mathbf{r}^0_\odot\right) \sin f = A_\odot \cos f + B_\odot \sin f \tag{3.78}$$

Where the complete expression of the coefficient $A_\odot$ and $A_\odot$ is reported in Appendix D. So that the Sun disturbing function, with $\delta_\odot = \frac{a}{r_\odot}$ is:

$$\mathcal{R}_\odot = \frac{\mu_\odot}{r_\odot} \sum_{l=2}^{4} \delta_\odot^l \, F_l(A_\odot, B_\odot, f, e) \tag{3.79}$$

For the Earth-Sun system, the mean anomaly $M_\odot$ and the mean longitude $\lambda_{mean,\odot}$ of the Sun depends on time, and in particular on T_{UTI} the number of Julian Centuries from 01/01/2000 (JD2000) (Vallado, [39]).

$$\lambda_{mean,\odot} = 280.460^\circ + 36000.770\, T_{UTI} \tag{3.80}$$

$$M_\odot = 357.527^\circ + 35999.050\, T_{UTI} \tag{3.81}$$

In particular those values shall be reduced to a value in $(0^\circ - 360^\circ)$.

3.5.5 Moon double averaged potential

The Moon double-averaged potential is recovered by substituting the $A_{\leftmoon}$ and $B_{\leftmoon}$ expressions in the single averaged one in Equation (3.67). Then, all the terms depending on the Moon's true anomaly $f_{\leftmoon}$ are collected and the integration is done for separately for different order terms: $\bar{\mathcal{R}}_{\leftmoon,2}$, $\bar{\mathcal{R}}_{\leftmoon,3}$, $\bar{\mathcal{R}}_{\leftmoon,4}$. To reduce the computational time, the integration is done separately only for the terms that depend on the true anomaly, and only then the overall expression is computed by substituting the results of integration.

Since the position of the third body appears in the denominator in Equation (3.67), it complicates the expressions to be averaged. A first simple approach is to consider the Moon orbiting on a circular orbit, as it was done in several studies (see Colombo, [25]). A more accurate model can then be developed by considering the actual orbit of the perturbing

body introducing also the eccentricity of the orbit.

Since the substitution of $A_{\leftmoon}$ and $B_{\leftmoon}$ in the single average expression leads to a very long term, the integrals are computed for each term separately.

Circular case of the Moon orbit

The first simplified approach considers the Moon orbiting on a circular orbit, but retains the inclination respect to the equatorial plane. In that case, the integration over the mean anomaly is equivalent to the integration over the true anomaly, since $e_{\leftmoon} = 0$:

$$f_{\leftmoon} = E_{\leftmoon} = M_{\leftmoon} \qquad \rightarrow \int \bar{\mathcal{R}}_{\leftmoon}\, dM_{\leftmoon} = \int \bar{\mathcal{R}}_{\leftmoon}\, df_{\leftmoon} \tag{3.82}$$

The double averaged expression then reads (Colombo, [25]):

$$\begin{aligned}
\bar{\bar{\mathcal{R}}}_{\leftmoon,2} = &\frac{\mu_{\leftmoon}\, a^2}{128\, a_{\leftmoon}^3}\Big[\cos 2i_{\leftmoon}\, \Big(6 + 9\,e^2 + 90\,e^2\cos 2\omega \sin^2 i\Big) + \\
&+ (2 + 3\,e^2 + 15\,e^2\cos 2\omega)(1 + 6\cos\delta\Omega \sin^2 i_{\leftmoon}) + \\
&+ 3\cos 2i_{\leftmoon}\, \Big((6 + 9\,e^2)\cos 2i_{\leftmoon} + \\
&+ (-2 - 3\,e^2 + 5\,e^2\cos 2\omega)(-1 + 2\cos\Delta\Omega \sin^2 i_{\leftmoon})\Big) + \\
&+ 12\,\Big(2 + 3\,e^2 - 5\,e^2\cos 2\omega\Big)\cos 2\delta\Omega \sin 2i \sin 2i_{\leftmoon} + \\
&+ 120\,e^2 \sin i \sin 2i_{\leftmoon}\, \sin\Delta\Omega + \\
&- 120 e^2 \cos i \sin^2 i_{\leftmoon}\, \sin 2\omega \sin 2\Delta\Omega\Big],
\end{aligned} \tag{3.83}$$

$$\bar{\bar{\mathcal{R}}}_{\leftmoon,3} = 0, \tag{3.84}$$

$$\begin{aligned}
\bar{\bar{\mathcal{R}}}_{\leftmoon,4} = &\frac{\mu_{\leftmoon}\, a^4}{65536\, a_{\leftmoon}^5}\Big[1680(15e^4 + 28\,\Big(e^2 + 2\Big)\, e^2\cos 2\omega + 40e^2 + 8 + \\
&+ \text{... long expression...}\Big].
\end{aligned} \tag{3.85}$$

Note that the third order term is null in this approximation, and this is due to the circular approximation of the orbit. In fact, in the following case, where the actual geometry of the orbit is retained, it would not be null any more. The full expression of the potential is simply the sum of each contribution: $\bar{\bar{\mathcal{R}}}_{3b} = \bar{\bar{\mathcal{R}}}_{3b,2} + \bar{\bar{\mathcal{R}}}_{3b,3} + \bar{\bar{\mathcal{R}}}_{3b,4}$.
The results obtained in this section are the same of the ones reported in Colombo, [25]. The full expression is reported in Appendix C.2. These results are very important since it verifies the results obtained in the integration, proving that the integration over the mean

anomaly is correctly performed. For this reason, this approach is used also for the elliptical case, since it works correctly.

Elliptical case of the Moon orbit

The second case considered and entirely developed in this work drops the circular orbit assumption: the Moon orbits on its actual elliptical orbit. In this case, the true anomaly does not vary along a circle any more, and this is the reason why the integration is done over the mean anomaly. Both circular and elliptical case, the mean anomaly is a linear function of time: $M = n(t - t_0)$. As for the case of the single averaging over the satellite f, the Moon true anomaly is averaged out through the mean anomaly of the third body $M_{\leftmoon}$, by using the expressions in Appendix A.

For each order term of the single average expression, the integrals are computed not on the whole equation, but on every single term that depends on $f_{\leftmoon}$. In this way, the substitution with the eccentric anomaly leads to short integrals easily solvable. Now the computation for each order term is reported in detail. Note that all the expressions are obtained by substituting $A_{\leftmoon}$ and $B_{\leftmoon}$ in the single average expression.

$\bar{\bar{\mathcal{R}}}_{moon,2}$ **term** The first term considered is the second order term. It is obtained from the single average expression, considering only the terms dependent on δ^2. Hence, at first δ is replaced by its expression: $a/r_{\leftmoon}$. Then the expression in Appendix C for $A_{\leftmoon}$ and $B_{\leftmoon}$ are replaced in the single-averaged expression. This procedure yields to a very long and complex expression (reported completely in Appendix C.3), where terms related to the true anomaly can be identified and collected together:

$$\begin{aligned}\bar{\mathcal{R}}_{moon,2} = &- \frac{\mu_{\leftmoon}\, a^2(2+3\,e^2)}{4\,r_{\leftmoon}^3} + \\ &+ \frac{3\,\mu_{\leftmoon}\, a^2 \sin^2 f_{\leftmoon}}{8\,r_{\leftmoon}^3}(...\text{term1}...) + \\ &+ \frac{3\,\mu_{\leftmoon}\, a^2 \cos^2 f_{\leftmoon}}{4\,r_{\leftmoon}^3}(...\text{term2}...) + \\ &- \frac{3\,\mu_{\leftmoon}\, a^2 \cos f_{\leftmoon}\, \sin f_{\leftmoon}}{8\,r_{\leftmoon}^3}(...\text{term3}...)\end{aligned} \tag{3.86}$$

Hence, four integrals can be identified: they depends only on the trigonometric functions of the true anomaly ($\cos f_{\leftmoon}$ and $\sin f_{\leftmoon}$) and on the Moon position vector ($r_{\leftmoon}$). The integration is done by reducing the terms at the second power ($\sin^2$ or $\cos^2$) to simple terms using trigonometric relations: $\cos^2 f_{\leftmoon} = (\cos 2f_{\leftmoon} + 1)/2$ and $\sin^2 f_{\leftmoon} = (1 - \cos 2f_{\leftmoon})/2$.

Then the substitution in terms of the true anomaly is performed: $dM = (1-e)^{3/2}/(e\cos f + 1)^2$, to make the integrals simpler. The solution to the four integrals is:

$$\frac{1}{2\pi}\int_0^{2\pi}\frac{1}{r_{\leftmoon}^3}dM_{\leftmoon} = \frac{1}{a_{\leftmoon}^3\,(1-e_{\leftmoon}^2\,)^{3/2}} \tag{3.87}$$

$$\frac{1}{2\pi}\int_0^{2\pi}\frac{\cos^2 f_{\leftmoon}}{r_{\leftmoon}^3}dM_{\leftmoon} = \frac{1}{2\,a_{\leftmoon}^3\,(1-e_{\leftmoon}^2\,)^{3/2}} \tag{3.88}$$

$$\frac{1}{2\pi}\int_0^{2\pi}\frac{\sin^2 f_{\leftmoon}}{r_{\leftmoon}^3}dM_{\leftmoon} = \frac{1}{2\,a_{\leftmoon}^3\,(1-e_{\leftmoon}^2\,)^{3/2}} \tag{3.89}$$

$$\frac{1}{2\pi}\int_0^{2\pi}\frac{\cos f_{\leftmoon}\,\sin f_{\leftmoon}}{r_{\leftmoon}^3}dM_{\leftmoon} = 0 \tag{3.90}$$

$$\tag{3.91}$$

At this point these expressions are placed in the single average expression, yielding to the final double averaged potential:

$$\begin{aligned}\bar{\bar{\mathcal{R}}}_{moon,2} =& \frac{\mu_{\leftmoon}}{32\,a_{\leftmoon}^3\,(1-e_{\leftmoon}^2\,)^{3/2}}\Big(30\,e^2\cos\,2\omega\cos^2\Delta\Omega + \\ &+(2+3\,e^2)(-5+3\cos 2\Delta\Omega)+ \\ &6(2+3\,e^2+5e^2\cos 2\omega)\sin^2\Delta\Omega\cos^2 i_{\leftmoon}\,+ \\ &-6(-2-3\,e^2+5e^2\cos 2\omega)\cos^2 i(\sin^2\Delta\Omega+\cos^2\Delta\Omega\cos^2 i_{\leftmoon}\,)+ \\ &-60\,e^2\sin 2\omega\sin\Delta\Omega\cos i_{\leftmoon}\,\sin i\sin i_{\leftmoon}\,+ \\ &+6(2+3\,e^2-5\,e^2\cos 2\omega)\sin^2 i\sin^2 i_{\leftmoon}\,+ \\ &+6\cos i(-5\,e^2\sin 2\omega\sin 2\Delta\Omega(1-\cos^2 i_{\leftmoon}\,)+ \\ &+2(2+3\,e^2-5\,e^2\cos 2\omega)\cos\Delta\Omega\cos i_{\leftmoon}\,\sin i\cos i_{\leftmoon}\,)\Big)\end{aligned} \tag{3.92}$$

$\bar{\bar{\mathcal{R}}}_{moon,3}$ **term** Now the third order term is considered. It depends on the term δ^3. The same procedure as before is followed, by substituting δ, $A_{\leftmoon}$ and $B_{\leftmoon}$ with their expressions. This procedure leads to a very complex and long form, which can be re-arranged to collect all the part that directly depends on the true anomaly:

$$\begin{aligned}\bar{\mathcal{R}}_{moon,3} =& \frac{5\mu_{\leftmoon}\,a^3\,e\,\sin f_{\leftmoon}}{16\,r_{\leftmoon}^4}(...\text{term1}...) + \frac{5\mu_{\leftmoon}\,a^3\,e\,\sin^3 f_{\leftmoon}}{16\,r_{\leftmoon}^4}(...\text{term2}...) \\ &+\frac{5\mu_{\leftmoon}\,a^3\,e\,\sin f_{\leftmoon}\,\cos^2 f_{\leftmoon}}{16\,r_{\leftmoon}^4}(...\text{term3}...) + \frac{5\mu_{\leftmoon}\,a^3\,e\,\cos^3 f_{\leftmoon}}{16\,r_{\leftmoon}^4}(...\text{term4}...) \\ &+\frac{5\mu_{\leftmoon}\,a^3\,e\,\cos f_{\leftmoon}}{16\,r_{\leftmoon}^4}(...\text{term5}...) + \frac{5\mu_{\leftmoon}\,a^3\,e\,\cos f_{\leftmoon}\,\sin^2 f_{\leftmoon}}{16\,r_{\leftmoon}^4}(...\text{term6}...)\end{aligned} \tag{3.93}$$

Hence, six integrals can be identified: they depends on $r_{\leftmoon}$, $\cos f_{\leftmoon}$ and $\sin f_{\leftmoon}$ only as before. The integration is done by reducing power terms of cos and sin using the trigonometric relations (this procedure is adopted to reduce the computational time):

$$\frac{1}{2\pi}\int_0^{2\pi}\frac{\cos f_{\leftmoon}}{r_{\leftmoon}^4}dM_{\leftmoon} = \frac{e_{\leftmoon}}{a_{\leftmoon}^4\,(1-e_{\leftmoon}^2\,)^{5/2}} \tag{3.94}$$

$$\frac{1}{2\pi}\int_0^{2\pi}\frac{\sin f_{\leftmoon}}{r_{\leftmoon}^4}dM_{\leftmoon} = 0 \tag{3.95}$$

$$\frac{1}{2\pi}\int_0^{2\pi}\frac{\cos^3 f_{\leftmoon}}{r_{\leftmoon}^4}dM_{\leftmoon} = \frac{e_{\leftmoon}}{4\,a_{\leftmoon}^4\,(1-e_{\leftmoon}^2\,)^{5/2}} \tag{3.96}$$

$$\frac{1}{2\pi}\int_0^{2\pi}\frac{\sin^3 f_{\leftmoon}}{r_{\leftmoon}^4}dM_{\leftmoon} = 0 \tag{3.97}$$

$$\frac{1}{2\pi}\int_0^{2\pi}\frac{\sin f_{\leftmoon}\,\cos^2 f_{\leftmoon}}{r_{\leftmoon}^4}dM_{\leftmoon} = 0 \tag{3.98}$$

$$\frac{1}{2\pi}\int_0^{2\pi}\frac{\cos f_{\leftmoon}\,\sin^2 f_{\leftmoon}}{r_{\leftmoon}^4}dM_{\leftmoon} = \frac{e_{\leftmoon}}{4\,a_{\leftmoon}^4\,(1-e_{\leftmoon}^2\,)^{5/2}} \tag{3.99}$$

Yielding to the final expression of the double averaged potential:

$$\begin{aligned}\bar{\bar{\mathcal{R}}}_{moon,3} =& \frac{\mu_{\leftmoon}\,15a^3\,e\,e_{\leftmoon}}{512a_{\leftmoon}^4\,(1-e_{\leftmoon}^2\,)^{5/2}}\Big(\cos\omega\cos\omega_{\leftmoon}\,\cos(\Omega-\Omega_{\leftmoon}\,)\\
&(35e^2\cos(2(\Omega_{\leftmoon}\,-\omega-\Omega))+35e^2\cos(2(\Omega_{\leftmoon}\,+\omega-\Omega))+\\
&+10(e^2+6)\cos(2(\Omega_{\leftmoon}\,-\Omega))+70e^2\cos 2\omega-86e^2-68)+\\
&-20\sin^2 i\cos\omega(7e^2\cos 2\omega-5e^2-2)\sin^2 i_{\leftmoon}\\
&\cos\omega_{\leftmoon}\,\cos(\Omega-\Omega_{\leftmoon}\,)+\sin i\sin\omega\sin i_{\leftmoon}\,\sin\omega_{\leftmoon}\\
&(35e^2\cos(2(\Omega_{\leftmoon}\,-\omega-\Omega))+35e^2\cos(2(\Omega_{\leftmoon}\,+\omega-\Omega))+\\
&+10(5e^2+2)\cos(2(\Omega_{\leftmoon}\,-\Omega))+70e^2\cos 2\omega-46e^2-108)+\\
&-20\sin^3 i\sin\omega(7e^2\cos 2\omega-e^2-6)\sin^3 i_{\leftmoon}\,\sin\omega_{\leftmoon}+\\
&\text{...long expression...}\Big)\end{aligned} \tag{3.100}$$

Note that the complete results is reported in Appendix C.3. The Equation (3.100) is long, and differently from the circular case (as previously discussed and in previous works Colombo, [25]), this term is not zero. In fact, the result is zero only in the circular perturbing body case, but most works considered the third body on a circular orbit, reducing all the integrals of the third order to zero. In this case, the full model was considered, and the Moon is on an elliptical trajectory.

$\bar{\bar{\mathcal{R}}}_{moon,4}$ **term** Finally, the procedure is repeated for the fourth order term, which is the last order of expansion necessary for a correct approximation of the actual motion of the satellite according to Colombo et al., [24]. Retaining higher order terms is necessary to have a good polynomial expansion as explained in Section 3.4.1. By collecting the terms either in $\cos f_{\leftmoon}$ or $\sin f_{\leftmoon}$, the expression becomes:

$$\begin{aligned}\bar{\mathcal{R}}_{moon,4} =& \frac{3\mu_{\leftmoon}\, a^4 \left(15\, e^4 + 40\, e^2 + 8\right)}{64\, r_{\leftmoon}^5} + \\ &+ \frac{3\mu_{\leftmoon}\, a^4 \sin^2 f_{\leftmoon}}{64\, r_{\leftmoon}^5}(...\text{term1}...) + \frac{3\mu_{\leftmoon}\, a^4 \sin^4 f_{\leftmoon}}{64\, r_{\leftmoon}^5}(...\text{term2}...) + \\ &+ \frac{3\mu_{\leftmoon}\, a^4 \cos^3 f_{\leftmoon}\, \sin f_{\leftmoon}}{64\, r_{\leftmoon}^5}(...\text{term3}...) + \\ &+ \frac{3\mu_{\leftmoon}\, a^4 \cos^4 f_{\leftmoon}}{64\, r_{\leftmoon}^5}(...\text{term4}...) + \frac{3\mu_{\leftmoon}\, a^4 \cos f_{\leftmoon}\, \sin f_{\leftmoon}}{64\, r_{\leftmoon}^5}(...\text{term5}...) + \\ &+ \frac{3\mu_{\leftmoon}\, a^4 \cos f_{\leftmoon}\, \sin^3 f_{\leftmoon}}{64\, r_{\leftmoon}^5}(...\text{term6}...) + \\ &+ \frac{3\mu_{\leftmoon}\, a^4 \cos^2 f_{\leftmoon}}{64\, r_{\leftmoon}^5}(...\text{term7}...) + \frac{3\mu_{\leftmoon}\, a^4 \cos^2 f_{\leftmoon}\, \sin^2 f_{\leftmoon}}{64\, r_{\leftmoon}^5}(...\text{term8}...) + \end{aligned} \tag{3.101}$$

Hence, nine integrals can be identified:

$$\frac{1}{2\pi}\int_0^{2\pi} \frac{1}{r_{\leftmoon}^5} dM_{\leftmoon} = \frac{2 + 3\, e_{\leftmoon}^2}{2\, a_{\leftmoon}^5\, (1 - e_{\leftmoon}^2\,)^{7/2}} \tag{3.102}$$

$$\frac{1}{2\pi}\int_0^{2\pi} \frac{\cos^2 f_{\leftmoon}}{r_{\leftmoon}^5} dM_{\leftmoon} = \frac{4 + 9\, e_{\leftmoon}^2}{8\, a_{\leftmoon}^5\, (1 - e_{\leftmoon}^2\,)^{7/2}} \tag{3.103}$$

$$\frac{1}{2\pi}\int_0^{2\pi} \frac{\sin^2 f_{\leftmoon}}{r_{\leftmoon}^5} dM_{\leftmoon} = \frac{4 + 3\, e_{\leftmoon}^2}{8\, a_{\leftmoon}^5\, (1 - e_{\leftmoon}^2\,)^{7/2}} \tag{3.104}$$

$$\frac{1}{2\pi}\int_0^{2\pi} \frac{\cos^4 f_{\leftmoon}}{r_{\leftmoon}^5} dM_{\leftmoon} = \frac{2(2 + 5\, e_{\leftmoon}^2\,)}{16\, a_{\leftmoon}^5\, (1 - e_{\leftmoon}^2\,)^{7/2}} \tag{3.105}$$

$$\frac{1}{2\pi}\int_0^{2\pi} \frac{\sin^4 f_{\leftmoon}}{r_{\leftmoon}^5} dM_{\leftmoon} = \frac{2(2 + 5\, e_{\leftmoon}^2\,)}{16\, a_{\leftmoon}^5\, (1 - e_{\leftmoon}^2\,)^{7/2}} \tag{3.106}$$

$$\frac{1}{2\pi}\int_0^{2\pi} \frac{\cos^2 f_{\leftmoon}\, \sin^2 f_{\leftmoon}}{r_{\leftmoon}^5} dM_{\leftmoon} = \frac{2 + 3\, e_{\leftmoon}^2}{16\, a_{\leftmoon}^5\, (1 - e_{\leftmoon}^2\,)^{7/2}} \tag{3.107}$$

$$\frac{1}{2\pi}\int_0^{2\pi} \frac{\cos f_{\leftmoon}\, \sin f_{\leftmoon}}{r_{\leftmoon}^5} dM_{\leftmoon} = 0 \tag{3.108}$$

$$\frac{1}{2\pi}\int_0^{2\pi} \frac{\cos f_{\leftmoon}\, \sin^3 f_{\leftmoon}}{r_{\leftmoon}^5} dM_{\leftmoon} = 0 \tag{3.109}$$

$$\frac{1}{2\pi}\int_0^{2\pi} \frac{\cos^3 f_{\leftmoon}\, \sin f_{\leftmoon}}{r_{\leftmoon}^5} dM_{\leftmoon} = 0 \tag{3.110}$$

Also in this case, most of the integrals are not null. By substituting them into Equation (3.101), a long expression is computed. Here only few terms are reported, for conciseness. An important note is that as for the second and the third order term, it depends on both the satellite and the Moon orbital parameters.
Yielding to the final expression of the double averaged potential:

$$\begin{aligned}\bar{\bar{\mathcal{R}}}_{moon,4} =& \frac{3a^4\left(15e^4+40e^2+8\right)\left(3e_{\leftmoon}^2+2\right)\mu_{\leftmoon}}{128a_{\leftmoon}^5\left(1-e_{\leftmoon}^2\right)^{7/2}}+\\ &\frac{9a^4\left(e_{\leftmoon}^2+2\right)\mu_{\leftmoon}}{1024a_{\leftmoon}^5\left(1-e_{\leftmoon}^2\right)^{7/2}}\Big(35(e^2-1)^2(\cos i\cos\omega(\cos \mathrm{i}_{\leftmoon}\cos\omega_{\leftmoon}\\ &\cos(\Omega-\Omega_{\leftmoon})+\sin\omega_{\leftmoon}\sin(\Omega-\Omega_{\leftmoon}))+\\ &+\sin i\cos\omega\sin \mathrm{i}_{\leftmoon}\cos\omega_{\leftmoon}+\\ &-\sin\omega\cos \mathrm{i}_{\leftmoon}\cos\omega_{\leftmoon}\sin(\Omega-\Omega_{\leftmoon})+\\ &+\sin\omega\sin\omega_{\leftmoon}\cos(\Omega-\Omega_{\leftmoon}))^4+\ldots\text{long expression}\ldots\end{aligned} \tag{3.111}$$

Double averaged Moon disturbing function At this point, the overall expression can be computed as the sum of second to fourth order terms in Equation (Equation (3.92)), (Equation (3.100)) and (Equation (3.111)). The complete expression is reported in Appendix Appendix C.3

$$\bar{\bar{\mathcal{R}}}_{\leftmoon} = \bar{\bar{\mathcal{R}}}_{moon,2}+\bar{\bar{\mathcal{R}}}_{moon,3}+\bar{\bar{\mathcal{R}}}_{moon,4} \tag{3.112}$$

The overall expression depends on

- satellite orbital parameters: $\{a,\ e,\ i,\ \omega,\ \Omega\}$,
- Moon orbital parameters: $\{a_{\leftmoon}\ ,\ e_{\leftmoon}\ ,\ i_{\leftmoon}\ ,\ \omega_{\leftmoon}\ ,\ \Omega_{\leftmoon}\ \}$,

The former set of Keplerian elements is expressed in the equatorial frame and is constant during one orbital revolution: the short-term variation was cancelled out in the first averaging. The latter set is expressed in the equatorial frame as well. Two main consideration shall be done at this level: the orbital parameters of the Moon with respect to the equator are not constant in time but shall be expressed through the analytical expression of the Moon ephemeris. The latter consideration derives from the second averaging that cancels out the short-term effects due to Moon revolution.

The Lunar ephemeris is taken from Vallado, [39], and the analytical expression is given with respect to the Julian days past the 01/01/2000 (JD2000). Vallado provides the Moon

ephemeris in the Ecliptic Earth Centred reference frame. For this reason, a rotation is applied to pass in the Equatorial plane, considering the obliquity of the ecliptic (ϵ =23.439°).

3.5.6 Sun double-averaged potential

The Sun double-averaged potential is recovered by substituting the $A_\odot$ and $B_\odot$ in the first averaged expression, reported in Equation (Equation (3.67)). In this case, it is not present the true anomaly of the Sun, but, thanks to the formulation in Section Section 3.5.4, those coefficients depend on the Sun ecliptic longitude λ_{ecl} and on the magnitude of the Sun vector $r_\odot$.

Both λ_{ecl} and $r_\odot$ depends on the Mean anomaly and the mean longitude of the Sun. As already reported in Section Section 3.5.4, they depends on T_{UTI} through a numerical expression. While the analytical expression is simply $\lambda_\odot = \omega_\odot + f_\odot$

Two main hypotheses are considered during the dissertation:

- the Sun is considered in a circular orbit, hence $r_\odot$ is constant in time: $r_\odot$ =1.000 140 612 AU, for the Earth-Sun system
- since the ecliptic longitude of the Sun varies in one year, during the motion of the Earth along its orbit, from 0° to 360°, as a first approximation, the double average is done over the ecliptic longitude instead of the mean anomaly.

By using these approximations, the double averaged disturbing function is computed with the following integration:

$$\frac{1}{2\pi}\int_0^{2\pi} \bar{\mathcal{R}}_\odot \, d\lambda_{ecl} \tag{3.113}$$

Then introducing the expressions of $A_\odot$ and $B_\odot$ in the single averaged expression, the integration can be done by isolating all the terms related to λ_{ecl}, which is the only term that varies in the integration. As for the Moon case, all the other parameters in the expression were considered constant during the integration. This is possible due to the hierarchy of timescales: the period of the satellite is much less than the period of the disturbing body, which is much less than the period of slow oscillation in the orbital elements.

Now, the results of the integration are reported for each order term. The procedure followed is the same as the Lunar case, so it is not reported.

$\bar{\bar{\mathcal{R}}}_{\odot,2}$ **term** The full expression for the second order term is reported. It depends on the satellites' orbital elements and on the obliquity of the ecliptic. On the other hand, the mean anomaly is not present any more, since it was averaged out.

Differently from the lunar case, where the coupling with the Moon RAAN, here only the satellite node appears. The final expression is the following:

$$\begin{aligned}\bar{\bar{\mathcal{R}}}_{\odot,2} =& \frac{\mu_\odot\, a^2}{16\, r_\odot^3}\Big[-8 - 12\, e^2 + 3(2 + 3\, e^2 + 5\, e^2 \cos 2\omega)\cos^2\Omega + \\ & - 15\, e^2 \sin 2\omega \sin 2\Omega \cos i - 3(-2 - 3\, e^2 + 5\, e^2 \cos 2\omega)\sin^2\Omega \cos^2 i + \\ & - \Big(-3(\cos\epsilon \sin\omega \sin\Omega + \cos\epsilon \cos\omega \cos\Omega \cos i + \cos\omega \sin\epsilon \sin i)^2 \\ & + 3\, e^2(-\cos\epsilon \sin\omega \sin\Omega + \cos\epsilon \cos\omega \cos\Omega \cos i + \\ & + \cos\epsilon \cos\omega \sin i) - 3(\cos\epsilon \cos\omega \sin\Omega + \cos\epsilon \cos\Omega \sin\omega \cos i \\ & \sin\epsilon \sin\omega \sin i)^2 - 12\, e^2(\cos\epsilon \cos\omega \sin\Omega + \\ & \cos\epsilon \cos\Omega \sin\omega \cos i + \sin\epsilon \sin\omega \sin i)^2\Big)\Big]\end{aligned} \tag{3.114}$$

$\bar{\bar{\mathcal{R}}}_{\odot,3}$ **term** Since the circular case was adopted, as demonstrated for the Lunar case, the third-order term is null (in particular all the odd order terms would be zero).

$$\bar{\bar{\mathcal{R}}}_{\odot,3} = 0 \tag{3.115}$$

$\bar{\bar{\mathcal{R}}}_{\odot,4}$ **term** The expression for this term is lengthy and therefore reported in the Appendix Appendix D.2.

Sun double averaged disturbing function The final expression of the double averaged disturbing function is recovered from the sum of the expressions for the second, third and fourth order terms:

$$\bar{\bar{\mathcal{R}}}_\odot = \bar{\bar{\mathcal{R}}}_{\odot,2} + \bar{\bar{\mathcal{R}}}_{\odot,3} + \bar{\bar{\mathcal{R}}}_{\odot,4} \tag{3.116}$$

The double average expression depends on the orbital parameters of the satellite ($\{a,\ e,\ i,\ \omega,\ \Omega,\ f\}$) and on the obliquity of the ecliptic ϵ. The variation due to the motion of the planet around the Sun in one year is not present any more, hence the order of magnitude of the disturbing potential depends mainly on the Sun gravitational constant and on the planet-Sun distance.

3.6 Validation of the secular and long-term evolution of the orbital parameters

This section contains the comparison between the accuracy of different models. In fact, it is important to validate the analytical model to see whether the averaging technique produces accurate results. For the validation the Earth-Moon-Sun system is taken as a reference, considering different scenarios:

- the orbital parameters evolution in case of Moon case, Moon-J_2 case, Moon-J_2-Sun case (both single (SA) and double (DA) averaged)
- the orbital parameters evolution in the double averaged model (DA), considering both the circular and the elliptic case for the Moon,
- the orbital parameters evolution in the single (DA) and double (DA) averaged model, considering both the Sun and the Moon as a third perturbing body,

First, the correct level of approximation is measured by comparing the single and the double-averaged model with the exact one. In figure Figure 3.6 shows the orbital propagation in time of certain initial conditions. The reference orbit under study is an INTEGRAL-like orbit with the following initial conditions (ephemeris taken at 22/03/2013 [2]):

Table 3.3 Orbital parameters of a INTEGRAL-like orbit.

a (km)	e (-)	i (deg)	ω (rad)	Ω (rad)	M (rad)
87705.22	0.8766	61.53	4.6385	2.2516	4.15

The propagation in time was done by integrating the Lagrange Planetary equations, considering as the overall disturbing potential the double averaged model: $\bar{\bar{\mathcal{R}}} = \bar{\bar{\mathcal{R}}}_{J2} + \bar{\bar{\mathcal{R}}}_{\mathbb{C}} + \bar{\bar{\mathcal{R}}}_{\odot}$. The exact time evolution is represented in red, where the short term oscillation are present. The Figure 3.7 shows the evolution over one year to underline the short term oscillations of the exact solution. The single averaged is in green, while the double is in red. Their time evolutions are a very good approximation of the exact dynamics, recalling that the semi-major axis is constant in those approximations.

Once the accuracy level of the double averaged model has been shown, it is important to justify the need of including the Sun and the J_2 effect, differently from many past models based on Kozai work [6], where only the Moon effect was taken into account. In Figure 3.8, the three different approximations are compared. The time evolution changes significantly

[2] NASA JPL Horizon Wb Interface: `https://ssd.jpl.nasa.gov/horizons.cgi`, latest visit on 10/2018

by considering different models the addition of J_2 affects significantly the propagation, and also the effect of the Sun is required to get the correct orbital evolution.

These considerations are important for the study of the end-of-life manoeuvres. In fact, they indicate the need for including the Sun effect. In fact, for closed Earth's satellite, J_2 is dominant: the orbital plane precesses around the equatorial plane. On the other hand, for far distant orbits, the third body effect (Moon/Sun) dominates and the orbital plane precesses around the ecliptic plane. It allows an easy expression of the Moon perturbations, but the addition of J_2 and Sun effect complicates the model. The Moon plane could still be used only by considering the Sun orbiting on the same plane of the Moon one. This is typically achieved by imposing that the Moon and the Sun have no relative inclination. This work tries to drop that approximation considering the real orbits for the perturbing bodies.

Finally, the results considering the Moon on a circular or an elliptical orbit are reported and define the need of dropping out also that approximation. As shown in Figure 3.9, the discrepancies start to become significant only after 30-40 year. Hence, for a very preliminary design of the disposal manoeuvre the circular Moon hypothesis can be retained, but only for a short period of observation (20-30 years), otherwise, the propagation would be inaccurate.

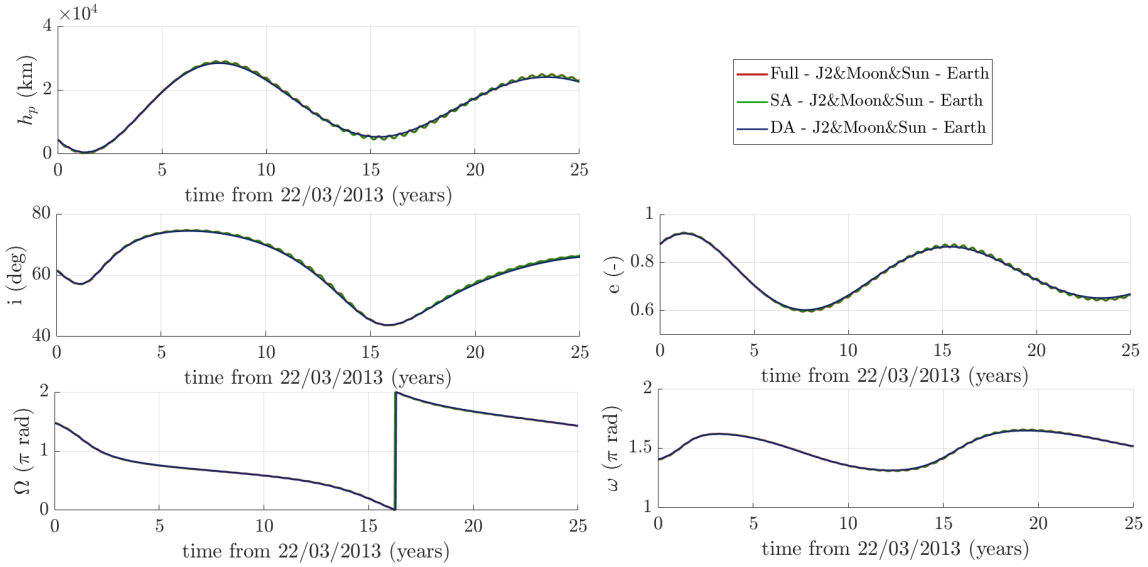

Figure 3.6 Comparison between the time evolution of the exact, single and double-averaged approximations.

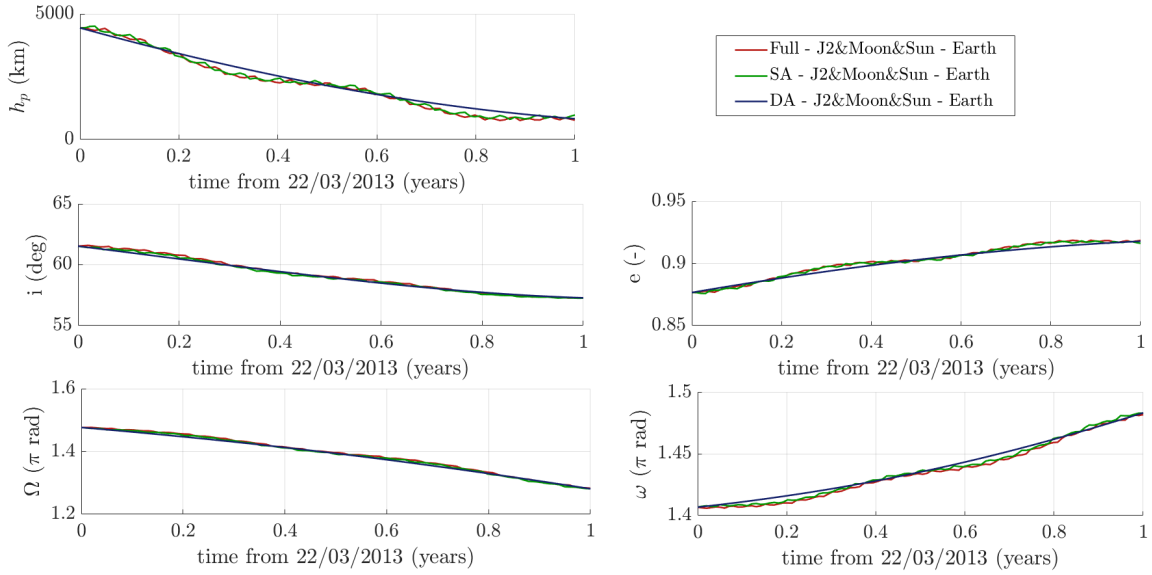

Figure 3.7 Focus on the first year of time evolution.

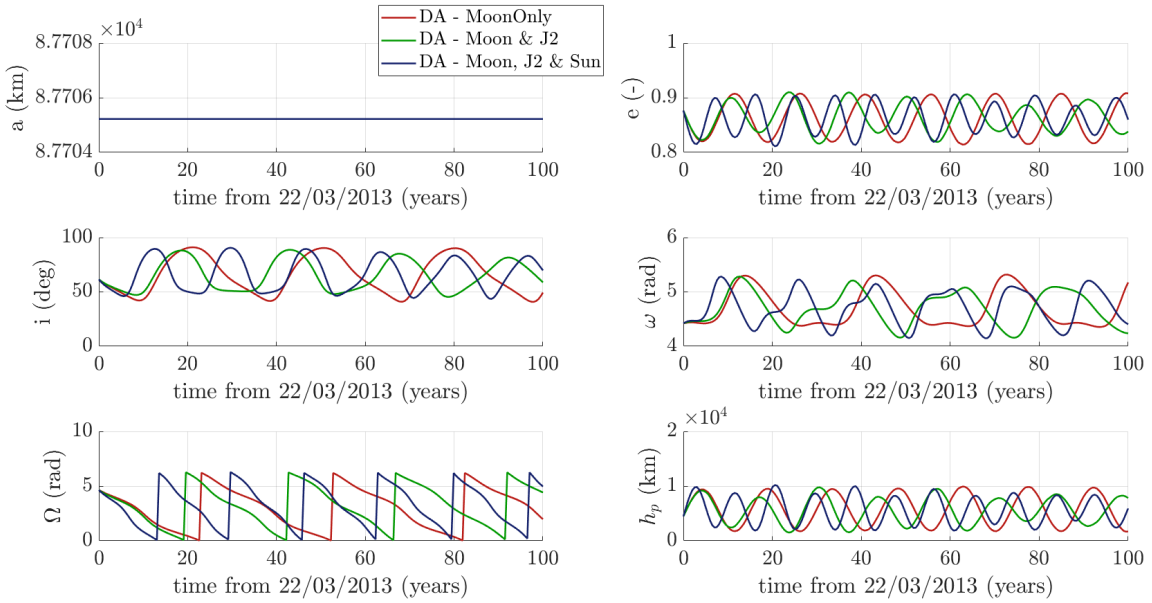

Figure 3.8 Different level of approximation of the orbital dynamics by considering at first only the Moon influence, then the J_2 zonal contribution is added, and finally also the Sun effect.

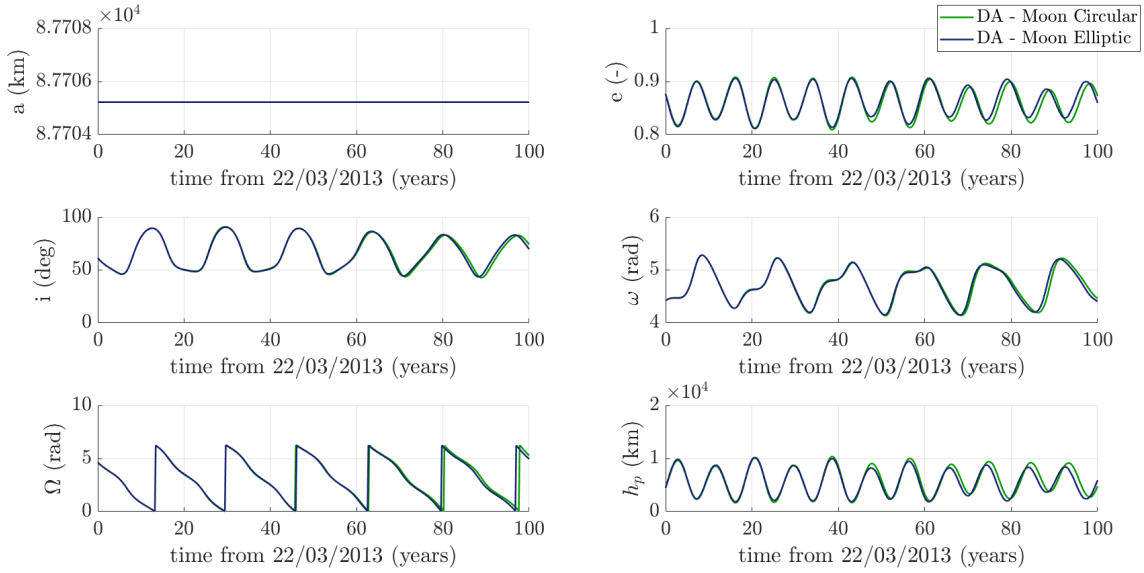

Figure 3.9 Satellite orbit propagation in case of circular Moon orbit (green) and elliptical Moon orbit (blue).

Chapter 4

Hamiltonian Formulation: Phase Space Maps

THE Hamiltonian formulation was discussed in Section 2.6. It depends on the disturbing potential of external sources of perturbation.

$$\mathcal{H} = -\frac{\mu}{2\,a} - \mathcal{R}_{\text{disturbances}}. \tag{4.1}$$

The Hamiltonian describes the dynamical evolution of the system. Since the aim is to study the disposal design with the goal to re-enter in 20-25 years, only the secular effect is retained, removing the short-periodic terms as shown in Chapter 3. This yields to a non-exact description for short period dynamics: the representation is independent of the evolution along the orbit in terms of the true anomaly. Therefore, all the periodic variations in the short period are not seen by this model, but they can be recovered for a full dynamical evolution. The main idea behind the secular effect is based on the averaging procedure, which behaves as a filtering technique, by cancelling out the high-frequency behaviour. The resulting effect upon the orbital parameter variation was already discussed in Section 3.6. As a case of study, two different systems are evaluated:

1. the Earth-Moon-Sun system with an Earth's satellite on a HEO.
2. the Sun-Venus system with a Venus orbiter in a trajectory equivalent to the Earth's HEO.

Both cases are studied to understand the effect of the third body perturbation and how this can be used for the manoeuvre design.

4.1 Earth-Moon-Sun system: Hamiltonian representation

The first study case is the Earth's satellite case. In this scenario a satellite placed on a HEO, as INTEGRAL or XMM-Newton, is considered. Its dynamics is affected by the perturbation caused by the Moon attraction, the J_2 effect of the Earth's oblateness and the Sun effect. Recalling the expression in Equation (2.23), the long-term representation of the Hamiltonian is computed by considering the double-averaged expression for the disturbing potentials: the third body potential in Equation (3.112) for the Moon and Equation (3.116) for the Sun and the J_2 potential in Equation (3.12).

$$\mathcal{H}_{\oplus\odot\leftmoon} = -\frac{\mu_\oplus}{2\,a} - \bar{\bar{\mathcal{R}}}_{J_2} - \bar{\bar{\mathcal{R}}}_{\leftmoon} - \bar{\bar{\mathcal{R}}}_{\odot}. \tag{4.2}$$

Considering only the long-term effect yields to some simplification:

- no more dependence on the true anomaly of the satellite: the orbital period for a satellite with a semi-major axis in the order of 4-8 $\times\, 10^4$ km is about

$$T = 2\pi\sqrt{\frac{a^3}{\mu}} \approx 22 \div 60\,\mathrm{h}$$

- no more dependence on the true anomaly of the Moon: with a orbital period of 27 d

- no more dependence on the ecliptic longitude of the Sun λ_{ecl}, with a apparent period of 365.25 year.

The independence from the actual time position of the satellite and the Moon has the advantage also to reduce the computational cost. Therefore, the Hamiltonian expression is a function of satellite orbital elements, Moon orbital elements and obliquity of the ecliptic:

$$\mathcal{H}_{\oplus\odot\leftmoon} = \mathcal{H}_{\oplus\odot\leftmoon}\,(a,\, e,\, i,\, \omega,\, \Omega,\, a_{\leftmoon}\,,\, e_{\leftmoon}\,,\, i_{\leftmoon}\,,\, \omega_{\leftmoon}\,,\, \Omega_{\leftmoon}\,,\, \epsilon)\,, \tag{4.3}$$

where in the part related to the Moon effect, the satellite's node appears coupled with the Moon node ($\Omega_{\leftmoon}$) as: $\Delta\Omega = \Omega - \Omega_{\leftmoon}$. This is a very important relation, since the Moon's node has a non-linear variation in time when it is expressed in the equatorial plane. Therefore, the resulting dynamics has a very complex behaviour.

4.2 Venus-Sun system: Hamiltonian representation

The second scenario considers the case of a Venus orbiter. The space probe is orbiting around Venus on an equivalent HEO Earth's orbit. This assumption allows studying the third body effect predicted by the Lidov-Kozai model. Venus has no natural satellite, hence, only the Sun disturbance is present. Moreover, the oblateness coefficient J_2 for Venus is much smaller than the Earth's case: the dynamics is dominated by the Sun disturbance.

As for the Earth's case, the Hamiltonian representation is obtained from the potential function of the external sources: the Sun effect and the J_2 potential.

$$\mathcal{H}_{♀\odot} = -\frac{\mu_{♀}}{2\,a} - \bar{\bar{\mathcal{R}}}_{J2} - \bar{\bar{\mathcal{R}}}_{\odot} \tag{4.4}$$

Also in this case, considering the double-averaged potentials brings some simplifications:

- no more dependence on the satellite's true anomaly,
- no more dependence on the Sun's position on its apparent orbit.

This representation is written in term of the mean orbital elements, instead of the osculating one, in the equatorial reference plane of Venus. The model, in this case, is subjected to some assumptions:

- the obliquity of the ecliptic for Venus is 177.4°: the equator is inclined over the ecliptic of an angle of 2.6°. Therefore, it is reasonable to consider the equatorial plane of Venus coincident with the ecliptic.
- the eccentricity of the heliocentric orbit of Venus is small: 0.007°. It is a good assumption to consider it as a circular orbit.

These two approximations simplify a lot the Hamiltonian expression. It is no more function of the third body node, inclination or eccentricity, but depends only on the Sun distance:

$$\mathcal{H}_{♀\odot} = \mathcal{H}_{♀\odot}\,(a,\, e,\, i,\, \omega,\, \Omega,\, r_{\odot}) \tag{4.5}$$

In this case, the satellite's node does not appear coupled with the third body one: understanding the dynamics of the vehicle is much simpler. In particular, it is an advantage for the Hamiltonian reduction for the description of the two-dimensional phase space. In fact, the third body node has a non-linear behaviour, which results in a complicated dynamics when coupled with the satellite node.

4.3 Two-Dimensional Hamiltonian phase space

After the double average, the Hamiltonian depends on several parameters, as already shown for both the Earth and the Venus case. To obtain two-dimensional phase space representation it is necessary to reduce the number of variables of the problem: a one-degree-of-freedom Hamiltonian is necessary. Therefore, the aim of this section is to identify a technique to reduce the Hamiltonian formulation to a one-degree-of-freedom expression.

A first consideration can be done upon the semi-major axis: in the single and in the double-averaged model it remains constant in time since the dependence on the true anomaly was cancelled out, as it was already shown in Section 3.6. This drops the dependence of the Hamiltonian form a, reducing the number of variables. In fact, it is a constant of motion and it is computed from the initial orbit condition: $a = a_0$. Different past studies (Kozai, [6]; Lidov, [5]) managed to represent the third body effect using a two-dimensional maps as function of eccentricity and argument of perigee. This procedure results from the elimination of the node dependence.

The removal of the longitude of the ascending node is commonly called 'elimination of the node'. This reduction was first introduced by Kozai [6]: he expressed the Hamiltonian of the system Jupiter-Asteroid-Sun adopting the invariable plane as the reference one. His case considers Jupiter as the perturber, and as it happens for the Moon effect in the Earth system, the longitude of the ascending node appears as a combination of $\Omega - \Omega_{3b}$. Kozai adopt the relations in the invariable planes among the Delaunay's variables:

$$h = h_{3b} \qquad \rightarrow \qquad \Omega = \Omega_{3b} \tag{4.6}$$

With this relation, and assuming that the inclination of Jupiter is near zero (Sun and Jupiter are on the same plane), he defines a constant of the motion: H constant. Hence, the definition of the Kozai parameter is presented as a constant of motion, [6]:

$$\Theta_{kozai} = \left(\frac{H}{L}\right)^2 = (1 - e^2)\cos i \tag{4.7}$$

The so-called, Kozai-Lidov parameter is a constant of the motion and can be defined only when the Hamiltonian does not depend any more on the RAAN. In particular, its power is the possibility to express the inclination of the satellite in the invariable plane as a function of the eccentricity, reducing for all purposes the Hamiltonian to a 2D expression. Defining

the initial condition of the motion for $\Theta_{kozai,0}$, the relation for the inclination is recovered:

$$\cos i = \frac{\Theta_{kozai,0}}{(1-e^2)} \tag{4.8}$$

Therefore, he was able to reduce the Hamiltonian expression to a function of the eccentricity and argument of perigee only: $\mathcal{H} = \mathcal{H}(e, \omega)$.

4.3.1 Elimination of the Node

The proposed double averaged model contains the influence of the satellite RAAN. For the Earth's satellite case, the argument of the node appears in two different ways. In the Moon potential $\bar{\bar{\mathcal{R}}}_{\leftmoon}$ it appears as a combination of $\Omega - \Omega_{\leftmoon}$, while in the Sun effect $\bar{\bar{\mathcal{R}}}_{\odot}$, it is not coupled with the Sun node, since two different mathematical models to describe the position vector of the perturber were used. For this reason, proceeding as Kozai did in his work is not possible, due to the presence of the Sun and the different reference system adopted. For the Venus' probe, instead, the plane of the third body coincide with the equatorial one. This is equivalent to consider the invariable plane. In addition, the node influence appears in the Sun double-averaged potential not coupled with the third body node.

In previous works (Colombo et al., [24]; Colombo, [25]) the elimination of the node from the Hamiltonian representation was done considering a rotating system with the x-axis in the direction of the node of the satellite orbit with respect to the Moon plane. In this way, the Hamiltonian is expressed with respect to the Moon node. Nevertheless, this was used only for the phase space representation, while the model for the orbital propagation considers the node influence.

The approach used to get rid of the argument of the node is based on the averaging procedure: a third integration is settled to average out the effect of Ω. This approach is similar to represent the Hamiltonian function in a new frame, where the dependence on the RAAN is not present any more. Nevertheless, the accuracy of this approximation shall be evaluated, to see whether it can correctly represent the orbital propagation. The elimination of the node is performed with an integration over Ω:

$$\mathcal{H}_{new} = \frac{1}{2\pi} \int_0^{2\pi} \mathcal{H}\, d\Omega. \tag{4.9}$$

The results of the integration are now reported for the two cases under study.

Earth's satellite

After the integration the Hamiltonian representation does not depend any more on the satellite node. Nevertheless, it is not a time-independent formulation: as already introduced, the Moon orbital elements are not constant in the equatorial frame, in particular, the inclination is subjected to a wide variation in the range 19°-29°. Therefore, to produce two-dimensional phase space maps, the time variation of Moon Keplerian elements should be dropped. In this way, the Hamiltonian becomes a function of eccentricity, inclination and argument of perigee only:

$$\mathcal{H}_{\oplus\odot\leftmoon}\ (a,\, e,\, i,\, \omega,\, \Omega,\, a_{\leftmoon}\,,\, e_{\leftmoon}\,,\, i_{\leftmoon}\,,\, \omega_{\leftmoon}\,,\, \Omega_{\leftmoon}\,,\, \epsilon) \quad \rightarrow \quad \mathcal{H}_{\oplus\odot\leftmoon}\ (e,\, i,\, \omega) \tag{4.10}$$

The following expressions reported the Hamiltonian due to the triple averaged potential of Sun and Moon (note that the contribution due to the Earth's oblateness is independent from the node). Only the second order terms are reported for the most general case with the Moon on an inclined eccentric orbit.

$$\begin{aligned}
\mathcal{H}_{new,\oplus\odot\leftmoon} \ =& -\frac{\mu}{2a} - \frac{\mathrm{J2}\mu R_{\oplus}^2(3\cos 2i+1)}{8a^3\,(1-e^2)^{3/2}} - \frac{\mu_{\leftmoon}\,a^2}{32,a_{\leftmoon}^3\,(1-e_{\leftmoon}^2\,)^{3/2}}\Big(15\,e^2\cos\omega((-1+\\
&+\cos^2 i)(1+\cos^2 i_{\leftmoon}\,)+2\sin^2 i\sin^2 i_{\leftmoon}\,)-(2+3\,e^2)(-5+\\
&+3\,\cos^2 i(1+\cos^2 i_{\leftmoon}\,)+6\sin^2 i\sin^2 i_{\leftmoon}\,)\Big)+\\
&-\frac{\mu_{\odot}a^2}{64\,r_{\odot}^3}\Big(10(-2-3\,e^2+3\,e^2\cos\omega)-3(3+\cos 2\epsilon)\cos^2 i(-2-3\,e^2+\\
&+5\,e^2\cos 2\omega)6\cos^2\epsilon(2+3\,e^2+3\,e^2\cos 2\omega)-12(-2-3\,e^2+\\
&+5\,e^2\cos 2\omega)\sin^2\epsilon\sin^2 i\Big)+\text{...higher order terms...}
\end{aligned} \tag{4.11}$$

Venus' probe

Similarly, the same procedure is applied for the Venus case. After the integration, the node dependence is dropped. The Hamiltonian representation is function of the eccentricity, inclination and argument of perigee only, it does not contain time dependent parameter as for the Earth's case. In fact, the Sun distance is assumed constant along the planet orbit.

$$\mathcal{H}_{\varphi\odot}\,(a,\, e,\, i,\, \omega,\, \Omega,\, r_{\odot}) \quad \rightarrow \quad \mathcal{H}_{\oplus\odot\leftmoon}\ (e,\, i,\, \omega) \tag{4.12}$$

The following expressions reported the Hamiltonian due to the triple averaged potential of Sun (note that the contribution due to the Venus' oblateness is independent from the node):

only the second order terms are reported.

$$\begin{aligned}\mathcal{H}_{new,\mathrm{♀}\odot} = &-\frac{\mu}{2a} - \frac{\mathrm{J2}\mu R_{\oplus}^2(3\cos 2i+1)}{8a^3\left(1-e^2\right)^{3/2}} - \frac{\mu_{\odot}a^2}{64\,r_{\odot}^3}\Big(10(-2-3\,e^2+3\,e^2\cos\omega)\\ &-3(3+\cos 2\epsilon)\cos^2 i(-2-3\,e^2+5\,e^2\cos 2\omega)6\cos^2\epsilon(2+3\,e^2\\ &+3\,e^2\cos 2\omega)-12(-2-3\,e^2+5\,e^2\cos 2\omega)\sin^2\epsilon\sin^2 i\Big)+...\end{aligned} \tag{4.13}$$

4.3.2 Kozai Parameter:

After the integration, a triple averaged model is produced: it does not depend any more on the satellite node. Since the new Hamiltonian formulation is a time-independent expression, the Kozai parameter can be applied.

The Kozai parameter is introduced to relate the inclination and the eccentricity variation in time. Since Θ_{kozai} is constant during the time evolution, the inclination can be written as a function of the eccentricity:

$$i = \arccos\Big(\frac{\Theta_{kozai,0}}{\sqrt{1-e^2}}\Big), \tag{4.14}$$

where $\Theta_{kozai,0}$ is related to the initial condition for orbit propagation.

By substituting this relation in the Hamiltonian expression, it is no more a function of the inclination. This is essential to obtain two-dimensional maps in the phase space.

$$\mathcal{H} = \mathcal{H}(e,\omega). \tag{4.15}$$

For the Earth-Moon-Sun system, the Kozai parameter would not be constant in the real dynamic, since the node elimination is an approximation for this system. Moreover, this will results in a numerical error with respect to the real propagation, but it can be used as a first approximation for manoeuvre design purposes.

4.4 Phase space maps

The new simplified Hamiltonian, as shown in Equation (4.15), depends on two variables: eccentricity and perigee anomaly (e,ω). To produce the two-dimensional maps, each phase space is produced in terms of fixed semi-major axis, which correspond to the initial condition for the orbit propagation. This means that each phase space is related to a defined value of a, and therefore to a fixed orbital initial condition. To produce the two-dimensional maps, a reference condition is chosen in terms of (e_0,ω_0), to compute the Kozai parameter $\Theta_{kozai,0}$.

The phase space maps are produced by computing the contour plot of the Hamiltonian function. From a generic initial condition, the Hamiltonian expresses the time evolution of eccentricity and perigee anomaly. The Hamiltonian function is therefore defined for a specific initial condition (e_0, ω_0).

$$\mathcal{F} = \mathcal{H}(e, \omega) - \mathcal{H}_0(e_0, \omega_0), \tag{4.16}$$

where (e_0, ω_0) are the initial condition for the orbital parameters. The phase space maps are now presented for the two cases of study. First, an INTEGRAL-like satellite is considered in the Earth-Moon-Sun system, then a Venus orbiter is analysed under the Sun third body effect.

Earth's satellite The satellite orbit was selected as an INTEGRAL-like orbit in HEO, with the following initial condition (from ephemeris at 22/03/2013[1]):

- sat orbital parameter: $\{87\,705.2\,\text{km}, 0.876, 1.074\,\text{rad}, 4.63\,\text{rad}, 2.25\,\text{rad}, 4.45\,\text{rad}\}$.

The orbital time evolution is described by the contour plot of the Hamiltonian function $\mathcal{F} = \mathcal{H}(e, \omega) - \mathcal{H}_0(e_0, \omega_0)$, generated by the initial conditions. This function is plotted over the Hamiltonian phase space generated with the corresponding conditions in terms of a_0, e_0, ω_0, i_0. Nevertheless, this approach is valid only in the case that all the other parameters in the Hamiltonian formulation (due to J_2, Moon and Sun) are constant in time. As already mentioned, this rises up an initial problem: most of the Moon Keplerian elements are fixed in the ecliptic reference system, only the node varies linearly in time, while in the equatorial frame, they oscillate in time, as for the inclination shown in Figure 4.1. As reference condition, the oscillation of the inclination is reported but obviously, the variation happens also in the other orbital elements. It is therefore evident that a significant variation happens in time, resulting in:

- Moon inclination oscillations in between 19° - 29°.

As a first approximation, the Keplerian elements of the Moon could be considered constant in time, and the average value is taken for the Hamiltonian computation.

The time propagation was done to compare the results gained from the exact model and the approximate one. The former computes at each time step the Moon ephemeris from the analytical description, the latter instead uses the average value of the moon orbital elements

[1]NASA JPL Horizon Wb Interface: `https://ssd.jpl.nasa.gov/horizons.cgi`, latest visit on 10/2018

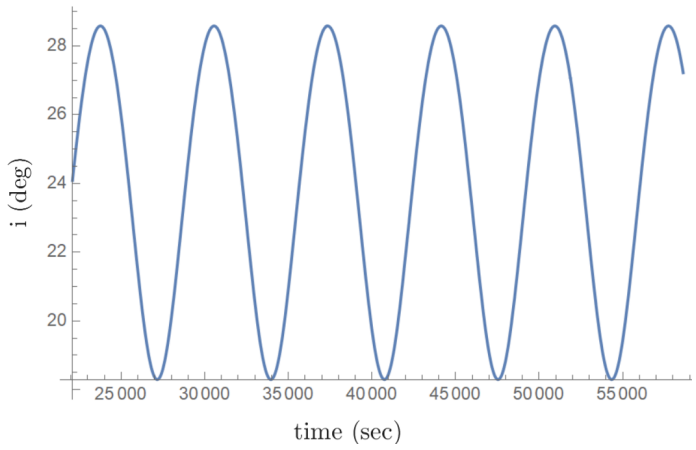

Figure 4.1 Time variation of Moon orbital plane inclination.

for the orbital determination:

$$\text{kep}_{\leftmoon,\text{av}} = \{3.834\,094 \times 10^5\,\text{km},\ 0.0554842,\ 23.769°,\ 179.206°,\ 182.23°\} \tag{4.17}$$

Graphs in Figure 4.2 compares the time evolution, using the triple averaged model, using at first the exact Moon ephemeris and then the average values. From these results, it appears that neglecting the time variation of the moon ephemeris does not change much the results. This condition is justified by the analytical expression of the triple averaged Hamiltonian, reported in Equation (4.11). Dropping the dependence on the satellite RAAN, decouples the disturbing function expression also from the Moon node $\Omega_{\leftmoon}$. In addition it is not a function of the anomaly of perigee $\omega_{\leftmoon}$ as well, but only of inclination $i_{\leftmoon}$, eccentricity $e_{\leftmoon}$ and semi-major axis $a_{\leftmoon}$. For this reason, the main effect is given by the inclination variation. The variation in the orbital parameters, considering the triple averaged model, is studied to see whether considering constant Moon parameters could be an acceptable solution for a first preliminary approach. Figure 4.2 shows the results, integrated in 100 years. For the first 20 years, the discrepancies in the results could be considered acceptable, since the results are very close to each other. Nevertheless, as time passes, the variation becomes more and more significant, defining the need for dropping this assumption.

A first way to solve this problem could be to model the dynamics of the satellite in the ecliptic plane: in this reference frame, the orbit of the Moon is fixed in time, producing constant Moon inclination. The phase space maps are produced from the two-dimensional Hamiltonian relation and describe the time evolution of e and ω of the satellite orbit under the effect of external disturbance.

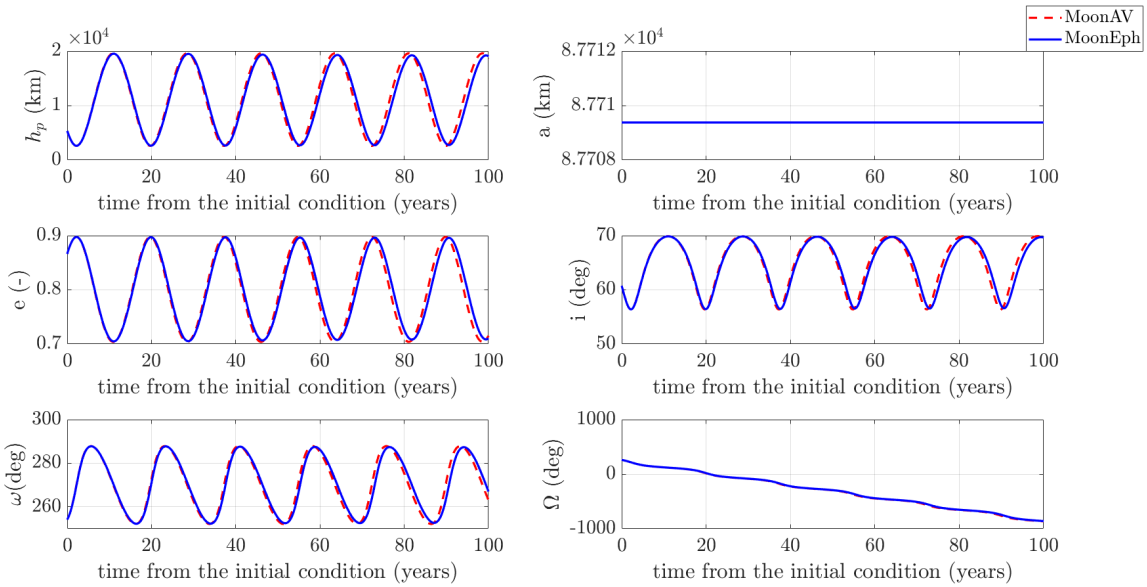

Figure 4.2 Orbital parameter variation, in the triple averaged approach, considering the influence of Moon ephemeris in time (blue line), and constant condition of Moon orbital parameter in time (red line).

The resulting maps are reported in Figure 4.3, where Figure 4.3a reports the solution obtained by Kozai in the Sun-Jupiter system, Figure 4.3b shows the results of Colombo et al. [4] in the Earth-Moon system, and Figure 4.3c presents the phase space produced with the model presented in this dissertation. A first important note is the similarity of the phase space structure, in all of them is evident the cyclicity of the eccentricity in time. Despite in the first two figures the reference plane is the disturber plane, the triple averaged model described in the third figure, was derived in the equatorial frame. The phase space presented in Figure 4.3c was obtained considering only the influence of the Moon and J_2; in addition, the averaged elements of the Moon was imposed. This very first simple approach was used to investigate the feasibility of the analytical recovery of the critical eccentricity condition in the phase space.

Venus' probe The Venus orbiter was selected to be on a highly elliptical and highly inclined orbit. In fact, Kozai demonstrates that the effect of the third body becomes relevant only for inclined orbits ([6]). Since Venus is very similar to Earth for dimensions and gravitational attractions, an orbit similar to the one followed by INTEGRAL or XMM-Newton were selected. In fact, most of the probes that visited Venus were on an orbit that was not affected by the Lidov-Kozai effect due to the low altitude, low eccentricity and inclination. In addition, some of them were very close to the atmospheric interface, and in those case

the drag perturbation becomes predominant. Considering the same initial condition used for the Earth, the phase space maps were produced, to describe the eccentricity oscillation in time. The phase space maps obtained for both the Earth's and Venus' cases have a very similar shape to the Kozai one. An observation can be done for the Venus' probe. The triple average model is used to describe the dynamics of the satellite. Differently, from the Earth's case, the hypothesis done for the third body are very reasonable and therefore they do not affect the real dynamics: the orbit of the Sun is almost equatorial and circular.

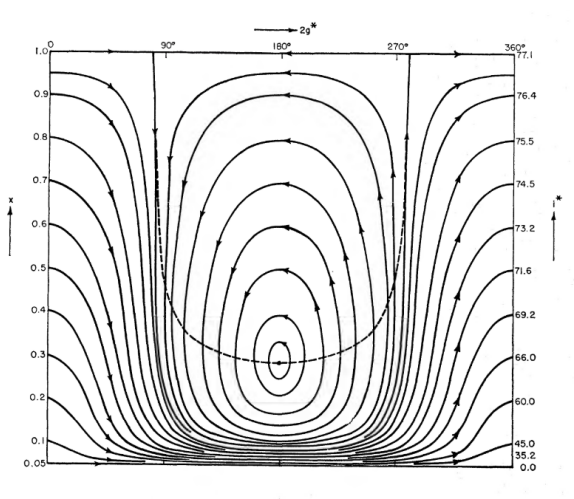

(a) Kozai phase space in Sun-Asteroid-Jupiter system: Jupiter disturbance only (Kozai, [6]).

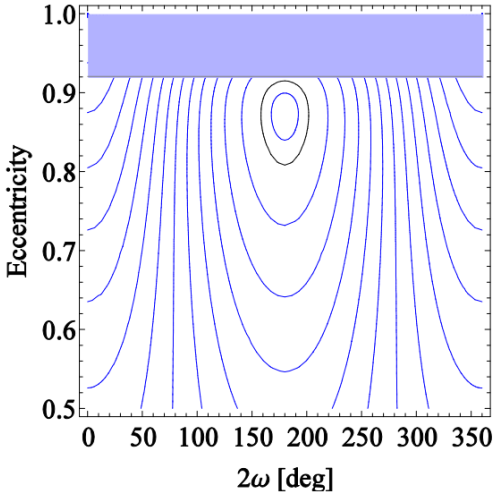

(b) Phase space in the Moon plane: Moon disturbance only (Colombo et al., [4]).

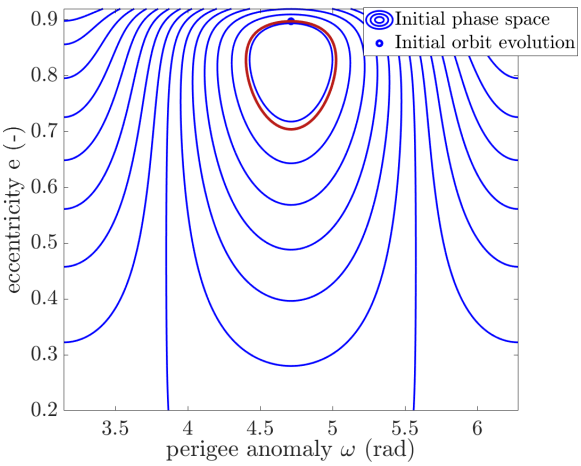

(c) Earth's satellite: Phase space in the Equatorial plane with Moon, J_2 and Sun perturbation.

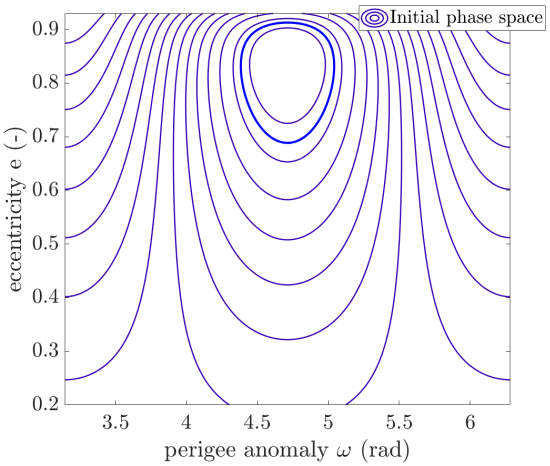

(d) Venus' probe: Phase space in the Equatorial plane with J_2 and Sun perturbation.

Figure 4.3 Phase space comparison between different approximation.

Semi-analytical recovery of critical eccentricity condition The importance of the recovery of a Hamiltonian expression in one degree of freedom lies in the possibility of computing in a fully-analytical way the maximum eccentricity condition. As it would be shown in Chapter 5, this is essential to reduce the computational time and cost for the disposal manoeuvre design. Once the satellite initial condition has been identified, the orbit evolution is described in the phase space by

$$\mathcal{H}(e, \omega) = \mathcal{H}_0(a_0, e_0, i_0, \omega_0) \tag{4.18}$$

This is an analytical expression in two variables only. Despite this, is it too complex to be solved completely in an analytical way, and therefore numerical methods shall be introduced for the computation of the eccentricity value as a function of the anomaly of perigee. Since from the phase space representation in Figure 4.3c, the stationary points in terms of eccentricity are in correspondence of $\frac{3\pi}{2}$, a first way to identify the stationary points by solving the Equation (4.18) for the eccentricity values. Iterative methods could be used, like the Newton method, since the system is non-linear. The solution was computed with MATLAB® using the `fsolve.m` function and imposing `Levenberg-Marquardt` algorithm.

The analysis of the contour level of the Hamiltonian is very important for the disposal strategy design. From the maps, it is possible to recover efficiently how the eccentricity change in time. Since the Kozai parameter was introduced, see Equation (4.14), the phase space can be evaluated also in terms of inclination and perigee anomaly, instead of the eccentricity. The (e, ω) representation is the most suitable for the de-orbit analysis. In fact, as explained in Chapter 5, the re-entry condition can be exploited in terms of a critical eccentricity, and this value can be easily represented on the planar phase space.

4.5 Accuracy analysis

Once the Hamiltonian phase space maps were produced, it is mandatory to verify that they describe the dynamics of the spacecraft under external perturbations. For this purpose, the triple averaged model of the system was propagated in time using Lagrangian Planetary Equations (Equation (2.8)) for the triple averaged potential. The resulting Keplerian elements describe the triple averaged evolution in time. Now, different maps in (e, ω) were produced to compare the effect of different levels of accuracy in the model. Two cases are studied: Earth's satellite system and Venus' probe system.

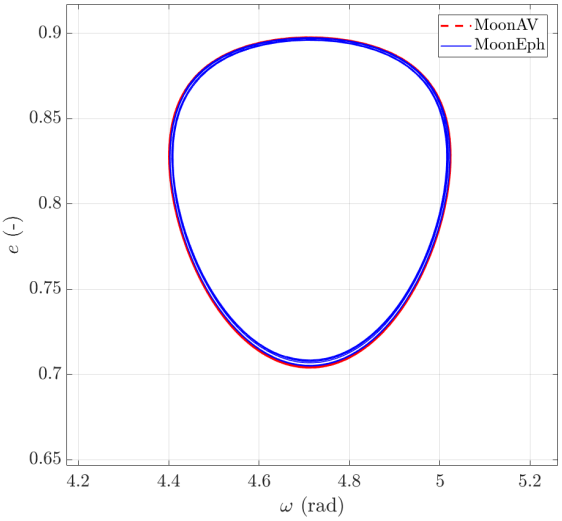

(a) Earth-Moon-Sun triple-averaged model: Orbit propagation considering the influence of Moon perturbation and zonal harmonic J_2. Comparison of the e, ω variation in two model: 1. constant Moon parameters, 2. actual ephemeris of the Moon.

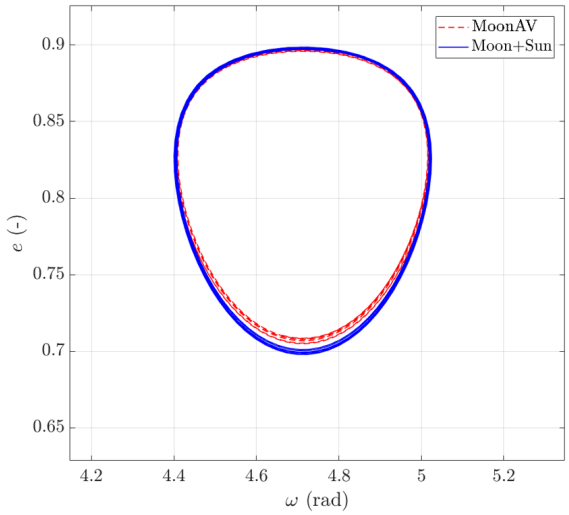

(b) Earth-Moon-Sun triple-averaged model: Orbit propagation comparing two models: 1. Moon and J_2 effect only, 2. Moon, J_2 plus the Sun effect of perturbation.

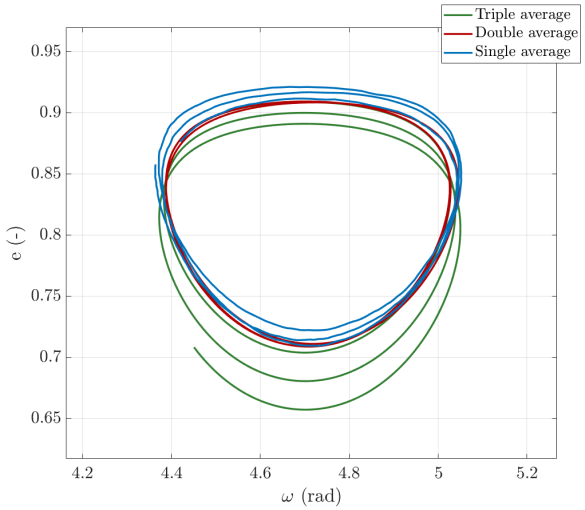

(c) Orbit propagation in the phase space to compare the Single, Double and Triple average model for the fictitious Earth-Moon-Sun system. Both the third bodies perturber are considered on the equatorial plane.

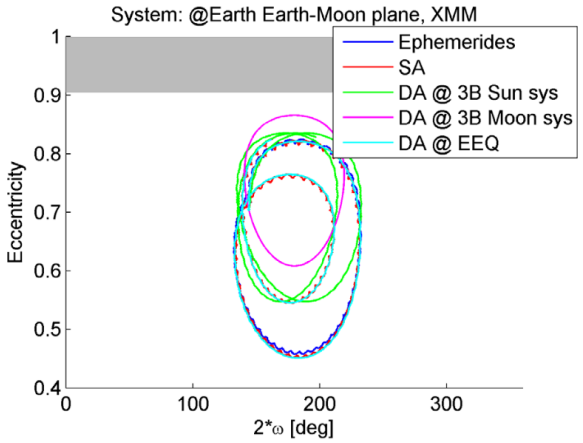

(d) Evolution of a high altitude orbit under the effect of luni-solar and zonal perturbations. Comparison of the actual ephemerides (blue) with single averaged (red) and double averaged (cyan) dynamics in the eccentricity-2ω phase space. (Colombo, [25])

Figure 4.4 Earth's satellite: Comparison of different models to describe the phase space maps.

Earth-Moon-Sun system Now, different maps in (e, ω) were produced to compare the effect of three different level of accuracy in the model:

- Moon and J_2 perturbation only, considering the averaged value of the Moon orbital elements: analytical phase space from the Hamiltonian expression,
- Moon and J_2 perturbation only, considering the actual ephemeris of the Moon at each time step: the (e, ω) evolution is computed by integrating the equations of motion,
- Moon, J_2 and Sun effect, considering the averaged value of the Moon orbital elements.

The results are shown in Figure 4.4. In the first figure (Figure 4.4a), in red is reported the ideal phase space considering constant elements for the Moon orbit, while in blue the corrected variation including the Moon plane effect. The difference in oscillation is present, meaning that the recovery of the real Moon motion is necessary for the analysis. The second figure (Figure 4.4b) shows the effect of introducing the Sun perturbation in the model, as already explained it is essential since it modifies significantly the orbital time evolution.

To understand whether this representation is appropriate for the satellite dynamics propagation, the time evolution was compared with the double averaged orbital elements (computed in Figure 3.6). From the results, it is evident that the approximation is not accurate. This behaviour is due to the strong hypothesis done in Section 4.3, during the node elimination, that the node variation could be cancelled out without changing the actual dynamic of the system. On the other hand, if a hypothetical system considering the Sun and the Moon orbiting on the equatorial plane is considered, the triple averaged model describes very accurately the real dynamics of the system, as in Figure 4.5b. The fictitious phase space is reported in Figure 4.4c. The triple averaged phase space is a good approximation of the single and the double one. Nevertheless, this is a fictitious case and cannot be used for manoeuvre modelling in the Earth environment. This approach is useful to solve the node of the Moon elimination problem.

The results obtained with the triple-averaged model are similar to the phse space obtained for the Earth-Moon system in the Colombo, [25]. The double averaged model, shown in pink in Figure 4.4d, was recovered in the Moon plane considering a rotating reference system to eliminate the node. The other models presented in the study consider also the Sun effect in the inertial equatorial reference frame (EEQ). It can be seen that the results for the single and double-averaged semi-analytical model propagation are a good representation of the real satellite ephemeris. The Earth-Moon-Sun system has a complex dynamics and the nodal elimination has some troubles in producing accurate approximation of the real model.

Venus' probe For the second case under study, phase space maps and numerical evolution of orbital parameter are produced. In this case, where the approximation of having the third body orbiting on the equatorial plane is reasonable, the results of the triple average model are very accurate. Even for a very long time of propagation, the single, double and triple models provide the same results, as shown in Figures 4.6b and 4.6a.

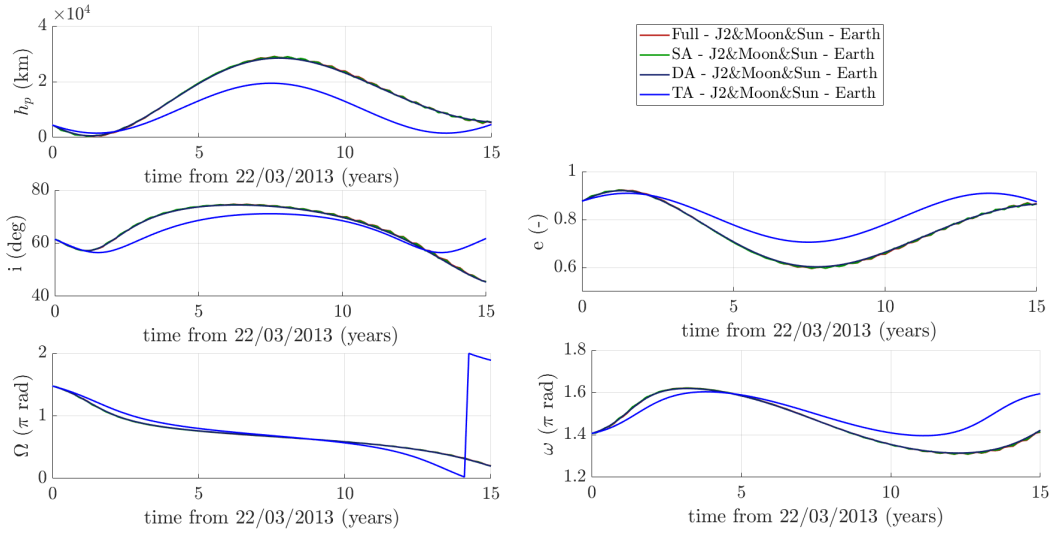

(a) Problem of the node elimination: the time evolution of the triple averaged model do not represent the actual time evolution of the orbit (described by the double and single averaged model).

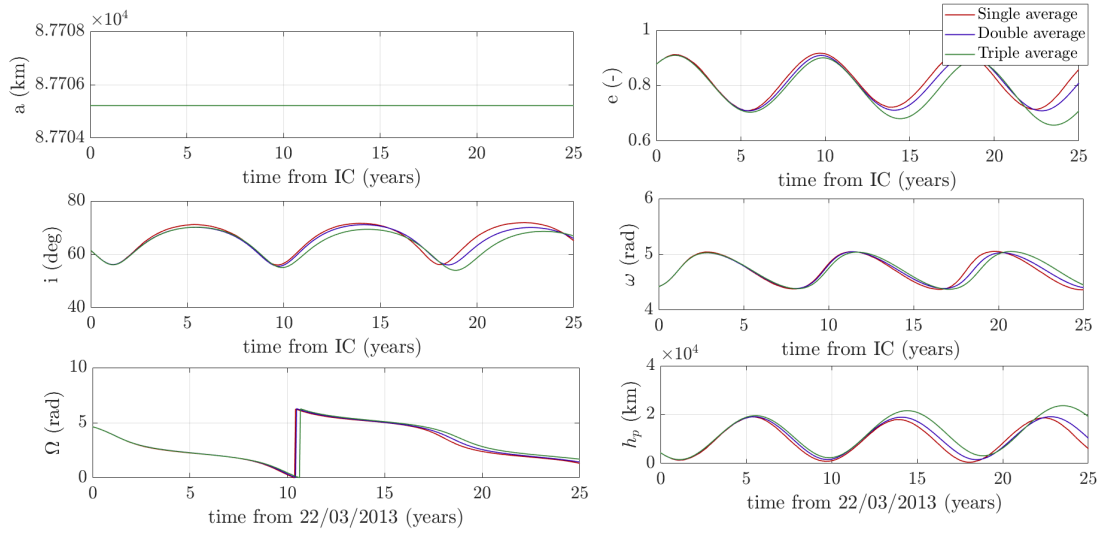

(b) Time evolution for the single, double and triple average model for the fictitious system considering Moon and Sun orbiting on the equatorial plane.

Figure 4.5 Earth's satellite: Comparison of different models to describe the orbital parameters time evolution.

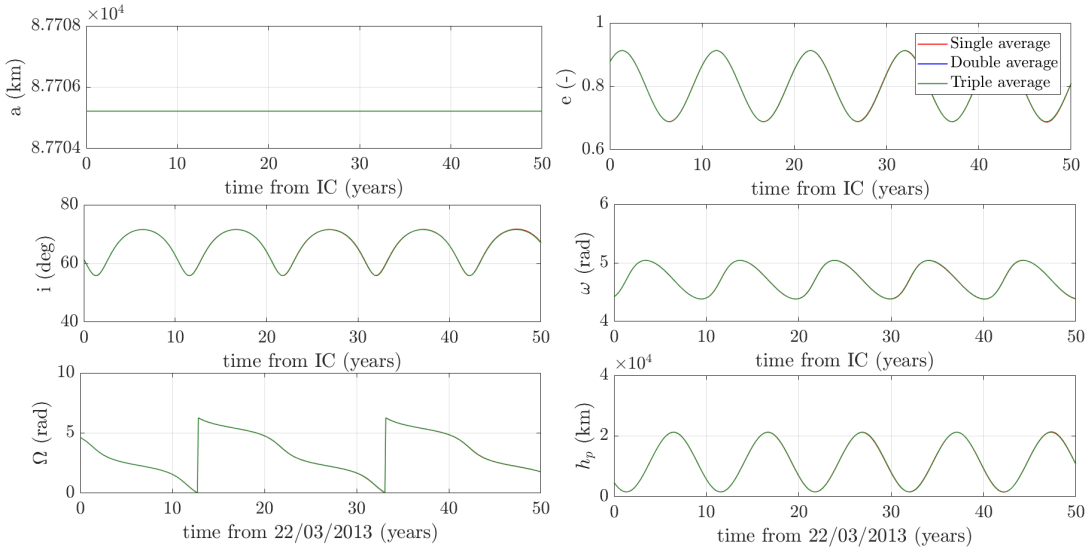

(a) Time evolution for different model (single, double and triple averaged) of a Venu's orbiter, considering Sun's and J_2's effects.

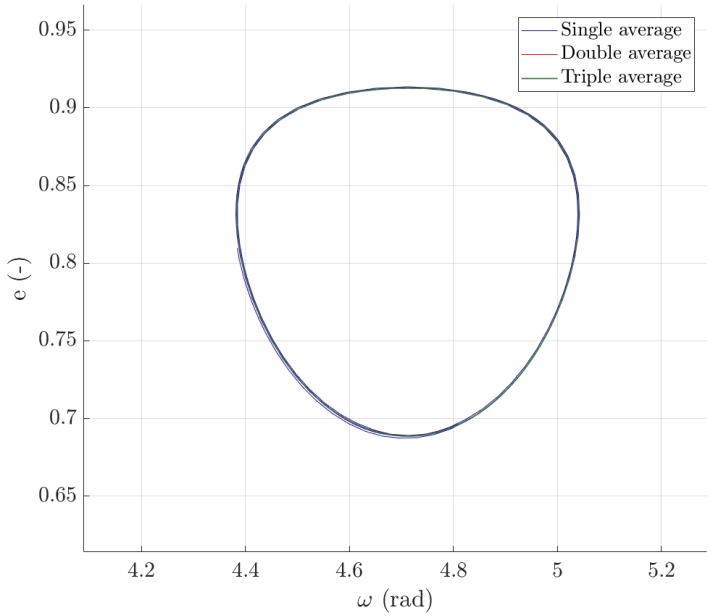

(b) Phase space for a Venus' orbiter under the effects of Sun and J_2 disturbance.

Figure 4.6 Venus' orbiter: Comparison of different models to describe the orbital parameters time evolution.

4.6 Problem of the node elimination

The results are given by the Earth-Moon-Sun model highlight the limitations in the triple-averaged model. In particular, the model developed correctly works for a system where the satellite node is not coupled with the third body node. As a result, approximating the Sun and the Moon on the equatorial plane provides good results as well as the Venus' case.

Nevertheless, the results for the equatorial case reveal how the Earth-Moon-Sun system has a complex behaviour. It is not as simple as the Venus' one, for which the Lidov-Kozai approximation perfectly works. This suggests that different approaches for the elimination of the node should be used. In fact, the idea is very powerful since allows the determination of the critical eccentricity (maximum eccentricity value in time) without propagating the dynamics, but simply by solving the Hamiltonian equation. The limitation of the present model is the non-correct elimination of the node procedure in case of an inclined perturber. This is a very complex problem and should be addressed in future works. Here, two main ideas are proposed to be considered in future works.

Test particle quadrupole approximation Since the variation of Ω is cyclic in time, for a test particle quadrupole approximation, described by Naoz [21], the problem can be written in the invariable plane. It is defined as the plane which has the z-axis aligned with the total angular momentum of the system Earth-Moon-particle. In this case, the total angular momentum is conserved, allowing the elimination of the node by imposing

$$\Omega - \Omega_{\leftmoon} = \pi \tag{4.19}$$

Nevertheless, the dependence upon the RAAN is recovered once the influence of the Sun is added in the model. What can be done in further studies is:

- study if an invariable plane exists for a more complex system, including the effect of both the Sun and the Moon
- the study shall consider Moon and Sun on their actual orbit, i.e. dropping the approximation that the perturbing body are on the same plane.

Semi-analytical solution for the four dofs Hamiltonian Since the double-averaged model was verified upon the actual evolution of the satellite (see also Colombo, [25]), the double-averaged model is appropriate to describe the orbital evolution. Nevertheless, its corresponding Hamiltonian expression is dependent on many variables. Even once the inclination of the

Moon is considered fixed, the Moon node has a very complex behaviour, non-linear in time. This results in four degrees of freedom model plus one (the Moon node). An idea could be to find an analytical or a semi-analytical solution for the stationary points of the expression, by fixing one or more variables in the Hamiltonian: this results in the computation of a local solution, for particular cases of the orbit. In particular, the maximum eccentricity condition is the most important term to recovered for disposal manoeuvre design. In this case, some consideration shall be done:

- the Hamiltonian $\mathcal{H}(e, \omega, i, \Omega) = \mathcal{H}_0(e_0, \omega_0, i, \Omega)$ depends on four variables plus the Moon node $\Omega_{\mathbb{C}}$. The only possible graphical representation is a 3D contour plot, using two variables as a parameter,
- all the coefficient in the Hamiltonian expressions shall be time-invariant: the Keplerian elements of the Moon cannot be updated at each time step by their ephemeris.
- the previous consideration yields to considering a better reference frame were the Moon orbital elements are constant, such as the ecliptic reference system. In this way, there is no need of assuming an averaged value of Moon Keplerian elements (see the studies conducted by Gkolias et al., [51]).

A brief analysis was done to understand the shape of such complicate expression. Since the aim, as it will be explained in Chapter 5, is to identify analytically the maximum eccentricity condition, a first representation could be done by imposing the argument of perigee equal to the value identified by Kozai in his studies. Considering an INTEGRAL-like orbit, the eccentricity stationary points are identified by imposing $\omega = \frac{3\pi}{2}$; moreover, the Moon's node was taken fixed equal to the mean value, otherwise, a 3D representation would not be possible. Hence, the Hamiltonian formulation can be representing in terms of a 3D contour plot, with $\omega = \frac{3\pi}{2}$, as shown in Figure 4.7. Obviously, this phase space does not represent the orbital dynamics, but only the shape of the function once the ω is fixed.

The next step would be to identify a proper analytical relation from the Hamiltonian expression to describe the eccentricity variation:

$$e = e(\omega, \Omega, i) \tag{4.20}$$

In this way the maximum eccentricity condition can be still recovered for defining an optimal disposal manoeuvre.

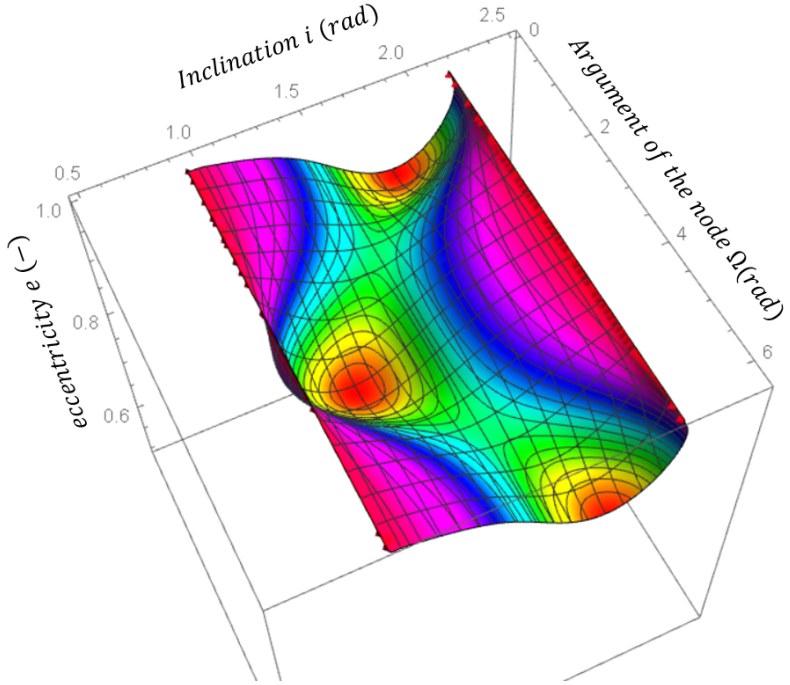

(a) 3D Hamiltonian phase space in the (e, Ω, i) space.

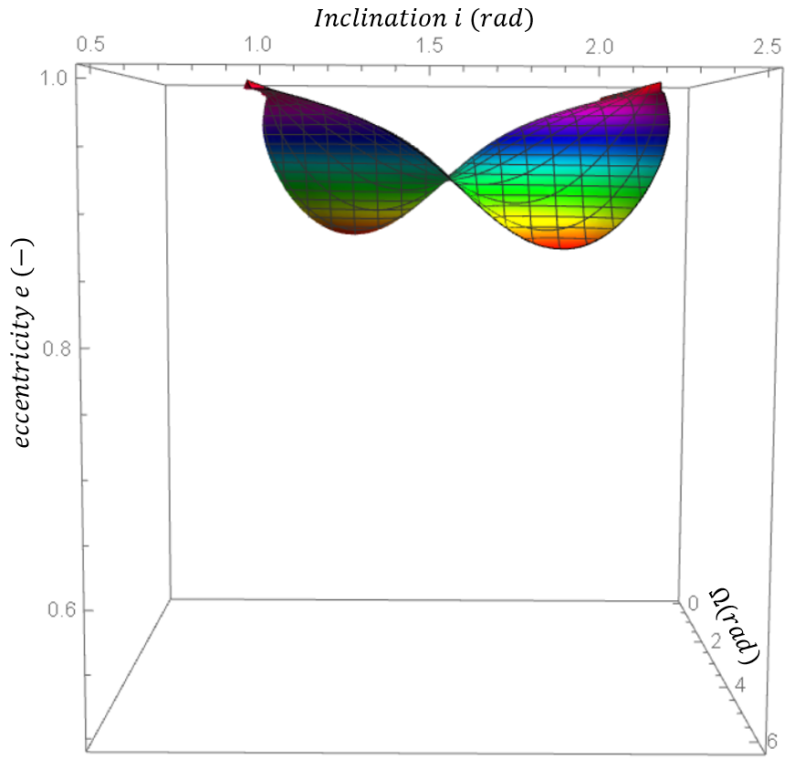

(b) 3D Hamiltonian phase space in the (e, i) plane.

Figure 4.7 3D Hamiltonian phase space for $\omega = 3\pi/2$.

Chapter 5

Disposal Manoeuvre Strategy

The disposal manoeuvre at the end-of-life is essential to reduce the amount of space debris in orbit and to control the collision probabilities of spacecraft-debris and debris-debris. In fact, as already introduced in Chapter 1, the Inter-Agency Space Debris Coordination Committee (IADC)[1] set some guidelines for space debris mitigation around the Earth. For the HEO, two possible strategies can be used (Colombo et al., [26]):

- target a re-entry trajectory, using the natural decay due to atmospheric drag for the satellite disintegration,
- target a graveyard orbit, whenever the re-entry is too expensive, by assuring no dangerous interaction with other orbiting objects.

In both cases, there should be no interaction at all with other orbiting objects, and some very stringent regulation exists in case of a passage in the protected region (GEO and LEO). In this chapter, both approaches are analysed. The former is based on the consideration that satellites, orbiting on a trajectory with at least the perigee below the atmospheric interface, suffer the drag effect and tends to naturally decay towards the Earth surface. The atmospheric interface is typically set at 120 km for the Earth, and at 250 km for Venus (Sgobba, [52]; Justus and Braun, [53]), above that altitude, the drag effect is not significant for the orbital parameters evolution. As a case of study, in this chapter, the disposal trajectory for the Earth is analysed, but the discussion is general, and the procedure is valid also in case of Venus' probe.

Below 120 km, the re-entry results in the space vehicle breakup. The major breakup shall result in a minimal amount of survival mass at the Earth's surface. The secondary

[1] `https://www.iadc-online.org/`, last visited 24/10/2018

risk is evaluated for each re-entry vehicle: the probability of impact with the ground must be minimised since it could lead also to human casualties. The risk for aviation or other operative satellites impact is considered as well, but it's very difficult to produce a precise model during the uncontrolled re-entry.

A better approach is to develop at least a semi-controlled re-entry, with known orbital parameters at the atmospheric interface (Gaudel et al., [54]; Comellini et al., [55]; ESA, [56]). In this way, the risk assessment is more accurate since the satellite is inserted in a specific trajectory. The second strategy aims to target a graveyard orbit. This is a special type of orbits out of the operational belts, where the orbital perturbations are so that the evolution in time maintain the orbit in a preselected area around the Earth: it almost impossible to have an atmospheric re-entry. This is a strategy currently adopted for geostationary satellites, that requires a high delta-v to de-orbit toward the Earth. The assessment of these family of orbits is achieved by raising the perigee of about 200 km (Ailor, [31]; Thompson et al., [57]). Note that IADC defines very stringent normative for satellites in GEO belts. The manoeuvre shall assure that the satellite remains in its end-of-life orbit without interfering with other space missions.

The strategy developed in this work consists of targeting specific condition for the disposal in terms of Keplerian parameters. A single manoeuvre is performed during the natural evolution of the spacecraft. The aim of the manoeuvre is to produce a change in the orbital parameter so that the resulting trajectory evolution in time produces a perigee altitude below 120 km in case of Earth's re-entry, or an increase of perigee that assures the minimum magnitude of oscillation of parameters in time. For the Venus' atmospheric entry the target perigee should be below 250 km. The new set of the orbital elements, after the Δv is produced, is propagated in time, considering the effect of external source of perturbation through the dual averaged disturbing potential function (Colombo, [25]).

Venus atmospheric entry condition The atmospheric entry for the disposal strategy of Venus' orbiter was adopted in the past for some missions, such as the Venus Express, which ends its operative life with a de-orbit trajectory (Svedhem et al., [58]). The de-orbit happens when the perigee altitude is below the atmospheric interface. Since the atmosphere of Venus is very dense, it is not necessary to set a low altitude as for the Earth's case. For Venus express, the drag effect starts being significant below 200 km. In addition, in the upper atmosphere very strong winds are presents (of about 400 m/s^2).

[2] from NASA Venus Express Mission Information: `https://pds.nasa.gov/ds-view/pds/viewMissionProfile.jsp?MISSION_NAME=VENUS%20EXPRESS`, last access: 11/2018

To maintain the operative orbit of Venus Express during the mission extension several perigee rising were performed to gain a altitude above 200 km. For this reason, the atmospheric entry condition was set at 130 km for Venus' orbiter:

$$h_{p,min} = \min\{h_{p,min}(t)\} < 130\,\text{km} \tag{5.1}$$

The minimum perigee altitude depends on the orbital elements:

$$\begin{aligned} r_p &= a(1-e) \\ h_p &= r_p - R_{\varnothing} \end{aligned} \tag{5.2}$$

Hence, the target perigee is related to critical eccentricity, once the semi-major axis is defined:

$$e_{cr} = 1 - \frac{h_{p,min} + R_{\varnothing}}{a} \tag{5.3}$$

Earth re-entry condition The condition for the re-entry is related to the minimum perigee altitude obtained during the evolution of the new orbital parameter:

$$h_{p,min} = \min\{h_{p,min}(t)\} < 120\,\text{km} \tag{5.4}$$

Note that from IADC normative, the time spent in LEO region should be at maximum 25 years. Nevertheless, the time span available for the re-entry can be even longer. This thesis investigates the possible solution for 25 years from the initial condition, setting a re-entry time window $\Delta t_{re-entry}$, where the target perigee is related to critical eccentricity, once the semi-major axis is defined:

$$e_{cr} = 1 - \frac{h_{p,min} + R_{\oplus}}{a} \tag{5.5}$$

This relation is very important, since allows the analysis in the (e, ω) phase space. Hence, the aim of the re-entry manoeuvre is to target both the minim perigee and the critical eccentricity for the orbit.

Graveyard orbit To target a graveyard orbit, the condition to be achieved is the reduction of the oscillation of the orbital parameters. In particular, the eccentricity variation in the new Keplerian elements during the time propagation shall be minimised:

$$\min \quad \Delta e, \tag{5.6}$$

where Δe is defined as $e_{max} - e_{min}$. In this case, looking at the (e, ω) phase space, the resulting final orbits is a smaller oval concentric to the first one: both the maximum and the minimum eccentricity changes, the former decreases, the latter increases. This causes also the argument of perigee to change, and its variation is reduced: min $\Delta\omega$ with $\Delta\omega = \omega_{max} - \omega_{min}$. This is a completely different approach respect to the earth re-entry and therefore would require a different treatment also for the manoeuvre optimisation. In fact, the reduction of the maximum eccentricity value during orbit propagation generates a rising in the minimum perigee altitude, as it was required by normative.

Delta-v design The delta-v design follows the approach described in Colombo et al., [24] and Colombo, [25]. The variation of the orbital parameter is studied through the Gauss equation in Section 2.5.3. The impulsive manoeuvre in terms of $\mathbf{\Delta v}$ is described in the $\hat{\mathbf{t}}, \hat{\mathbf{n}}, \hat{\mathbf{h}}$ frame by:

- the magnitude of the impulse Δv,
- the in-plane angle: α,
- the out-of plane angle: β.

The $\hat{\mathbf{t}}, \hat{\mathbf{n}}, \hat{\mathbf{h}}$ frame is defined as: $\hat{\mathbf{t}}$ tangent to the orbit to the velocity vector, $\hat{\mathbf{h}}$ in the direction of orbit angular momentum and $\hat{\mathbf{n}}$ to complete the orthogonal frame.

$$\hat{\mathbf{t}} = \frac{\mathbf{v}}{||\mathbf{v}||} \tag{5.7}$$

$$\hat{\mathbf{n}} = \hat{\mathbf{h}} \times \hat{\mathbf{t}} \tag{5.8}$$

$$\hat{\mathbf{h}} = \frac{\mathbf{r} \times \mathbf{v}}{||\mathbf{r} \times \mathbf{v}||} \tag{5.9}$$

The geometry of the $\mathbf{\Delta v}$ is represented in Figure 5.1. The impulse is characterised by three components: tangential, normal and out-of-plane. The mathematical description is provided in terms of the angles α, β.

$$\mathbf{\Delta v} = \Delta v \begin{bmatrix} \cos\alpha\cos\beta \\ \sin\alpha\cos\beta \\ \sin\beta \end{bmatrix} \tag{5.10}$$

This $\mathbf{\Delta v}$ provides a finite variation in the orbital elements as $\Delta\mathsf{kep} = \mathsf{Gauss}\Big(\mathsf{kep}(t_m), f_m, \mathbf{\Delta v}\Big)$. Once the variation of the orbital elements is computed from the manoeuvre, the new orbital

parameters are computed as:

$$\mathsf{kep}_{\mathsf{new}} = \mathsf{kep}(t_m) + \Delta\mathsf{kep} \tag{5.11}$$

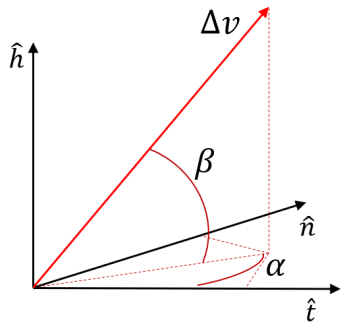

Figure 5.1 Impulse representation of the in-plane and out-of-plane angle α, β in the t, n, h reference frame.

5.1 Disposal manoeuvre design

To understand how the delta-v changes the orbit, the phase space can be used to compute the eccentricity evolution of the orbit, as proposed in Colombo et al., [4]. In fact, the phase space representation is very intuitive and allows the visualisation of the manoeuvre effect. The delta-v will change the condition of the orbital parameter so that the final trajectory in the phase space would target the critical eccentricity. This means that the final trajectory is tangent to that value, indicating that in time the re-entry condition is achieved.

A first simple approach is to target another trajectory in the same phase space, for which the maximum eccentricity is the critical one. The impulsive manoeuvre shall provide a variation in eccentricity and anomaly of perigee only, maintaining the semi-major axis invariant. This approach is represented in Figure 5.2a. A second approach is to provide an impulsive manoeuvre, which changes also the semi-major axis. This provides a variation of the phase space representation. Depending on the new value of the semi-major axis, the Hamiltonian contour line could translate up or down. For a reduction of a, the phase space translates towards higher values of the eccentricity, enhancing the disposal condition. These approaches are represented in Figure 5.2b.

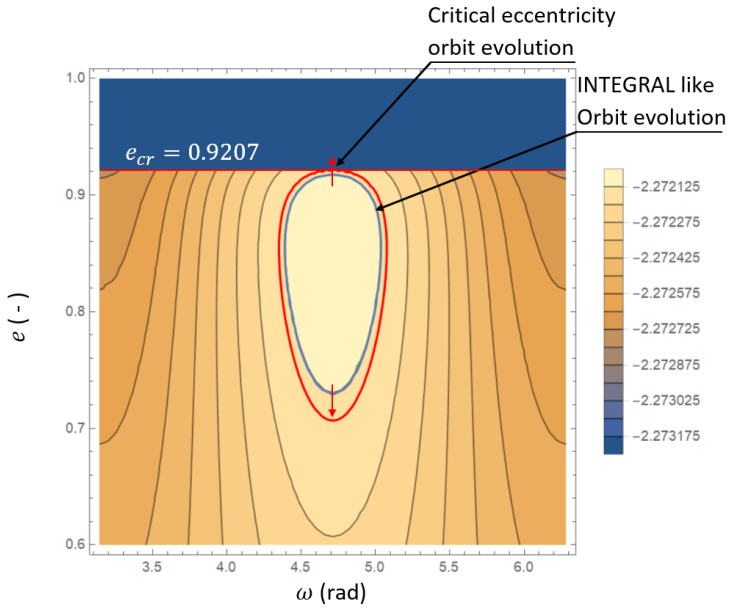

(a) Phase space for a = 87 702.5 km and $\Theta_{kozai,0}$ = 0.215192. The blue trajectory represents the time evolution of the initial orbit. The red trajectory is the target trajectory corresponding with to the critical eccentricity.

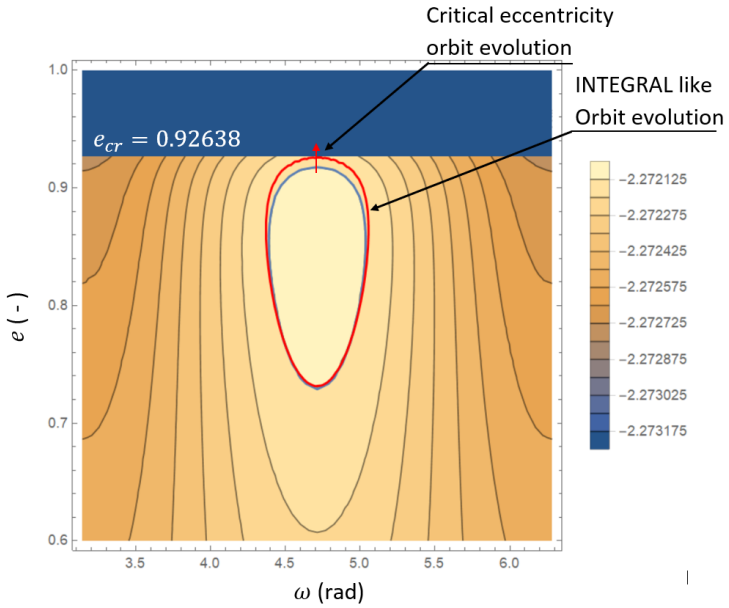

(b) Initial phase space for a = 87 702.5 km and $\Theta_{kozai,0}$ = 0.215192. The blue trajectory represents the time evolution of the initial orbit. After the manoeuvre, new phase space with a = 87 319.2 km and $\Theta_{kozai,0}$ = 0.20437. The red trajectory is the target trajectory corresponding with to the critical eccentricity.

Figure 5.2 Representation of different strategy for the disposal.

5.2 First case: impulse in normal direction ($\alpha = 90°$)

The first case analysed consist of a manoeuvre that does not change the orbit semi-major axis. This is the case of an impulse with null tangential component, hence, the in-plane contribution is all in the normal direction: the in-plane angle is set to α =90°. The impulse is described by the magnitude Δv and the out of plane angle β, while α is fixed. From the analytical expression of the semi-major axis variation in the Gauss equation, the constancy of a is demonstrated if the $\mathbf{\Delta v}$ component in the tangential direction is null: $\delta v_t = 0\,\mathrm{km/s}$:

$$\delta a = \frac{2a^2 v_d}{\mu}\delta v_t = 0 \qquad \rightarrow \qquad a = const \tag{5.12}$$

The manoeuvre changes the parameters of the satellites in terms of e, ω, i, Ω, according to Gauss equations of motions (Equation (2.15))). Since the semi-major axis stays constant, the assessment of a lower perigee is due to an increase of the maximum value of the eccentricity in time. Therefore, the amplitude in eccentricity oscillations is enlarged.

5.3 Second case: impulse in a generic direction

This second case, differently from the previous one, consists of an impulse given in a generic direction: both angles α and β can assume a generic value. This results in a variation also in the semi-major axis. Given the impulse $\mathbf{\Delta v}$, the variation in the Keplerian elements are given by the Gauss equations, reminding that the target is always a trajectory with a lower perigee, i.e. it reaches the critical eccentricity value, as the red trajectory in Figure 4.4. The variation in the orbital parameters shall provide a trajectory with the maximum eccentricity equal to the critical one, hence the phase space contours translate up through higher eccentricity values. The translation upwards is obtained with a reduction of the semi-major axis for the final orbit.

5.4 Optimisation procedure

An optimisation procedure is necessary to evaluate which is the optimal impulse that provides the desired solution, not only the magnitude of the impulse is optimised, but also its direction. For each initial condition, the re-entry manoeuvre is assessed through an optimisation procedure. This aims to determine the optimal parameters for the definition of the $\mathbf{\Delta v}$ impulse and the optimal true anomaly for the manoeuvre f_m. An optimal set of parameter is defined: $\mathbf{x} = [\alpha, \beta, \Delta v, f_m]$. The optimisation procedure is used to

determine the optimal solution for the target eccentricity and the minimum $\mathbf{\Delta v}$. Hence, it is a multi-objective optimisation, but the former condition related to the minimum perigee has a higher relative importance than the delta-v optimisation. A multi-objective optimisation (Shirazi,[59]) aims to optimise more than one function of merit. The cost function for the optimal control problem is select as a quadratic function, that shall provide the solution with the desired accuracy. The general expression of a multi-objective cost function is:

$$\begin{aligned} J &= \frac{1}{2}\sum_i \lambda_i J_i \\ J_i &\rightarrow \text{quadratic function} \\ \lambda_i &\rightarrow \text{weighting function} \end{aligned} \tag{5.13}$$

5.4.1 Cost function for the optimal altitude: Earth's or Venus' re-entry

The aim of the optimisation is to target the re-entry altitude, set below the atmospheric interface. The disposal manoeuvre shall target the critical eccentricity, corresponding to 50 km of altitude for the Earth's case and to 130 km for Venus. The maximum eccentricity value reached during the long-term propagation shall be compared with the critical one e_{cr}, so that the goal of the optimisation is

$$e(t*) = e_{cr}. \tag{5.14}$$

Nevertheless, the eccentricity is a very small value and for the optimisation is better to switch to the altitude difference. From the eccentricity, the value of the perigee altitude is easily recovered as:

$$h_p = r_p - R_\alpha, \qquad \text{where} \qquad r_p = a(1-e^2), \tag{5.15}$$

where $r_{p,min}$ is the perigee radius, and R_α is the planet mean equatorial radius. The altitude accuracy is defined through the following cost function:

$$J_{h_p} = \max\left(\frac{h_{p,min} - h_{p,target}}{h_{p,target}}, 0\right)^2 \tag{5.16}$$

Differently from the cost function used in Colombo et al., [24], the variation in the perigee altitude is divided by the target altitude since it represents the accuracy coefficient for solution determination and acts as a weighting coefficient for the objective function, resulting in an a-dimensional cost function.

5.4.2 Cost function for the optimal graveyard trajectory

For the orbits whose Earth's re-entry is too expensive or it is not feasible due to the violation of normative, the end-of-life is designed through a graveyard trajectory. In this case the eccentricity and the argument of perigee oscillations shall be minimised together with a rise of the perigee. Hence that the goal of the optimisation is

$$\min \quad \Delta e(t) \tag{5.17}$$

Moreover, the variation of the perigee anomaly $\Delta\omega$ is minimised as well to enhance the convergence of the solution. Hence, the cost function shall consider both conditions:

$$J_{grv} = \max\left(\frac{e_{max} - e_{min}}{e_{min}}\right)^2 + \max\left(\frac{\omega_{max} - \omega_{min}}{\omega_{min}}\right)^2 \tag{5.18}$$

5.4.3 Cost function for the optimal Δv cost

The second objective of the optimisation is to maintain the Δv cost the smallest as possible. The onboard fuel at the end of mission is typically very low, and the aim of the strategy shall be to use as much as possible the natural evolution and reducing the propellant consumption. The mass of the propellant used during the manoeuvre is:

$$\Delta v = g_0\, I_{sp}\, \ln(MR), \tag{5.19}$$

where $g_0 = 9.81\,\mathrm{m/s^2}$, I_{sp} is the specific impulse, MR is the mass ratio: $\frac{1}{MR} = 1 - \frac{m_p}{m_0}$, with m_p the propellant mass and m_0 the initial total mass. The cost function for the Δv cost is selected as a quadratic function as:

$$J_{\Delta v} = \left(\frac{\Delta v}{\sigma_v}\right)^2 \tag{5.20}$$

where $\sigma_{\Delta v}$ is set equal to $1\,\mathrm{km/s}$ to have an a-dimensional representation of the cost function.

5.4.4 Cost function for the optimisation procedure

The goals for the cost function are identified by the performance indexes previously defined by J_{h_p}, J_{grv} and $J_{\Delta v}$. Two cost functions are identified for the different end-of-life strategy.

In case of EARTH'S RE-ENTRY, the cost function used in the optimisation is:

$$\begin{aligned} J =& \frac{1}{2}\left(\mathcal{K}J_{h_p} + \mathcal{W}J_{\Delta v}\right) \\ =& \frac{1}{2}\left(\mathcal{K}\max\left(\frac{h_{p,min} - h_{p,target}}{h_{p,target}}, 0\right)^2 + \mathcal{W}\left(\frac{\Delta v}{\sigma_v}\right)^2\right) \end{aligned} \tag{5.21}$$

where $\mathcal{K}, \mathcal{W}$ are the weighting constants for the optimisation, set as:

$$\mathcal{K} = 1 \qquad \text{and} \qquad \mathcal{W} = 1 \times 10^{-2} \tag{5.22}$$

On the other hand, the cost function used for the GRAVEYARD ORBIT is:

$$\begin{aligned} J =& \frac{1}{2}\left(\mathcal{K}J_{grv} + \mathcal{W}J_{\Delta v}\right) \\ =& \frac{1}{2}\left(\mathcal{K}\left(\frac{e_{max} - e_{min}}{e_{min}}\right)^2 + \left(\frac{\omega_{max} - \omega_{min}}{\omega_{min}}\right)^2 + \mathcal{W}\left(\frac{\Delta v}{\sigma_v}\right)^2\right) \end{aligned} \tag{5.23}$$

Where $\mathcal{K}, \mathcal{W}$ are the weighting constants for the optimisation, set as:

$$\mathcal{K} = 1 \qquad \text{and} \qquad \mathcal{W} = 5 \times 10^{-4} \tag{5.24}$$

The main difference with the cost function used in previous works, Colombo et al., [24] and Colombo, [25], is the insertion of the weighting factors ($h_{p,target}$, σ_v, e_{min} and ω_{min}) to refer the cost function to the target condition. The weights act as accuracy coefficient and make the cost function a-dimensional. The weighting constant $\mathcal{K}$ and $\mathcal{W}$ have been selected to grant the convergence in terms of target perigee for the re-entry condition and minimum variation of the eccentricity for the graveyard case. The delta-v is optimised only after the target condition has been reached.

The procedure is performed with a multi-start method, for the search of the best local minima. The `MultiStart.m` algorithm in MATLAB® generates multiple local solutions starting from various initial points. The solution is generated in the `GlobalOptimSolution.m`. This is a MATLAB® object containing information on the local minima: the value of the local minimum, the objective function value, the start and the point that leads to the minimum. On the other hand, in Colombo et al., [24], the optimisation was done with the genetic algorithm only. In that work, the optimisation was performed introducing the tournament selection and mutation to maintain the genetic diversity and enhance the algorithm convergence.

5.4.5 Disposal constraint

The optimisation problem is not an un-constrain problem but requires the setting of bounds and constraints. Linear and non-linear constraints can be imposed on the procedure, using the `createOptimProblem.m` function. The optimisation is based on the set of parameters $[\alpha, \beta, \Delta v, \theta_m]$, that, during the optimisation process, can varies in a certain interval:

$$\begin{aligned} &\alpha \in (-\pi, \pi) && \beta \in (-\pi/2, \pi/2) \\ &\Delta v \in (\Delta v_{min}, \Delta v_{max}) && \theta_m \in (-\pi, \pi) \end{aligned} \tag{5.25}$$

Where the bounds in Δv are mission dependant. On the other hand, some nonlinear constraints are imposed on the minimisation.

1. The perigee radius shall be higher than the Earth radius: $h_p > 0$.

2. The new target orbit shall be elliptical: $e_{new} \in (0, 1)$

5.4.6 Optimal single impulse design

The strategy adopted in this work consists of exploiting one single manoeuvre to assess the final orbit. In a further study, a multi-manoeuvre design can be developed. The design of the manoeuvre is different depending on the application, which could be both an atmospheric re-entry or a graveyard trajectory. For both cases, a semi-analytical and a fully-analytical one is described.

Semi-analytical approach

The numerical modelling of the disposal trajectory was developed in several past works (Colombo et al., [4]; Colombo et al., [24]; Colombo, [25]). The strategy is based on the assessment of the target condition by integrating numerically the orbital elements of the satellite, using the double averaged model derived in Chapter 3. The orbit propagation defines if the spacecraft reaches the desired condition. At first, the delta-v impulse is applied to the initial conditions, then from Gauss equations (Equation (2.15)), the new Keplerian elements are defined as:

$$\mathrm{kep_{new}} = \mathrm{kep(t_m)} + \Delta\mathrm{kep} \tag{5.26}$$

The orbital propagation is performed using the double averaged model of the disturbing function using the Lagrange Planetary equations (Equation (2.8)), which results in a

high computational cost for the algorithm. From the numerical propagation, the disposal condition is checked:
For planets' re-entry case (either Earth or Venus), the maximum eccentricity condition is investigated to search the minimum perigee condition:

$$e_{max} = \max\left(e_{new}(t)\right) \quad \Rightarrow \quad h_{min}(e_{max}) \tag{5.27}$$

If the minimum perigee is equal or below the target one, the re-entry is assessed.
For the graveyard orbit definition, the maximum variation in eccentricity and perigee anomaly is detected:

$$e_{max} = \max\left(e_{new}(t)\right) \tag{5.28}$$

$$e_{min} = \min\left(e_{new}(t)\right) \tag{5.29}$$

$$\omega_{max} = \max\left(\omega_{new}(t)\right) \tag{5.30}$$

$$\omega_{min} = \min\left(\omega_{new}(t)\right) \tag{5.31}$$

From these conditions, the approach is to make the orbit as stable as possible using the available on-board fuel, minimising the variations: $e_{max} - e_{min} \rightarrow 0$ and $\omega_{max} - \omega_{min} \rightarrow 0$.

Fully-analytical approach

Differently from the semi-analytical approach, the fully-analytical one, developed in this work, relies on the Hamiltonian formulation to compute the maximum eccentricity condition. This approach was firstly investigated by Colombo et al., [4], considering only the Moon perturbing effect and using the Moon plane as the reference one. The power of this approach consists in avoiding the numerical propagation of the orbit. In this way, the computational effort is reduced in the optimisation, resulting in a much lower overall time.

Differently, from the previous work, Colombo et al., [4], the triple-averaged approximation considers a more complex model: it includes the J_2 effect and the Luni-Solar disturbance for the Earth-Moon-Sun system and the Sun and the J_2 effect for the Venus-Sun system. The previous works add those contributions numerically to the semi-analytical code, to recover the accuracy of the representation. The novelty of this work is, therefore, the development of a fully-analytical model including all the major disturbance contribution for an orbiter on a HEO around a generic planet (Earth or Venus). Note that the main limitation of the presented model is the low accuracy for the Earth-Moon-Sun system, where the dynamics are very complex and the triple averaged model, resulting from the elimination of the node,

does not represent the actual dynamics, differently from the second averaged model, and can be used only for a very preliminary design. Nevertheless, this model is able to compute the target eccentricity condition by solving the analytical expression of the triple-averaged Hamiltonian representation: starting from the satellite initial condition, the orbit dynamics is described by one equation only. Therefore, the computational time for the optimisation is significantly reduced with respect to the semi-analytical approach.

The following approach was selected. As for the semi-analytical case, the delta-v impulse is applied to the initial conditions through the Gauss equations:

$$\mathrm{kep}_{\mathrm{new}} = \mathrm{kep}(\mathrm{t_m}) + \Delta\mathrm{kep} \tag{5.32}$$

The new orbital parameters define a new trajectory in the phase space. By considering the Hamiltonian as a function of (e, ω) only, the stationary conditions could be identified simply by solving an equation. The stationary points of the Hamiltonian can be investigated considering the function $f = \mathcal{H}(e, \omega) - \mathcal{H}(e_0, \omega_0)$. The solutions are recovered by imposing correctly the initial guess in the `fsolve.m` function of MATLAB® . The maximum and minimum eccentricity condition is in correspondence of $\frac{3\pi}{2}$, while the stationary points of ω are orbit dependant. For the Earth's re-entry case, using the maximum e, the minimum perigee altitude can be recovered. While for the graveyard orbits, the stationary conditions directly enter in the cost function. The power of the fully-analytical approach is based on the computational time to find the stationary points conditions. The difference in time spent by the algorithm is reported in Table 5.1. The performances are referred to the following processor: 2.60 GHz and 16.0 GB of RAM. It is evident that the computational time is reduced significantly, yielding to the necessity of developing a much more accurate analytical model.

Table 5.1 Difference in computational time between a numerical and a semi-analytical approach.

Semi-Analytical	
Orbit propagation for 25 year	30.63 s
Optimisation with `MultiSart.m`	3-4 h
Fully-Analytical	
Stationary points solution with `fsolve.m`	0.021 63 s
Optimisation with `MultiStart.m`	10-15 min

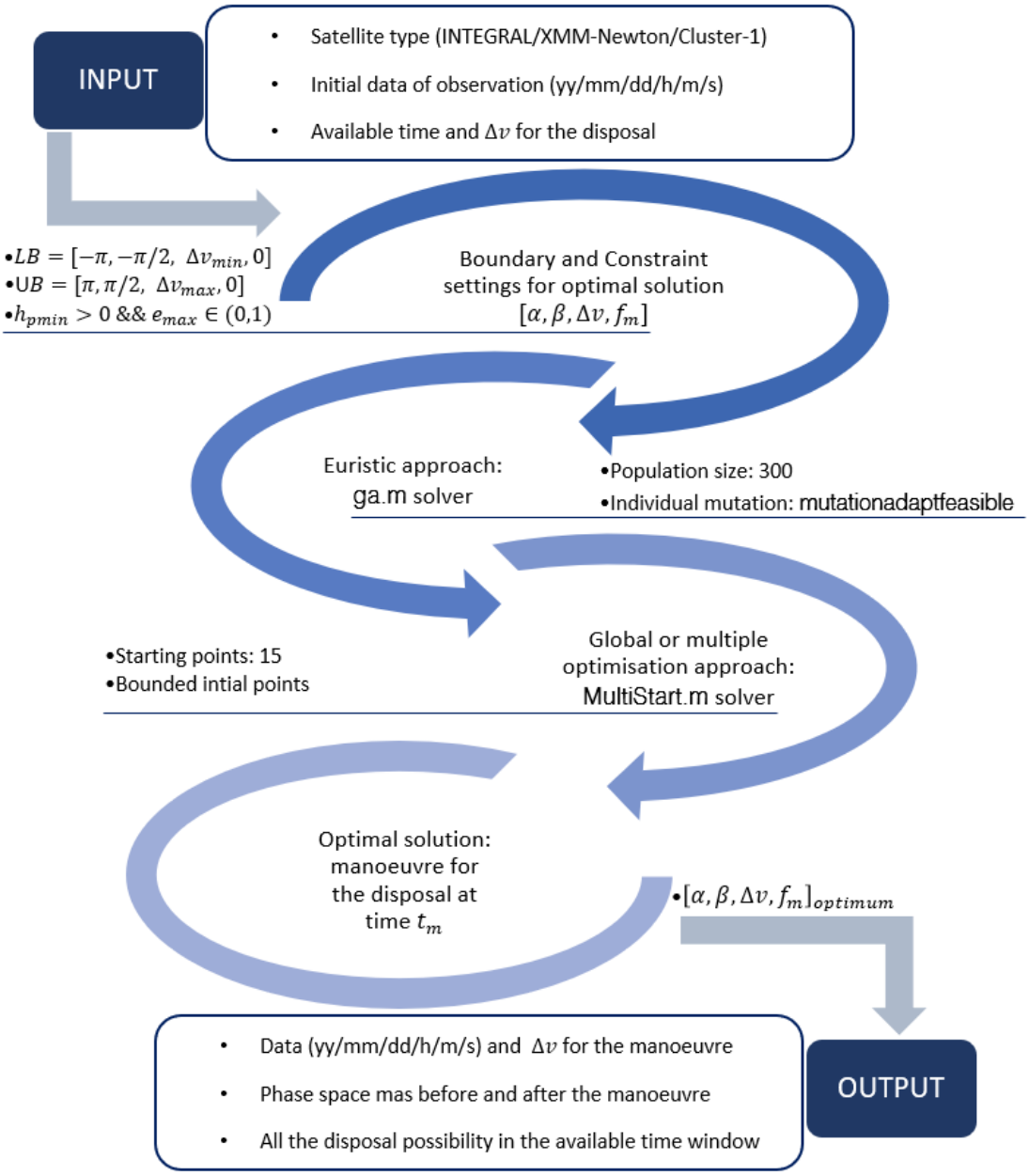

Figure 5.3 Flow chart of the optimisation procedure algorithm used in the manoeuvre design.

5.4.7 Disposal Algorithm

The logic behind the disposal algorithm is shown in figure Figure 5.3. Starting from the initial orbital parameters of the satellite, the algorithm requires in the input only three initial conditions:

1. initial data of observation at $T_0 = [yy, mm, dd, h, min, sec]$,
2. Satellite ephemeris at T_0: $\text{kep}_0 = \{a_0,\, e_0,\, i_0,\, \omega_0,\, \Omega_0,\, M_0\}$,
3. maximum Δv available onboard.

Then, two different solvers are used to validate the procedure. At first the `ga.m` solver was used, as in Colombo, [25]. The Genetic Algorithm (`ga.m`) is a heuristic method based on the natural evolution theory. It is based on the natural selection process to eliminates the bad conditions from one generation to another: during the iterations only, the best solution passes at the successive generation yielding to the best fitness selection. In addition, during the process the mutation was introduced to maintain the diversity within the population: this prevents a premature convergence and ensures that the algorithm terminates once there is no significant difference between two consecutive generations.

On the other hand, the same solution was computed with `MultiStart.m`. It does not rely on a heuristic method, but the solver searches the best solution by running multiple local solvers starting from various points. It uses a non-linear programming solver (`fmincon.m`) to find the minimum of a constrained multi-variable function. The assessment of the convergence of this algorithm is more difficult than for the Genetic Algorithm. It is very important to correctly impose the initial conditions and the solver options: the settings of the number of initial points to run is essential to achieve the convergence. In addition, it must be specified that the initial points should be within the bounds of the inequalities constraints.

The initial conditions for the optimisation are defined by the delta-v parameters: angles (α, β) and magnitude Δv. In addition, the solver can select the best true anomaly for the manoeuvre, since in the single and double-averaged approach the dependence on it was cancelled out: each solution is valid for any value of the true anomaly values along the orbit. This should be in any case checked at the end of the optimisation, verifying that the target condition is reached.

$$x = [\alpha,\, \beta,\, \Delta v, f] \tag{5.33}$$

The value of the objective function defines the accuracy of the solution: one solution is better than another if the objective function is smaller. In particular, `MultiStart.m` and

`ga.m` take more or less the same function evaluations for the computation of the optimal solution, providing two equivalent optimum points. Nevertheless, MultiStart takes about half of the time to find the minima, hence it results more efficient for the case under study.

For both the solvers, the same objective function was considered. For the Earth and Venus re-entry cases it is reported in Equation (5.21), while for the Graveyard orbit see the relation in Equation (5.23):

$$\begin{aligned} J_{re-entry} &= \frac{1}{2}\left(\mathcal{K}\max\left(\frac{h_{p,min}-h_{p,target}}{h_{p,target}},0\right)^2+\mathcal{W}\left(\frac{\Delta v}{\sigma_v}\right)^2\right) \\ J_{graveyard} &= \frac{1}{2}\left(\mathcal{K}\left(\left(\frac{e_{max}-e_{min}}{e_{min}}\right)^2+\left(\frac{\omega_{max}-\omega_{min}}{\omega_{min}}\right)^2\right)+\mathcal{W}\left(\frac{\Delta v}{\sigma_v}\right)^2\right) \end{aligned} \tag{5.34}$$

Finally from the optimisation procedure, the optimal parameters of the manoeuvre are defined: epoch of the manoeuvre (date and f_m), optimal impulse (α_{opt}, β_{opt}, Δv_{opt}).

MultiStart option settings To have a correct optimisation procedure, the algorithm shall be set correctly. Upper and lower bounds as well as the constraint tolerance should be identified. The bounds for the optimal parameter, $x = [\alpha, \beta, \Delta v, \theta_m]$, are defined as:

```
LB = [-pi   -pi/2   Dv_min    0  ]; % low boundary
UB = [ pi    pi/2   Dv_max   2*pi]; % upper boundary
```

Where the constraint upon the delta-v is mission dependent. For what concerns the tolerance definition, the Optimality and the Constraint should not be less than 10^{-9} to avoid convergence problems in the algorithm. On the other hand, the tolerance between two successive function evaluations should be more stringent to assure the correct convergence. The options for the `MultiStart.m` solver can be set with `optimoptions.m`

```
options = optimoptions(@fmincon,'TolFun',1e-20,'PlotFcns',@optimplotfval,...
'ConstraintTolerance',1e-9,'OptimalityTolerance',1e-9);
```

MultiStart problem definition Here the settings for the MultiStart solver are presented and analysed. Once the bounds and the options are set up, the problem should be defined by the function `createOptimProblem.m`. The initial conditions were set equal to the lower boundary; then the bounds and the non-linear constraints were applied.

```
problemMS = createOptimProblem('fmincon','x0',LB,...
'objective',@(x)optimalDV_disposal_3(x, IC, DATA),...
'lb',LB,'ub',UB,'nonlcon',@(x) myConstrain(x,IC,DATA),'options',options);
```

At this point the `MultiStart.m` algorithm is set, imposing the constraint that the points to be run should belong to the bounded region. Then the optimisation is run: k defines the number of starting points to find a solution or multiple local solutions to problem.

```
ms = MultiStart('TolFun', 1e-20,'StartPointsToRun','bounds');
[x_ga,opt_costFun] = run(ms,problemMS,k);
```

Performances comparison of MultiStart and Genetic Algorithm In Table 5.2 the solutions are compared obtained by using the two different solvers. The difference in the final value of the cost function is negligible, while the main aspect to point out is the difference in the computational time. The MultiStart solver is faster in reaching the solution and can be used to generate a family of results for many initial conditions on the original orbit. In this way, the best solution in terms of the propellant consumption can be identified: each of them is connected to an optimal epoch for the disposal. These performances are for the fully-analytical methods, where the solver must solve the Hamiltonian for the critical eccentricity condition. Similar results are obtained with the semi-analytical propagation method. In the latter case, the computational time is very high (2-4 h).

Table 5.2 The result obtained for the MultiStart and the Genetic Algorithm methods for an Integral like orbit, using a semi-analytical method. Notice the difference in the computational time.

Parameters	MultiStart	Genetic Algorithm
kep_{in}	$\{\ 8.7709 \times 10^4\,\text{km}, 0.8975, 0.9841\,\text{rad}, 4.7123\,\text{rad}, 3.0596\,\text{rad}, 3.141\,\text{rad}\ \}$	
α_{opt}	$-3.137\,\text{rad}$	$-3.140\,\text{rad}$
β_{opt}	$7.05 \times 10^{-5}\,\text{rad}$	$7.06 \times 10^{-5}\,\text{rad}$
Δv_{opt}	$67.9\,\text{m/s}$	$67.9\,\text{m/s}$
f_{opt}	$3.1411\,\text{rad}$	$3.1415\,\text{rad}$
Cost fun J_{opt}	0.023	0.0052
$h_{p,min}$	$50.0048\,\text{km}$	$50.00\,\text{km}$
kep_{new}	$\{\ 8.6412 \times 10^4\,\text{km}, 0.9256, 0.9841\,\text{rad}, 4.7123\,\text{rad}, 3.0596\,\text{rad}, 3.141\,\text{rad}\ \}$	
Computational time	2.55 min	11.21 min

Chapter 6

Numerical results for the study case missions

In this chapter, the numerical results for three different case studies are analysed. The fully-analytical approach is applied to all of them to verify the potential efficiency of this new approach. In addition, the results were compared with the classical numerical optimisation to validate the solution.

1. Venus' orbiter: the disposal trajectory is designed as an atmospheric re-entry. The triple-averaged potential is used in the Hamiltonian formulation to recover in a fully-analytical way the maximum eccentricity of the target orbit after the manoeuvre. An altitude of 130 km is set as the target condition. The results from the fully-analytical codes are compared with the optimisation using the semi-analytical propagation of the double-averaged model of the disturbing potentials.

2. Earth's satellite atmospheric re-entry. The case of the INTEGRAL satellite is considered for the design of the disposal manoeuvre, both the fully-analytical and semi-analytical optimisations are considered. In addition, the results of both codes are compared with the manoeuvre options computed in literature.

3. Earth's satellite graveyard orbit. The case of XMM-Newton is analysed. The results from the fully-analytical approach are compared with the semi-analytical results obtained in the literature.

6.1 Venus' Orbiter disposal design

6.1.1 Mission Definition

In the past years, many space probes visited Venus for scientific purposes. Since 1960s, NASA starts planning future scientific missions to Venus (Bienstock, [60]). In particular, the opportunity to study the atmosphere and clouds of Venus was of great interest: Pioneer Venus probes, Venera missions, Magellan and Venus Express are just some example of missions that visits the planet (Titov et al., [61]). Nevertheless, none of them is a suitable case of study to see how the third body perturbation can be used for orbital navigation. In fact, the inclination, the eccentricity or the semi-major axis were not suitable for the analysis, or their trajectory was much affected by the atmospheric drag.

For this reason, a fictitious orbiter was considered. It is the equivalent of a HEO trajectory in the Earth-Moon system. In particular, since the dimension and the gravitational attraction of Venus and Earth are quite similar, the parameters for the HEO are considered similar to the INTEGRAL mission. The initial trajectory of the orbiter, chosen for this analysis, is reported in Table 6.1

Table 6.1 Orbital parameters of a fictitious Venus' orbiter.

a (km)	e (-)	i (deg)	ω (rad)	Ω (rad)	M (rad)
87000	0.87	60	4.42	4.64	2.25

6.1.2 Mission strategy and constraint.

The manoeuvre strategy consists in an atmospheric entry, that can be exploited for different purposes. Most of the orbiters, already sent to Venus, were equipped with a lander: this should enter the atmosphere after the separation from the orbiter. The trajectory shall grant the correct entrance angle and velocity. Nevertheless, this kind of study shall be very accurate to assure the survival of the lander. On the other hand, the satellite de-orbit was already studied for the end-of-life strategy of the Venus Express mission, which ended its operative life with a de-orbit trajectory (Svedhem et al., [58]).

In this section, an atmospheric re-entry was designed targeting the atmospheric interface. It is set at 250 km (Justus and Braun, [53]), but the target altitude was taken a bit lower to assure the entrance in the atmospheric layer. The aim of this work is the design of re-entry trajectory in the Venus atmosphere. The results of the numerical and semi-analytical model are compared to validate the results.

For the numerical propagation, the double averaged model is used to describe the orbital dynamics. For the optimisation procedure, the following constraints were identified:

- disposal window of 15 years,
- delta-v interval for the optimisation: 0 - 1.20 km/s,
- target perigee 130 km.

The target perigee corresponds to a critical eccentricity condition:

$$e_{cr} = 1 - \frac{h_{p,cr} + R_{\varphi}}{a} = 0.9281 \tag{6.1}$$

The phase space is recovered from the triple-averaged Hamiltonian representation. Remember that it is described in the Venus equatorial frame, considering the effects of J_2 and Sun attraction. Figure 6.1 represents the two dimensional phase space. Each contour line represents a trajectory for a specific initial condition: in other words, given the initial condition, one phase space line is selected and the satellite moves on this line for its future evolution. In blue is represented the trajectory followed by the satellite under study. The critical eccentricity is represented in red: the satellite time evolution never reaches that condition, meaning that a manoeuvre is necessary to perform the atmospheric entry.

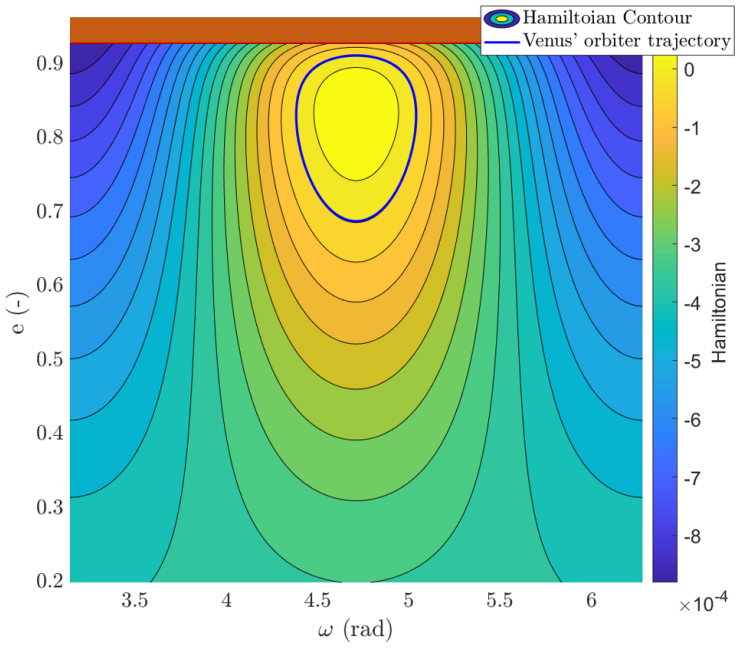

Figure 6.1 Venus' orbiter two dimensional phase space. In blue the spacecraft trajectory, in red the target eccentricity.

6.1.3 Numerical Results

Maximum and minimum eccentricity condition.

The first optimisation was done for the maximum and the minimum eccentricity point to define the interval of the manoeuvre cost. The manoeuvre was modelled both with the fully-analytical and semi-analytical approach, presented in Chapter 3, to verify the accuracy of the results. As reported in Table 6.2, the manoeuvre is more expensive at the maximum eccentricity condition.

Table 6.2 Results for maximum and minimum eccentricity condition of the Venus' orbiter.

	Semi-analytical propagation	Fully-analytical solution
Manoeuvre - M1		
Δv at e_{min}	60 m/s	57.0 m/s
Minimum perigee altitude	130.0 km	130.0 km
Computational time	1 h	3 min
Manoeuvre - M2		
Δv at e_{max}	84 m/s	86.5 m/s
Minimum perigee altitude	130.0 km	130.0 km
Computational time	1 h	5 min

The time evolution of the resulting trajectories after the manoeuvre is reported in Figure 6.2c, while the phase space of the manoeuvres is reported in Figure 6.2a. In both cases the target trajectory results in the atmospheric re-entry (see Figures 6.2c and 6.2d). Moreover, the same results are achieved also with the semi-analytical optimisation, verifying the fully-analytical design process itself. Nevertheless, since the numerical approach is more expensive computationally (1 hour instead of 3-5 minutes), for the optimisation of a generic set of initial conditions along the orbit, only the fully-analytical approach is proposed, since the two models for the Venus-Sun system are equivalent.

The manoeuvre at the maximum eccentricity (M2) is more expensive since it results in a direct reduction of the perigee altitude to the critical condition. On the other hand, for the minimum eccentricity (M1) condition, it results in a tangent manoeuvre: the consumption of propellant is less. M2 consists in a manoeuvre at the apogee to change the perigee altitude, increasing instantaneously the eccentricity of the orbit. On the other hand, the manoeuvre at M1 maintains constant the eccentricity of the orbit, resulting in a δe almost zero, the delta-v produces a variation in the semi-major axis, decreasing it and in a reduction of the orbital inclination.

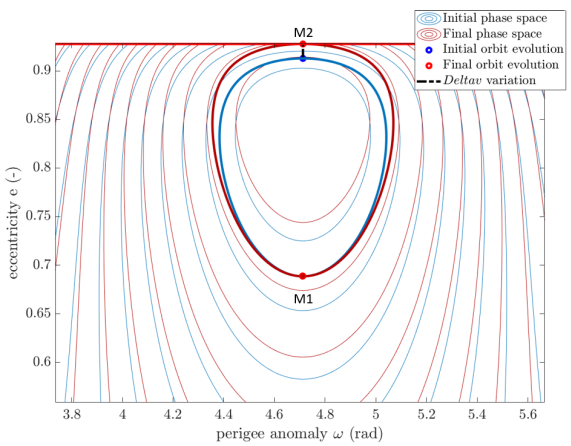

(a) Phase space trajectory in (ω, e) to target the critical condition for the re-entry. The initial phase space is in blue line, while the final phase space is in red.

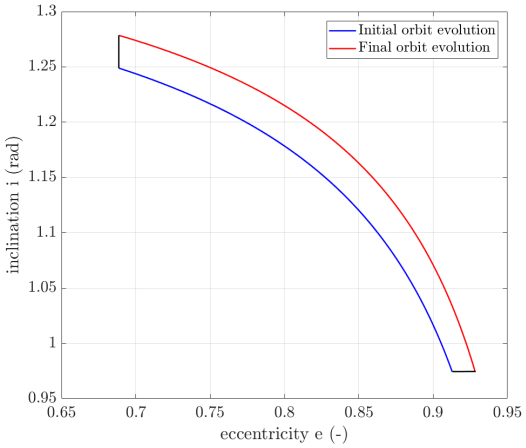

(b) Initial and final trajectory in the (e, i) space. The manoeuvre at the maximum eccentricity point does not change the orbit inclination, while at the e_{min} it slightly increases it.

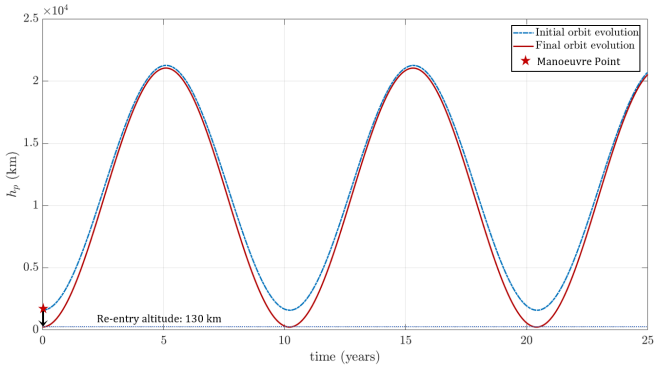

(c) Time evolution of the final trajectory after the re-entry manoeuvre at the maximum eccentricity point. It results in a direct re-entry in atmosphere.

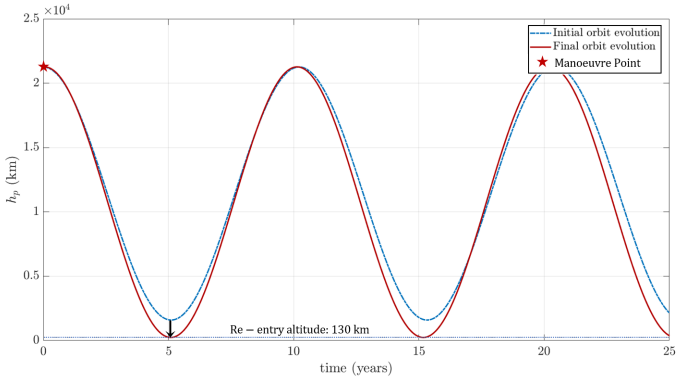

(d) Time evolution of the final trajectory after the re-entry manoeuvre at the minimum eccentricity point. It results in a tangent manoeuvre: the target trajectory is reached in time.

Figure 6.2 Representation of minimum (M1) and maximum (M2) eccentricity condition for the manoeuvre.

Venus' orbiter de-orbit options

In this paragraph, different initial condition along the orbit is investigated, producing different possible disposal manoeuvre for a different initial epoch. The results for the fully-analytical approach are reported in Figure 6.3. The minimum perigee altitude below 130 km is assured for each initial condition. The solution is shown in terms of the optimal angle of the delta-v firings and the optimal true anomaly for the manoeuvre. The computational time for the optimisation is about 45-60 minutes. It's a very efficient optimisation, remembering that for optimising just one initial condition with semi-analytical propagation one hour or even more time is required. The mission considered has the following initial condition, reported in Table 6.3:

Table 6.3 Orbital parameters of a fictitious Venus' orbiter.

a (km)	e (-)	i (deg)	ω (rad)	Ω (rad)	M (rad)
87000	0.87	60	4.42	4.64	2.25

The numerical results from the fully-numerical approach are reported in Table 6.4. Ten initial conditions are investigated for the period of 2013-2022. The minimum perigee altitude is reached by each disposal options. Nevertheless, the cost of the manoeuvre depends on the orbital elements of the satellite and in particular on the couple (e, ω): depending on the position in the phase space the cost of the manoeuvre is different, varying from a minimum of 55.3 m/s to a maximum of 70.2 m/s.

Table 6.4 Venus' probe optimal solution from the fully-analytical approach using the Hamiltonian triple averaged model: starting date 22/03/2013.

	Fully-Analytical model			
Manoeuvre date (dd/mm/yy)	$h_{p,min}$ (km)	Δv (m/s)	α (rad)	β (rad)
22/03/2013	130.60	56.6	-2.51	0.60
25/03/2014	130.53	55.3	-2.90	0.17
29/03/2015	130.56	56.1	-3.14	-0.31
01/04/2016	130.62	57.2	2.49	-0.73
04/04/2017	130.69	59.2	2.59	-0.97
08/04/2018	130.83	63.0	2.76	-1.11
12/04/2019	131.13	70.2	2.98	-1.20
14/04/2020	131.04	68.1	-2.92	1.18
18/04/2021	130.79	61.9	-2.72	1.08
22/04/2022	130.67	58.6	-2.55	0.92
computational time	$\sim$1 h			

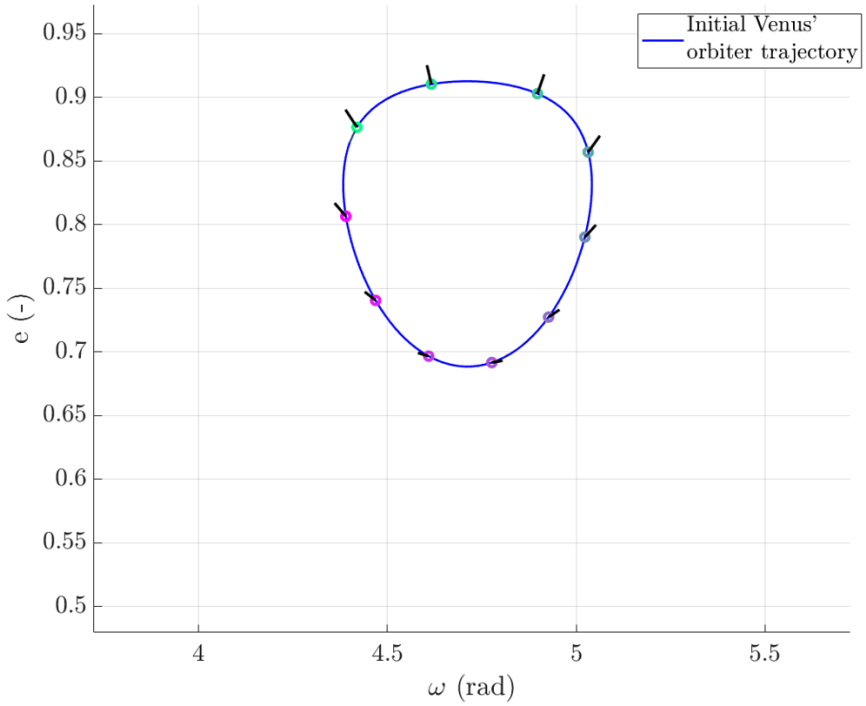

(a) Phase space representation of he initial trajectory. The black lines correspond to the possible manoeuvre for the re-entry.

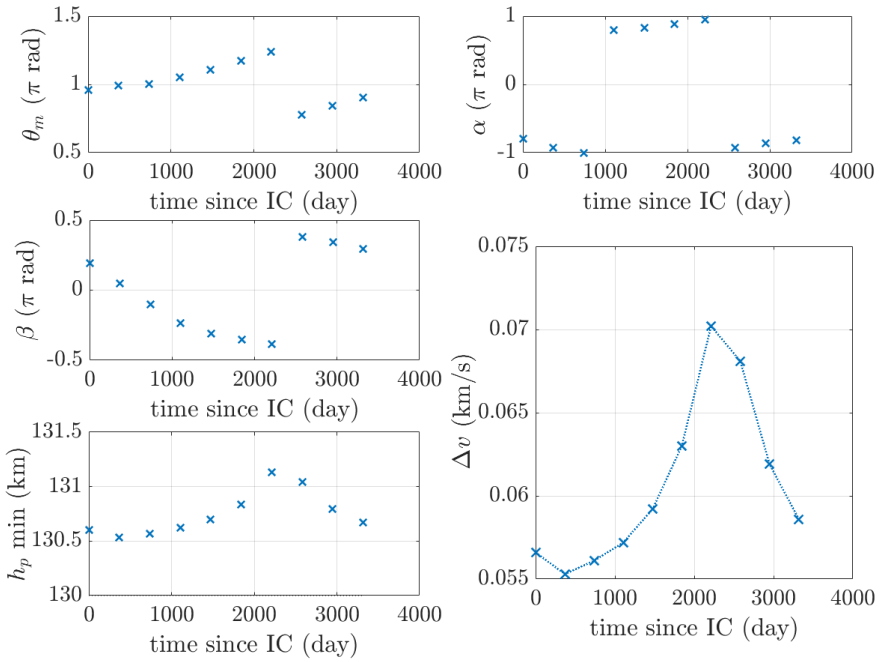

(b) Optimal manoeuvres parameters: the in and out of plane angles are reported (α and β), together with the magnitude of the Δv. Finally, the optimal true anomaly for the manoeuvre is reported

Figure 6.3 Representation of optimal disposal options for the Venus' orbiter.

6.2 INTEGRAL disposal design

6.2.1 Mission Definition

The INTErnational Gamma-Ray Astrophysics Laboratory (INTEGRAL) was an European mission of ESA for the "Horizon 2000" programme. It was dedicated to spectroscopy and imaging of gamma-ray sources (Winkler et al., [62]; Parmar et al., [63]; Pralet and Verfaillie, [64]). It was conceived by ESA with the contribution of Russia and NASA. INTEGRAL was launched on 17 October 2002 from Baikonur (Kazakhstan), which hosts the Russian launch pad. It was designed to have a nominal mission of two years, but its lifetime was then extended from 2004 to 31 December 2021[1].

The main characteristics of INTEGRAL mission are described in Table 6.5, where the initial situation of the spacecraft where compared with the known condition on January 2013, Colombo et al., [4].

Table 6.5 Most important data of INTEGRAL mission.

	Launch on Nov 2002 [65]	Condition on Jan 2013 [24]
Operational orbit	h_p =9050 km h_a =153 657 km i =52.2° ω =302° Ω =103°	h_p =10 822 km h_a =164 587 km i =61.5° ω =253° Ω =265°
Fuel mass	540 kg	61.5 kg
Equivalent delta-v	543 m/s	61.9 m/s

6.2.2 Disposal strategy and constraint

The end-of-life strategy of INTEGRAL mission was already studied in many works, see for example Colombo et al., [24] and Armellin et al., [67]. In both works, they exploit a semi-analytical orbit propagator to describe with high fidelity the orbit motion of the satellite. To speed up the long-term computations they removed the satellite mean anomaly influence by averaging it out. The former works investigate the Earth's atmospheric re-entry possibility for the satellite in the time window 2013-2029, the latter focused his works on the design of a graveyard trajectory. The aim of this work is to design an Earth's re-entry trajectory, using both the semi-analytical propagation of the orbit and the fully-analytical recovery of the critical condition.

[1]Extended life for ESA's science missions: `http://sci.esa.int/director-desk/60943-extended-life-for-esas-science-missions/`

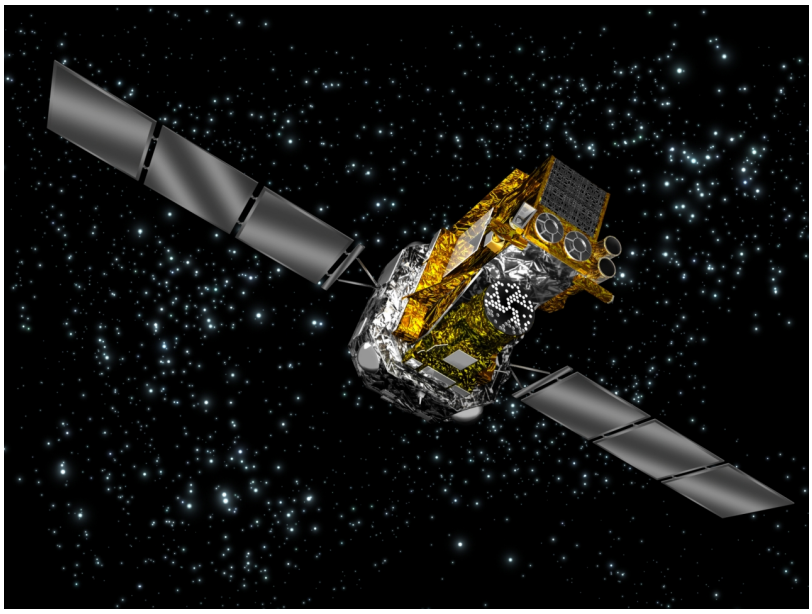

Figure 6.4 INTEGRAL satellite, image retrieved from ESA website [66]

As explained in Colombo et al., [24], the typical target perigee altitude for an earth re-entry is equal or lower than 80 km. Moreover, since this condition refers to missions with a lower initial perigee than INTEGRAL, it is assumed a perigee equal or below 50 km. This is due to the higher velocity at the atmospheric interface, which could results in a partial fragmentation or the bouncing on the atmosphere if the target perigee is above 50 km.

For the optimisation procedure, the following constraints were identified:

- disposal time window: 2013-2029
- delta-v interval for the optimisation: 0-1.20 km/s
- target perigee altitude after the manoeuvre 50 km

From the target altitude, the critical eccentricity condition can be identified:

$$e_{cr} = 1 - \frac{h_{p,cr} + R_{\oplus}}{a} = 0.9267 \tag{6.2}$$

From the triple-averaged model of the Hamiltonian, the 2D phase space of an INTEGRAL-like spacecraft can be recovered. The phase space is represented in the Equatorial frame, starting from the initial condition on Jan 2013. The influence of the Moon, J_2 and Sun perturbation is retained. Each contour line represents a phase space trajectory for the long-term evolution of the initial condition. The critical eccentricity condition is shown in the Figure 6.5 as a red line, in correspondence of $e_{cr} = 0.9267$. The strategy is to modify

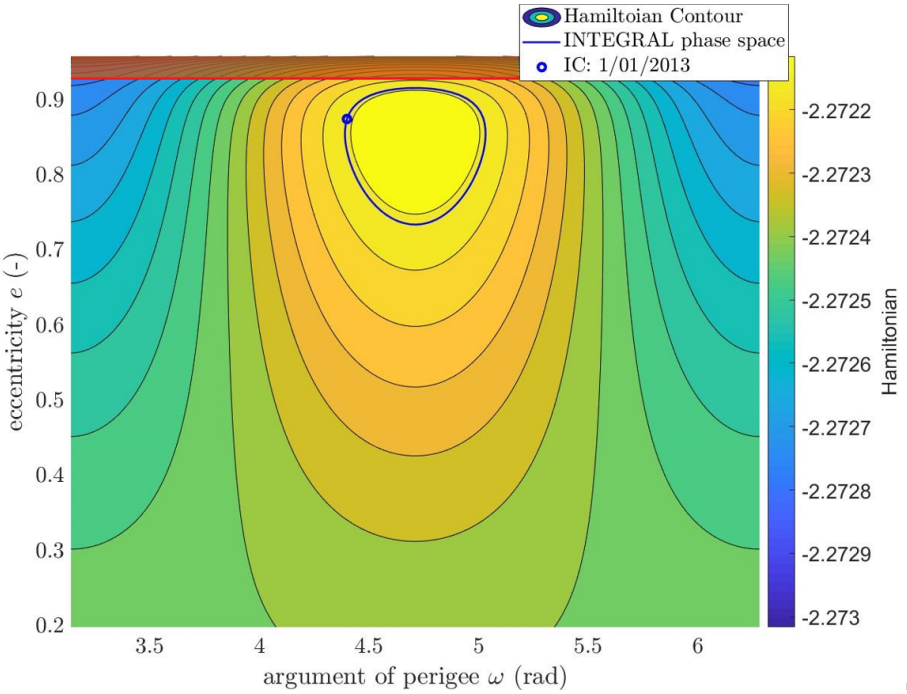

Figure 6.5 INTEGRAL Phase Space two-dimensional representation

the phase space with a single impulsive manoeuvre so that the resulting contour line is tangent to the critical condition.

Since the triple averaged model is not so accurate as the double-averaged one (see Chapter 4), the results are compared with the numerical propagation of the satellite dynamics in time. The semi-analytical propagation is a more accurate model, and it can describe the satellite dynamics. For a very accurate propagation, an high fidelity code is necessary, as the one developed by Colombo in the PlanODyn suite, which considers a much more complicated model (Moon effect up to the fourth order, Sun effect up to the fourth order, SRP effect, zonal gravity up to J_{10}, tesseral harmonics and atmospheric drag).

The numerical results from the phase space approach and the numerical propagation are compared with the INTEGRAL disposal options described in Colombo et al., [24]. This works provides a series of delta-v manoeuvre in the time interval 2013-2029 for the assessment of the atmospheric re-entry. The aim is to decide if a simplified model can be used for a preliminary manoeuvre design. In particular, from the new definition of INTEGRAL lifetime, good disposal options starting from 2021 could require a minimum of 17 m/s. This result is suitable with the onboard available propellant corresponding to 62 m/s. In addition, these results match the time window ESA is considering to dismiss the satellite.

6.2.3 Numerical Results

Maximum and maximum eccentricity condition The first optimisation was set to define the cost of the manoeuvre at the minimum and at the maximum eccentricity condition. Two manoeuvres were investigated:

- M_1 at the minimum eccentricity condition,
- M_2 at the maximum eccentricity condition.

The manoeuvre was modelled both with the semi-analytical propagation optimisation and with the fully-analytical approach in the phase space. The results are shown in Table 6.6.

Table 6.6 Results for maximum and minimum eccentricity of INTEGRAL mission.

	Numerical propagation	Semi-analytical solution
Manoeuvre - M1		
Δv at e_{min}	45.7 m/s	106 m/s
Minimum perigee altitude	50.0 km	50.0012 km
Computational time	3 h	3 min
Manoeuvre - M2		
Δv at e_{max}	97.2 m/s	67 m/s
Minimum perigee altitude	50.0 km	50.0048 km
Computational time	3 h	5 min

The results from the fully-analytical model are comparable with the study in Colombo et al., [4]. The Figure 6.6 shows how the phase space change after the manoeuvre. Both for the minimum and the maximum eccentricity condition, the spacecraft reaches the same final trajectory. The solution was recovered by considering as an initial condition the following Keplerian elements:

$$\text{kep}_{\text{in}} = \{8.7709 \times 10^4 \,\text{km},\, 0.8975,\, 0.9841 \,\text{rad},\, 4.7124 \,\text{rad},\, 4.625 \,\text{rad},\, 3.141 \,\text{rad}\} \tag{6.3}$$

The target trajectory results in a maximum eccentricity value equal to the critical one, yielding to a correct perigee altitude value. The final trajectory corresponds to manoeuvre that reduce the perigee altitude. Nevertheless, the results from the fully-analytical method are just the opposite than the results from the semi-analytical one, and can be used only for very preliminary estimation of the delta-v magnitude. This difference is the consequence of the non-accuracy of the triple averaged model used to recover the maximum eccentricity. Moreover, the numerical solution computes the orbit propagation in a more accurate way. For

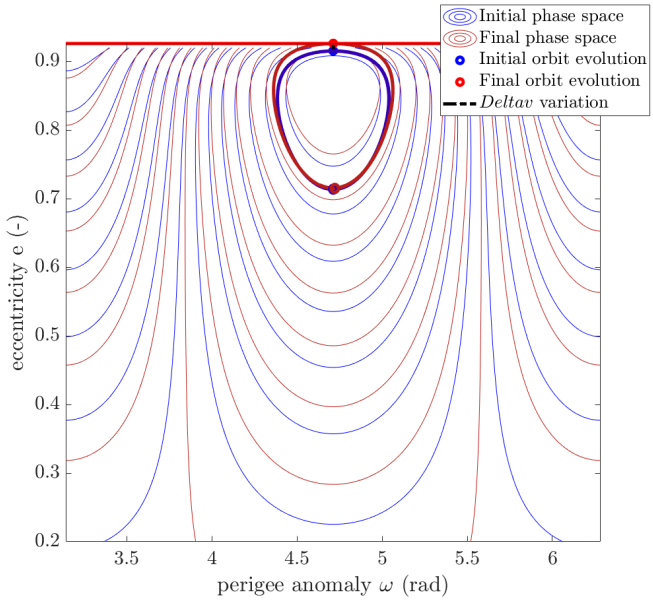

(a) Phase space trajectory in (ω, e)to target the crital condition for the re-entry. The initial phase space is in blue line, while the final phase space is in red. The blue bold trajectory represents the initial orbit. The red bold trajectory is the target trajectory corresponding to the critical eccentricity.

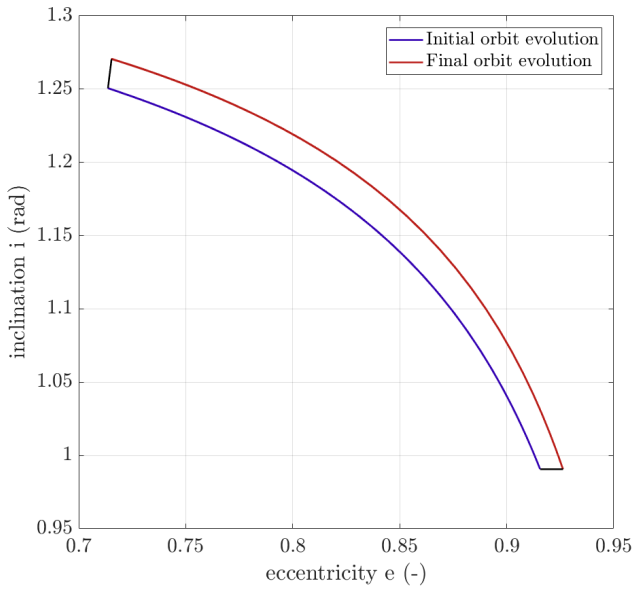

(b) Initial and final trajectory in the (e, i) space. The manoeuvre at the maximum eccentricity point does not change the orbit inclination, while at the minimum e it slightly increase it.

Figure 6.6 Representation of different strategy for INTEGRAL disposal.

the M1, the fully-analytical solution results in a higher delta-v requirement: it overestimates the manoeuvre effort. On the other hand, for M2 the behaviour is just the opposite, it underestimates the delta-v cost. This behaviour is due to the non-correct approximation of the semi-analytical model: the node elimination cancels out the complex dynamics of the Moon node, which is fundamental for a correct orbit prediction. These results are qualitatively the same reported in Colombo et al., [4]: the manoeuvre starting at lower eccentricity was more expensive. This is caused by the node elimination.

Integral re-entry disposal options The possible re-entry options were computed starting an optimisation procedure at different initial epochs. Therefore, the orbital dynamics was propagated from 2013 for 25 years, and several manoeuvre points were selected in a different epoch. The Figure 6.7a presents the manoeuvres for different initial conditions, computed with the fully and the semi-analytical method. Those results were compared with the ones in Colombo et al., [24]. It results that the computations performed with the semi-analytical method are much more accurate than the one from the fully-analytical model. In fact, the results computed with the triple averaged Hamiltonian formula yield to cheaper manoeuvre

when actually it is more expensive and vice-versa.

The numerical results are reported in Table 6.7. The Δv value changes significantly in the two different approaches. In particular, the semi-analytical model has a behaviour like the results obtained by Colombo et al., [24]. In the table, the best solutions are coloured in blue. There are three best options: the first in 2014, which would not be considered, it is already passed. The second in 2023, it is a very good option, since in this analysis it requires the lowest value of delta-v. The third option on 2032, with a delta-v of 25.6 m/s.

The best period to perform the disposal appears to be around 2023. In particular there, the delta-v necessary for the re-entry is only 17.2 m/s. This is a very good solution since it is in the same period ESA wants to dismiss it. Note that the fully-analytical method is not able to provide the correct estimation of the manoeuvre cost. This results from the low accuracy level for the Earth-Moon-Sun system of the triple-averaged model, as described in Figure 4.5a.

Table 6.7 INTEGRAL solution from the fully-analytical approach using the Hamiltonian triple averaged model and the semi-analytical propagation using the double-averaged potential function. The results from the semi-analytical approach are comparable with the literature results of Colombo et al., [24]

	Fully-Analytical model		Semi-analytical model	
Manoeuvre date	Δv (m/s)	$h_{p,min}$ (km)	Δv (m/s)	$h_{p,min}$ (km)
01/06/2013	73.3	34.69	75.2	50.02
04/06/2014	67.7	33.18	35.5	49.5
08/06/2015	67.4	43.45	36.5	50.3
11/06/2016	73.1	43.17	48.8	49.8
14/06/2017	74.9	53.23	50.6	49.7
18/06/2018	77.7	38.76	100.1	49.1
22/06/2019	83.7	44.37	112.8	50.2
24/06/2020	94.0	32.37	100.3	49.4
28/06/2021	97.8	35.37	118.5	49.9
02/07/2022	85.9	44.38	50.1	50.0
05/07/2023	78.9	37.43	17.2	47.8
08/07/2024	75.5	37.21	47.9	45.6
12/07/2025	73.8	37.63	52.6	48.5
15/07/2026	68.8	33.12	80.4	49.7
19/07/2027	66.8	52.19	96.3	50.8
22/07/2028	74.2	40.47	83.2	47.3
25/07/2029	74.8	43.05	70.6	50.3
29/07/2030	77.3	45.10	55.3	46.2
02/08/2031	83.0	40.85	37.2	48.8
05/08/2032	92.2	42.49	25.6	49.3
computational time	1 h		∼8 h	

Studying the results in Figure 6.7, the solution obtained in previous works is more accurate since a bigger number of initial conditions were studied. Nevertheless, the behaviour of the semi-analytical method is very similar to those results, indicating an equal trend in time. In fact, the red and the green lines have the maximum and the minimum in the same time period. On the other hand, the results from the fully-analytical model are not accurate, in the first part seems to follow at least the average trend, but then it behaves just the opposite as the real delta-v required. Moreover, the big difference in the computational time justifies the need of finding a better approximation with the fully-analytical model, as demonstrated for the Venus system, where the model perfectly works.

The manoeuvre parameters for the fully-analytical model are shown in Figure 6.7c. Those values are related to the semi-analytical approach. The optimal angle is around π, hence in the phase space, the best manoeuvre is obtained at the apogee. The in-plane angle, α varies in $-\pi$ and π, and the optimisation exploits values of α around π. This means that the manoeuvre is in the opposite direction of the velocity vector and therefore it reduces the energy of the orbit decreasing the semi-major axis. In fact, it aims to increase the eccentricity value, reducing the perigee altitude. This logic is valid also in the semi-analytical approach. On the other hand, the β angle varies in $-\pi/2$, $\pi/2$ cyclically, hence, it only depends on the time evolution of the orbit.

Finally, the orbit time evolution in terms of perigee altitude is reported. The Figure 6.8 reports the effect of the single optimal manoeuvre in time. The results are reported for the fully-analytical approach. The manoeuvre aims to decrease the perigee altitude, make it reaches the re-entry condition in time. The evolution was studied for 25 years. All the conditions satisfy the re-entry altitude, as can be seen in the zoomed part of the graph.

The blue line represents the original orbit time evolution, the manoeuvres are indicated as black lines with red dots. They decrease the perigee altitude resulting in proper time evolution to target the disposal condition. Note that this serves only as a preliminary study. Further analysis including the atmospheric drag and the SRP is necessary, to understand how those components can change the behaviour of the satellite in time. Hence, a new model shall be developed, for a high-fidelity propagation. The atmospheric leg design is necessary for analysing the casualty risk and the probability of impact on the ground. Moreover, since with this method the Keplerian elements at the entry altitude are known, the earth's re-entry happens as a semi-controlled disposal. This is very good for the risk statistics analysis.

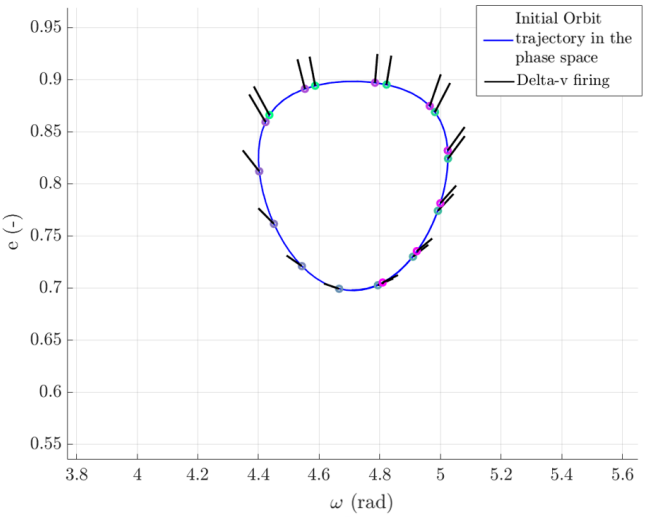

(a) Visualization in the phase space of the manoeuvre firings. The black lines indicates in which direction the couple (ω, e) is moving respect to the initial space.

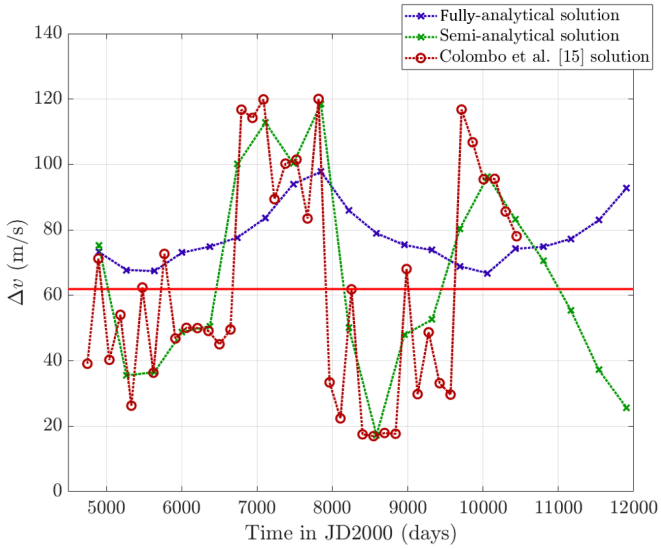

(b) Delta-v variation for different manoeuvre epoch.

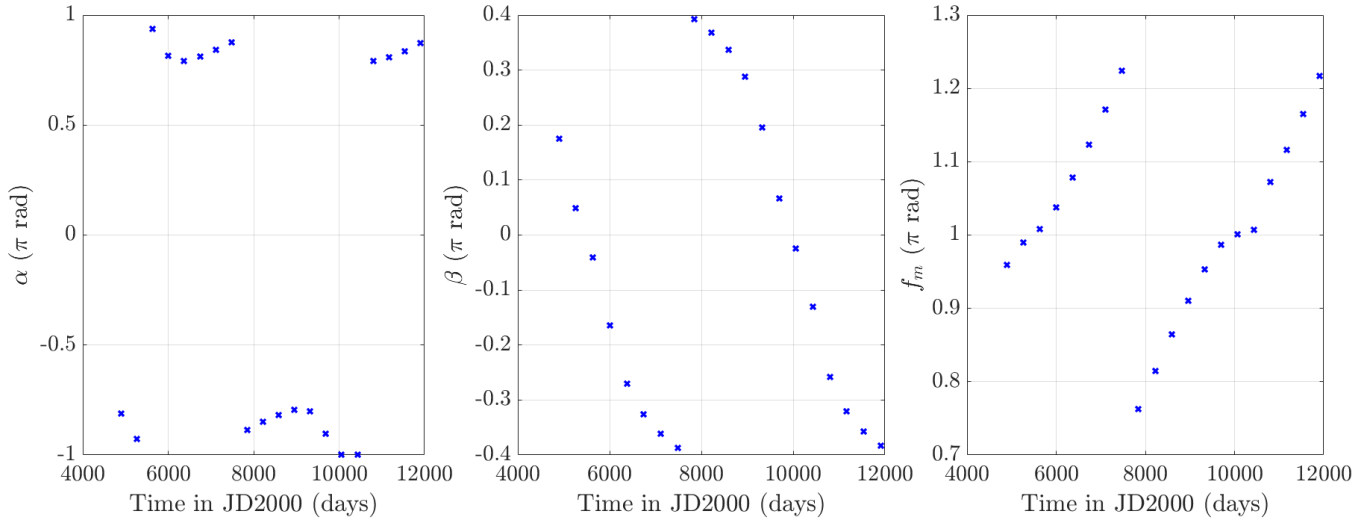

(c) Fully-analytical model: optimisation results for the delta-v in and out of plane angles α, β and the true anomaly of the manoeuvre f

Figure 6.7 Representation of new phase space for both minimum and maximum eccentricity conditions.

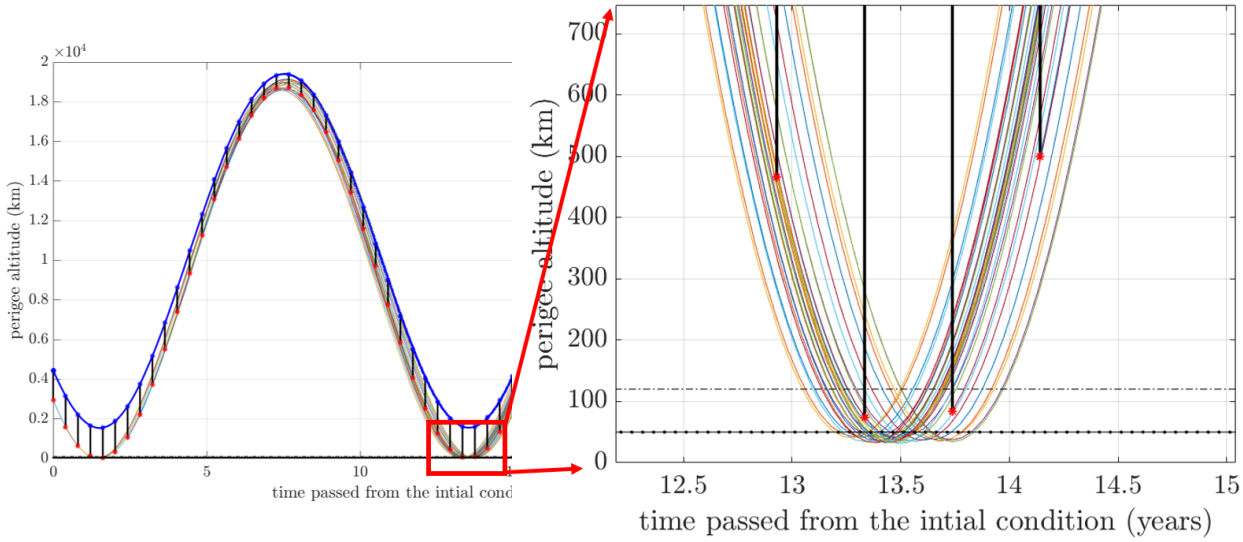

Figure 6.8 Time evolution of Integral-like orbit. Orbital propagation after the delta-v impulse. In blue the original trajectory, The change in the perigee altitude shows that the manoeuvre assess the target value for the re-entry.

6.3 XMM-Newton disposal design

6.3.1 Mission Definition

The X-ray Multi-Mirror Mission-Newton (XMM-Newton) is an European mission of ESA for the "Horizon 2000" programme. It has onboard a high-quality X-ray telescope with the aim to identify faint X-ray sources in the universe (Jansen et al., [68]). It was launched in 1999 in Kourou launch pad, and its operative orbit is a HEO trajectory. The mission was scheduled to end in 2018, but on 14 November 2018, its nominal life was extended up to 2022[2]. The main characteristics of XMM-Newton are reported in Table 6.8, where the initial condition is reported together with the condition in January 2013.

6.3.2 Disposal strategy and constraint

The end of life disposal of XMM-Newton follows a different strategy than the INTEGRAL case. The Earth re-entry is not feasible due to small amount of on-board propellant in 2013 (33 km/s). This approach was studied in Colombo, [25]. For this of orbit, the Luni-Solar attraction has a smaller beneficial effect for achieving the re-entry. This is mainly due to a smaller eccentricity respect to the INTEGRAL one: 0.728 respect to 0.879. In fact, for the

[2]Extended life for ESA's science missions: `http://sci.esa.int/director-desk/60943-extended-life-for-esas-science-missions/`

Table 6.8 Most important data of XMM-Newton mission.

	Launch on Dec 1999 [25]	Condition on Jan 2013 [24]
Operational orbit	h_p =13 737 km h_a =120 352 km i =38.95° ω =56.8° Ω =103°	h_p =19 642 km h_a =114 209 km i =64.15° ω =95.1° Ω =73.11°
Fuel mass	NA	47 kg
Equivalent delta-v	NA	35 m/s

Figure 6.9 XMM-Newton satellite, image retrieved from ESA website [69].

re-entry purpose, the Moon and Sun perturbations become more significant as the orbit is more elliptical and inclined. Hence, a bigger effect is exploited when e and i of the orbit are higher. From the preliminary study of the Earth re-entry, the minimum delta-v condition identified is too expensive for the satellite. Hence a graveyard trajectory is designed, by imposing that the eccentricity oscillation in time shall be as smallest as possible. Also in this case, the optimisation procedure is exploited, constraining the delta-v to be as small as the available one.

The aim in the phase space is to reach the central libration point. Moreover, the manoeuvre is constrained, so it will tend in that direction but will not reach that condition. It is important that after the manoeuvre, the orbit becomes more stable under the Luni-Solar attraction, and in particular, a good parameter of merit can be identified as the time that the satellite spends on its new orbit with a higher stability level than the initial one.

For the optimisation procedure the following constraints were identified:

- disposal time window: 2013-2029,
- maximum delta-v available 40 km/s
- the target conditions are: $\min \Delta e$ and $\min \Delta \omega$

From the triple averaged model, the Hamiltonian phase space in the Equatorial frame starts from the initial condition in January 2013. As for the INTEGRAL mission, the effect of Moon, J_2 and Sun is studied for the long-term behaviour of the orbit. The results are then compared with the numerical one, to verify the level of accuracy of the semi-analytical solution.

The (e, ω) phase space is shown in Figure 6.10: the critical eccentricity corresponding to the orbit evolution is 0.906. It can be seen that its evolution is closer to the central libration points than the INTEGRAL case. This justifies the necessity to change the disposal approach, targeting a graveyard orbit.

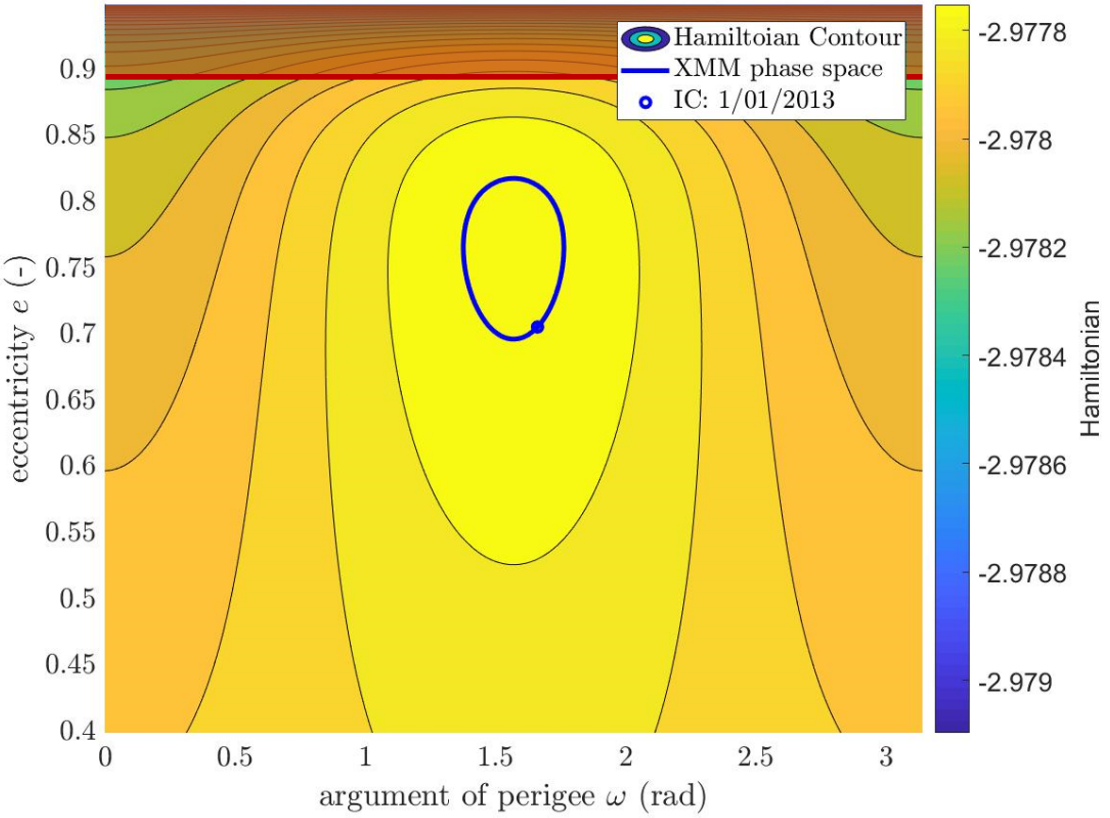

Figure 6.10 XMM-Newton Phase Space two-dimensional representation

6.3.3 Numerical Results

Maximum and minimum eccentricity condition The first optimisation is done considering as manoeuvre point the maximum and minimum eccentricity conditions. The delta-v in the procedure was limited by 120 km/s, even if, only manoeuvres that requires less than 40 km/s are actually feasible.

The results highlight that even using all the 120 km/s, the new orbital conditions are not suitable for an atmospheric re-entry. In fact, the maximum eccentricity value is significantly lower than the critical one.

Now the results for the two different manoeuvres are reported, note that the min e condition is defined by M_1, while the maximum by M_2. Only the results obtained with the fully-analytical approach are reported, but the considerations are valid also with a semi-analytical propagation (see also Colombo, [26]).

Table 6.9 Results for the minimum and the maximum eccentricity condition for INTEGRAL mission.

	Fully-analytical approach
Manoeuvre - M1	
Δv at e_{min}	120 m/s
Minimum perigee altitude	1.9737×10^3 km
Manoeuvre - M2	
Δv at e_{max}	120 m/s
Minimum perigee altitude	3.037×10^3 km

Hence, the minimum perigee reached is far above the atmospheric interface: the Earth's re-entry is not available. This is shown also in the new phase space after the manoeuvre, reported in Figure 6.11. Note that the new red bold trajectory is far below the critical condition. In addition, since the convergence was not reached, the two phase spaces generated at the minimum and maximum conditions are not the same.

XMM re-entry disposal options From the considerations done for the maximum and the minimum eccentricity conditions, the only possibility is to switch to a graveyard disposal orbit. The concept of this kind of orbits is well represented in the phase space in Figure 6.12a. Hence the aim is to reduce the eccentricity oscillation in time. The phase space representation in this work is represented in the equatorial plane. On different works, the Earth-Moon plane was used instead, as reported in Figure 6.12b. Even if the two reference frames are different, hence they would have a different shape, the logic behind is the same: the manoeuvre shall aim to contain the eccentricity oscillation, making the orbit more stable.

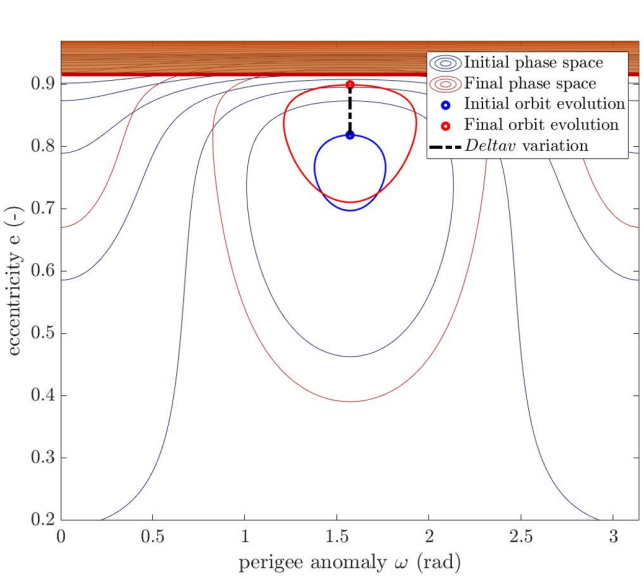

(a) Phase space trajectory in (ω, e) in correspondence of the maximum eccentricity condition. The initial phase space is in blue line, while the final phase space is in red. The blue bold trajectory represents the initial orbit, the red one the final.

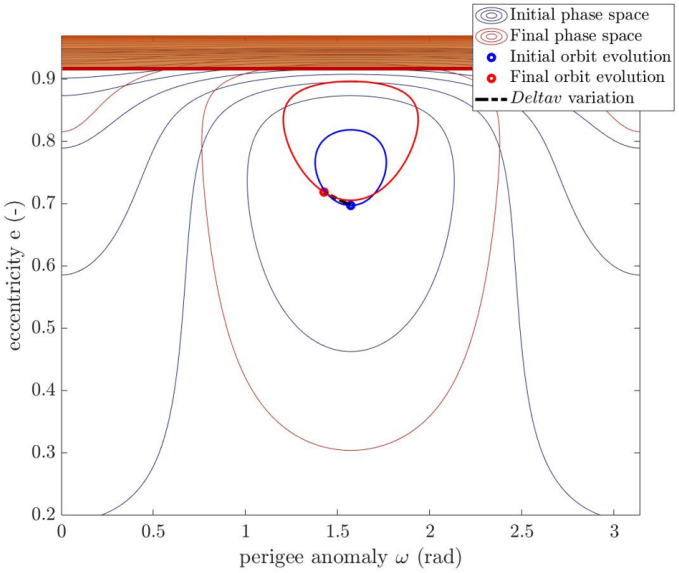

(b) Minimum eccentricity phase space. The original trajectory is the blue bold line, the final is the red bold line.

Figure 6.11 Representation of new phase space for both minimum and maximum eccentricity conditions: the critical condition for the re-entry is not reached in both cases.

For this satellite, only a preliminary study was computed using the fully-analytical approach to see which kind of results it provides. Those solutions are then compared with the ones in Colombo, [25]. The possible results obtained for the graveyard orbit are reported in Table 6.10. The delta-v was used completely, since the aim, in this case, is not to optimise the fuel consumption, but to go as close as possible to the central libration point of the phase space. Obviously, the higher the amount of the remaining fuel, better the solution will be in terms of long-term stability.

For the XMM-Newton, the maximum amount of fuel was used: 35 m/s. In the Table 6.10 also the value for the design of the delta-v are reported: in and out of plane angle. Their values change with the manoeuvre epoch and are optimised to provide the best direction of the impulse. Moreover, the true anomaly of the manoeuvre is reported. As for the other cases under study, this value represents the best condition along the orbit to achieve the final trajectory. The true anomaly is left free in the optimisation since the model used averaged out the short terms effect due to one orbit revolution of the satellite. For this reason, a more accurate analysis shall verify that the manoeuvre condition is reached by the satellite and that the graveyard orbit is assessed.

Finally, also the information upon the minimum perigee altitude is reported. This never

goes below 6000 km. This is a very good result and assures that the spacecraft does not enter in the atmosphere layer during its long-time evolution. Moreover, some solutions are better than others, even at constant delta-v consumption, since they grant a higher minimum perigee: till 12 000 km. This is due to the different value of the couple (ω, e) during the time evolution, which represents a different initial data of the manoeuvre.

Nevertheless, as already explained for the INTEGRAL mission, the elimination of the node in the semi-analytical model does not produce a very accurate representation of the orbital dynamics. The triple averaged Hamiltonian which is used for the phase space representation, is used here only for a very preliminary study. The results should be compared with the semi-analytical optimisation, which relies on the double averaged model. Moreover, the fully-analytical approach has the great advantage of reducing significantly the computational time, hence further investigations would be essential to better characterize the one degree of freedom Hamiltonian.

Table 6.10 XMM-Newton solution from the fully-analytical approach using the Hamiltonian triple averaged model.

	Fully-Analytical model				
Manoeuvre date	Δv (m/s)	α (rad)	β (rad)	f_m (rad)	$h_{p,min}$ (km)
1/1/2013	35	3.14	-0.02	2.98	1.1627e4
10/8/2013	35	-2.39	0.44	2.71	1.2297e4
19/3/2014	35	2.12	-0.83	3.54	1.2872e4
26/10/2014	35	2.53	-0.41	3.39	1.2341e4
4/06/2015	35	2.47	-0.37	3.47	1.2273e4
12/1/2016	35	2.48	-0.33	3.54	1.2061e4
20/08/2016	35	2.51	-0.18	3.57	1.1625e4
29/03/2016	35	-0.73	1.12	2.68	1.2485e4
5/11/2017	35	2.56	0.05	3.64	1.0536e4
14/06/2018	35	2.61	0.22	3.66	9.8718e3
22/01/2019	35	2.61	0.28	3.73	9.2055e3
31/08/2019	35	2.60	0.42	3.77	8.4952e3
8/04/2020	35	2.65	0.60	3.79	9.2055e3
15/11/2020	35	2.72	0.80	3.77	8.4952e3
24/06/2021	35	0.72	-0.31	2.53	7.8188e3
1/02/2022	35	0.80	-0.51	2.58	7.7794e3
10/09/2022	35	0.85	-0.67	2.63	7.1877e3
19/04/2023	35	0.93	-0.87	2.66	6.7471e3
26/11/2023	35	-0.96	0.92	3.62	6.4206e3
5/07/2024	35	-0.85	0.72	3.63	6.3569e3
11/02/2025	35	-0.80	0.54	3.68	7.0866e3
20/09/2025	35	-0.73	0.36	3.73	7.4634e3

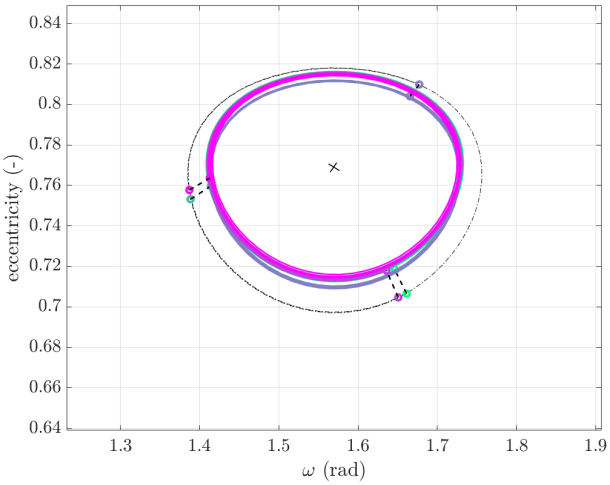

(a) Possible graveyard orbit for XMM-Newton mission. Phase space in the Equatorial Refrence frame

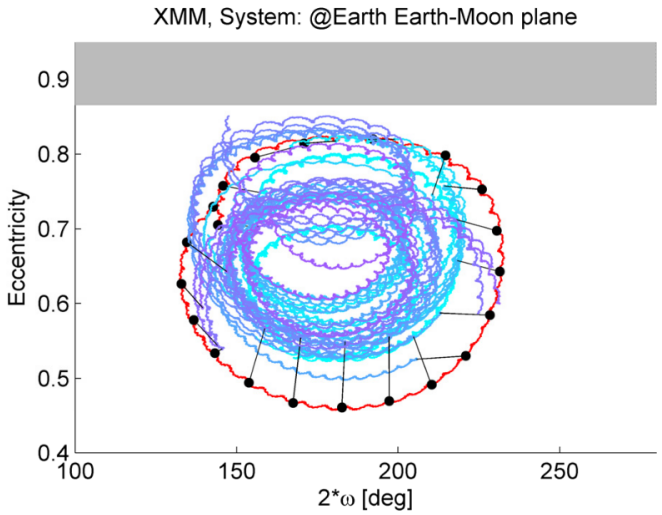

(b) Real XMM-Newton phase space in the Earth-Moon plane, from Colombo, [25].

Figure 6.12 XMM-Newton: Representation of new phase space for both minimum and maximum eccentricity conditions.

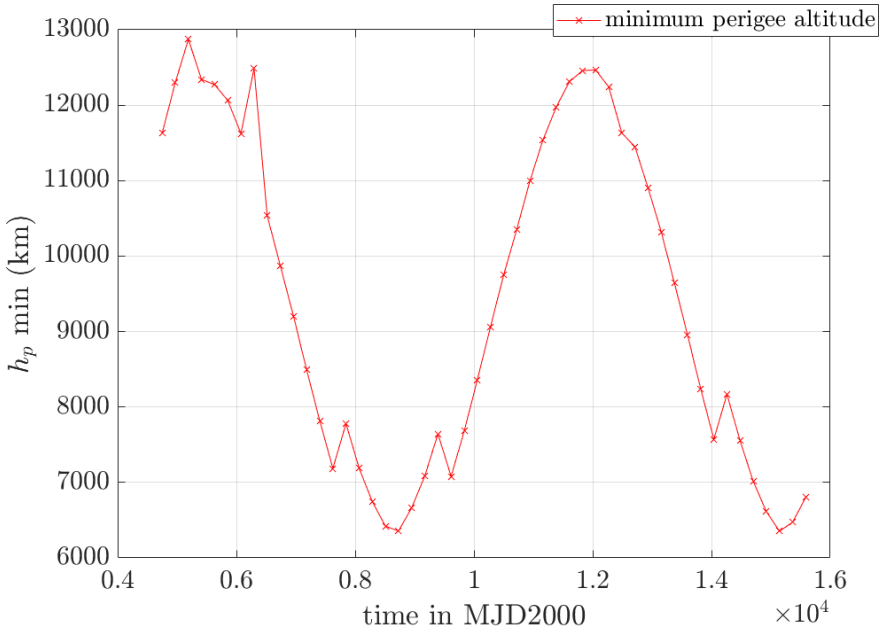

(a) Minimum perigee altitude for different orbital manoeuvre disposal, computed with the fully-analytical approach.

Figure 6.13 XMM-Newton: Representation of the perigee altitude for different initial condition of the manoeuvre (different epoch).

Chapter 7

Conclusions and further developments

THE aim of this thesis was to investigate the feasibility of a fully-analytical approach to design disposal manoeuvres for HEO spacecraft. The end-of-life strategy relies on the exploitation of the coupled behaviour of the third body attraction with the J_2 effect of the planet's oblateness. It was already demonstrated that for highly inclined orbits, these contributions to the satellite dynamics are very important to define the long-term and the secular effect (Kozai, [6]; Lidov, [5]). The main difference with respect to the previous works was the development of a dynamical model of the orbit perturbations in the Equatorial reference frame to write the Hamiltonian system for the study of the phase space maps to investigate possible disposal strategies. Moreover, to deal with the node effect upon the long-term dynamics, a possible technique was studied for the elimination of the node: a reduced Hamiltonian in one-degree-of freedom is recovered. Then the analytical expression of the Hamiltonian was used to derive the critical eccentricity conditions for the end-of-life disposal trajectory.

In the previous works, starting from Kozai, [6], the phase space maps were typically produced in the planet-perturber plane. Moreover, the Hamiltonian formulation in this reference frame was very simple whenever only the Moon effect was considered. In that case only, the Hamiltonian could be reduced to a time-invariant formulation, which allows the derivation of critical eccentricity condition in a semi-analytical way (Colombo et al., [4]). The analytical model developed in this thesis aims to introduce all the contributions of the external perturbations: for the Earth's satellite, both J_2 and the third body influence of the Sun and the Moon is analysed. On the other hand, for Venus's probe, both J_2 and Sun's

disturbance are introduced. For both cases, the double-averaged model is very accurate in the description of the satellite dynamics. Moreover, in this thesis it was demonstrated that the node elimination in the equatorial frame produces accurate results only when the third body orbit can be approximated on the equator: a non-inclined perturber. For this reason, the triple-averaged model is very accurate to describe a system where the perturber has a very small inclination on the equatorial plane. Hence, the results obtained for the Venus' orbiter are exact: both semi-analytical propagations of the double average model and the fully-analytical approach using the triple averaged Hamiltonian provide the same results. The Venus-Sun system is only an example where this model describes the exact dynamics. Other examples could be studied, like a Europa's orbiter with the third body disturbance of Jupiter.

This thesis demonstrates that using a semi-analytical propagation for the manoeuvre optimisation is more expensive than a full analytical method based on the solution of the Hamiltonian, while it is more time efficient with respect to a full dynamics integrator. It could take several hours to produce the optimal results. For this reason, the optimal solution shall be computed on ground and then the instructions are sent to the onboard system. Instead, the approach presented in this thesis aims to reduce significantly the computational time for the optimisation design. The elimination of the node effect in the long-term evolution of the satellite was adopted with the aim to simplify the Hamiltonian expression to be solved in a fully-analytical way. Moreover, the equatorial plane was chosen for the representation, since it is the most common frame for the description of orbit evolution and allows a simple representation of the overall disturbing effect present in orbit. In fact, in this representation, the node elimination allows writing a reduced one-dimensional Hamiltonian formulation: the satellite dynamics is simply described by solving the Hamiltonian equation. The numerical integration is no more necessary: this is the innovative potential efficiency for future orbit determination. This procedure is not so accurate due to the elimination of node in the Earth-Moon-Sun system, but it can be used as first guess solution of the disposal manoeuvre.

In this thesis, two different strategies were analysed for the end-of-life disposal. The first one considers a target orbit that during the time evolution produces a perigee altitude below the atmospheric re-entry limit: this yields to an Earth's re-entry trajectory where the satellite is destroyed by the aerodynamic forces due to the interaction with the atmospheric layers. The second one, instead, targets a graveyard orbit. The manoeuvres were designed through an optimisation procedure, using the satellite ephemeris and the available on-board fuel as initial conditions.

The innovative approach presented in this thesis is the design of the manoeuvre fully-analytically: the Hamiltonian equation in one degree of freedom can be solved for the target condition. This approach demonstrates the potential computational efficiency of a fully-analytical solver. The computational time reduces significantly with respect to the semi-analytical optimisation, which relies on numerical integration of the satellite's double-averaged dynamics.

The validation of the model was done comparing the results from the fully-analytical approach with the classical propagation model, using the double-averaged potential. From the comparison, the potential efficiency of having a fully-analytical model on-board is evident. Using the Hamiltonian expression to evaluate the Venus' orbiter disposal takes just a few minutes for one initial condition and about one hour for different disposal option selection.

The reduction of the Hamiltonian to a one-degree-of-freedom equation allows solving the dynamical behaviour of the satellite with one equation only, without even the need of propagating in time. This is the most important starting point for future works. A simple code, which is low computationally expensive, can be placed on-board of future space mission even for orbital navigation: it can predict long-term propagation just starting from the initial condition.

The main drawback of this model appears in the Earth-Moon-Sun system. This system is very complex, and the Hamiltonian reduction is based on too stringent hypotheses to describe in an accurate way the real satellite dynamic. The problematic arises from the node elimination. Since the right ascension of the satellite is coupled with the Moon node, by eliminating Ω very complex dynamics are discharged: the Moon node has a non-linear time behaviour in the equatorial frame. As reported both in Chapter 4 and 6, the model is not accurate for the Earth's system. On the other hand, the semi-analytical model, considering the orbit propagation in time produces suitable results for the disposal strategy of INTEGRAL mission.

This thesis opens to a variety of future development. First, the node reduction works perfectly for low inclined perturber, which orbit can be approximated to be on the equator. On the other hand, for the Earth-Sun-Moon system, this opens to different approaches. Since the main achievement is the the optimal single manoeuvre design for the Venus-Sun system, future works could investigate more accurate analysis comparing the triple-averaged model and the second-averaged model with a full numerical propagation of the orbit evolution for future mission. Moreover, the phase space maps of the triple-averaged Hamiltonian could be used also for other applications, like frozen conditions for a Venus' orbiter.

On the other hand, for the Earth-Moon-Sun system, the nodal reduction should be

analysed. A first study could investigate the feasibility of finding a solution to the 2.5 degree of freedom Hamiltonian, that is produced after the double averaging. The investigation of possible phase space maps of this model could be much more accurate for the preliminary design of the disposal. Another important issue is the time dependence of the Moon orbital elements from time. A first approach could try to solve the same problem developed in this thesis, starting from a model in the ecliptic plane, see the works of Gkolias et al., [51]. This removes the time dependence of most of the Moon elements, apart from the Moon node.

Moreover, the need to reduce the computational time is related to the possibility of generating a software that can compute the optimal disposal trajectory from the current ephemeris of the satellite. If this software is light enough (computationally speaking), it could be placed on board the satellite, removing the necessity of sending information from the ground. The fully-analytical method, due to its potential efficiency can be used on-board of the satellite for a preliminary mission definition ans design. Moreover, this can be used to design the station-keeping requirements and operations for those kind of orbits. This is fundamental during the missions design, since it allows the correct dimensioning of each satellite's subsystem. This idea is very revolutionary and could be achieved only by solving the satellite dynamics in a fully-analytical way, as it was done in this work.

This thesis was part of the COMPASS project: "Control for orbit manoeuvring by surfing through orbit perturbations" (Grant agreement No 679086). This project is European Research Council (ERC) funded project under the European Unions Horizon 2020 research.

Acknowledgements

The research leading to these results is part of the European Research Council (ERC) under the European Unions Horizon 2020 research and innovation programme as part of project COMPASS (Grant agreement No 679086). The author acknowledges the use of the Milkyway High Performance Computing Facility, and associated support services at the Politecnico di Milano, in the completion of this work. The datasets generated for this study can be found on the project page `www.compass.polimi.it`.

Appendix A

Fundamental Relations

A.1 Trigonometric relation for true, mean and eccentric anomaly

The mean and the eccentric anomaly were introduced to relate the actual position of the satellite, described through the true anomaly, to the time along the orbit, as in Vallado [39].

The Mean Anomaly M correspond to uniform angular motion on a circle of radius a, and it is defined as function of the orbital period:

$$M = \int_T^t n\, dt = n(t - T) \tag{A.1}$$

On the other hand, by defining the auxiliary circle around the ellipse of the orbit, a new angle can be defined as the Eccentric Anomaly E. It is related to both the Mean and the true anomaly of the body:

$$M = E - e \sin E \tag{A.2}$$

$$\sin E = \frac{\sqrt{1 - e^2} \sin f}{1 + e \cos f} \tag{A.3}$$

$$\cos E = \frac{e + \cos f}{1 + e \cos f} \tag{A.4}$$

$$\tan\left(\frac{E}{2}\right) = \sqrt{\frac{1 - e}{1 + e}} \tan\left(\frac{f}{2}\right) \tag{A.5}$$

And in particular this results in useful relation for $\cos f$ and $\sin f$, which would be used for the averaging procedure:

$$\cos f = \frac{\cos E - e}{1 - e \cos E} \qquad \sin f = \frac{\sqrt{1 - e^2} \sin E}{1 - e \cos E} \tag{A.6}$$

Averaging procedure The averaging procedure can be solved in two different ways. The first one consists in express all the terms related to the body's potion along the orbit as function of the Eccentric anomaly. The second one, instead, exploit the relation between the mean and the true anomaly to express the integral in terms of the latter one.

Integral in terms of the eccentric anomaly Since the satellite position depends on the true anomaly, it is expressed in terms of the eccentric anomaly:

$$r = a(1 - e\cos E) \tag{A.7}$$

Therefore, the averaging procedure results in

$$\frac{1}{2\pi}\int_0^{2\pi} fun(M)\, dM = \frac{1}{2\pi}\int_0^{2\pi} fun(E)(1 - e\cos E)\, dE \tag{A.8}$$

In addition, in the zonal and in the third body disturbing potential, the terms related to the true anomaly appears as functions of $\cos nf$ and $\sin nf$. Those terms are reported to the basic relations in Equation (A.6) thanks to the trigonometric relations:

$$\cos 2f = 2\cos^2 f - 1 = 2\left(\frac{\cos E - e}{1 - e\cos E}\right)^2 - 1 \tag{A.9}$$

$$\sin 2f = 2\cos f \sin f = 2\frac{\cos E - e}{1 - e\cos E}\frac{\sqrt{1 - e^2}\sin E}{1 - e\cos E} \tag{A.10}$$

$$\cos 4f = 2\cos^2 2f - 1 \tag{A.11}$$

$$\sin 4f = 2\cos 2f \sin 2f \tag{A.12}$$

It is fundamental to write each term function of the true anomaly in terms of the eccentric one, otherwise, the integral cannot be solved.

Integral in terms of the true anomaly In this case the integrals is expressed through the true anomaly by using the relations recovered by ecliptic expansion (Danby, [70]; Hu and Scheeres, [71]):

$$dM = \frac{r^2}{a^2(1 - e^2)^{1/2}}\, df, \tag{A.13}$$

$$r = \frac{a(1 - e^2)}{1 + e\cos f}, \tag{A.14}$$

yielding to a new expression of the averaging procedure, which is completely equivalent ot the previous one:

$$\frac{1}{2\pi}\int_0^{2\pi} fun(M)\,dM = \frac{1}{2\pi}\int_0^{2\pi} fun(f)\frac{r^2(f)}{a^2(1-e^2)^{1/2}}\,df \tag{A.15}$$

A.2 Latitude and argument of latitude

An other important part is to correctly express the satellite latitude δ in terms of the equatorial satellite elements. Starting from the geometric representation, shown in figure A.1, the sine law in the spheric geometry is introduced.

Sine Theorem in spherical geometry:

$$\frac{\sin A}{\sin a} = \frac{\sin B}{\sin b} \qquad \rightarrow \qquad \sin\delta = \sin i \sin u \tag{A.16}$$

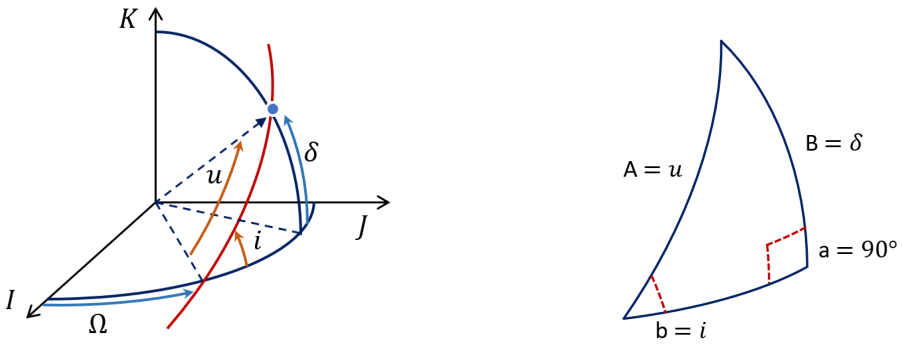

(a) Orbital Geometry in the equatorial frame.

(b) Spherical Triangle.

Figure A.1 Spherical Geometry in the equatorial frame I, J, K with I aligned with the γ direction to the equinox.

Appendix B

Planetary Fact Sheet

The numerical values used during the disturbing potential computations are reported in this appendix. Sun, Moon, Earth and Venus main characteristics are described in table B.1. All the data are retrieved from NASA website[1]: "Planetary fact Sheet"

Table B.1 Planetary Fact Sheet in metric units

	Venus	Earth	Moon	Sun
Mass (10^{24} kg)	4.87	5.97	0.073	1988500
Diameter (km)	12104	12756	3475	-
μ ($1 \times 10^6\,\mathrm{km}^3/\mathrm{s}^2$)	0.32486	0.39860	0.00490	132712
Orbital period (days)	224.7	365.2	27.3	-
Orbit semi-major axis (1×10^6 km)	108.21	149.60	0.3844	-
Orbit inclination (deg)	3.4	0.0	5.1	-
Obliquity of the orbit	177.4	23.4	6.7	-
J_2 $\times 10^{-6}$	4.458	1082.63	202.7	-
Atmospheric altitude (km)	250	120	-	-

[1] `https://nssdc.gsfc.nasa.gov/planetary/factsheet/`

Appendix C

Third body disturbing potential: Moon

C.1 A and B coefficient

A coefficient

$$\begin{aligned} A_{moon} = &\sin\omega((\cos i\cos i_{moon}\cos(\Omega-\Omega_{moon})+ \\ &+\sin i\sin i_{moon})\sin(\omega_{moon}+f_{moon})+ \\ &-\cos i\cos(\omega_{moon}+f_{moon})\sin(\Omega-\Omega_{moon}))+ \\ &\cos\omega(\cos(\omega_{moon}+f_{moon})\cos(\Omega-\Omega_{moon})+ \\ &+\cos i_{moon}\sin(\omega_{moon}+f_{moon}\sin(\Omega-\Omega_{moon})) \end{aligned} \tag{C.1}$$

B coefficient

$$\begin{aligned} B_{moon} = &\cos\omega\sin i\sin i_{moon}\sin(\omega_{moon}+f_{moon})+ \\ &(\cos i\cos\omega\cos\Omega-\sin\omega\sin\Omega) \\ &(\cos i_{moon}\cos\Omega_{moon}\sin(\omega_{moon}+f_{moon})+ \\ &+\cos(\omega_{moon}+f_{moon}\sin\Omega_{moon}))+ \\ &+(\cos\Omega\sin\omega+\cos i\cos\omega\sin\Omega) \\ &(-\cos(\omega_{moon}+f_{moon})\cos\Omega_{moon}+ \\ &\cos i_{moon}\sin(\omega_{moon}+f_{moon})\sin\Omega_{moon}) \end{aligned} \tag{C.2}$$

C.2 Double averaged Moon disturbing function: Circular case

$$\begin{aligned}\bar{\bar{\mathcal{R}}}_{3b,2} =& \frac{\mu_{moon}\, a^2}{128\, a_{moon}^3}\Big[\cos 2i_{moon}\left(6+9\,e^2+90\,e^2\cos 2\omega\sin^2 i\right)+\\ &+(2+3\,e^2+15\,e^2\cos 2\omega)(1+6\cos\delta\Omega\sin^2 i_{moon})+\\ &+3\cos 2i_{moon}\Big(\left((6+9\,e^2\right)\cos 2i_{moon}+\\ &+(-2-3\,e^2+5\,e^2\cos 2\omega)(-1+2\cos\Delta\Omega\sin^2 i_{moon})\Big)+\\ &+12\left(2+3\,e^2-5\,e^2\cos 2\omega\right)\cos 2\delta\Omega\sin 2i\sin 2i_{moon}+\\ &+120\,e^2\sin i\sin 2i_{moon}\sin\Delta\Omega+\\ &-120e^2\cos i\sin^2 i_{moon}\sin 2\omega\sin 2\Delta\Omega\Big]\end{aligned} \tag{C.3}$$

$$\bar{\bar{\mathcal{R}}}_{3b,3} = 0 \tag{C.4}$$

$$\begin{aligned}\bar{\bar{\mathcal{R}}}_{3b,4} =& \frac{3\mu_{\mathbb{C}}\, a^4}{65536 a_{\mathbb{C}}^5}\Big(-47040\cos 2\omega\sin^4 i\sin^4 i_{\mathbb{C}}\, e^4+35280\cos 4\omega\sin^4 i\sin^4 i_{\mathbb{C}}\, e^4+25200\sin^4 i\sin^4 i_{\mathbb{C}}\, e^4\\ &+8400\cos 2\Delta\Omega\sin^2 i\sin^2 i_{\mathbb{C}}\, e^4+53760\cos 2\omega\sin^2 i\sin^2 i_{\mathbb{C}}\, e^4-35280\cos 4\omega\sin^2 i\sin^2 i_{\mathbb{C}}\, e^4\\ &-17640\cos(2(2\omega-\Delta\Omega))\sin^2 i\sin^2 i_{\mathbb{C}}\, e^4-17640\cos(2(-\Delta\Omega-2\omega))\sin^2 i\sin^2 i_{\mathbb{C}}\, e^4\\ &-30000\sin^2 i\sin^2 i_{\mathbb{C}}\, e^4-6600\cos 2\Delta\Omega e^4+3150\cos 4\Delta\Omega e^4\\ &-1680\cos(2(-\Delta\Omega-\omega))e^4+2205\cos(4(-\Delta\Omega-\omega))e^4+8820\cos(2(2\omega-\Delta\Omega))e^4\\ &-9240\cos 2\omega e^4+13230\cos 4\omega e^4-1680\cos(2(\omega-\Delta\Omega))e^4+2205\cos(4(\omega-\Delta\Omega))e^4\\ &+8820\cos(2(-\Delta\Omega-2\omega))e^4+2940\cos(2(\omega-2\Omega+2\Omega_{\mathbb{C}}))e^4+2940\cos(2(\omega+2\Omega)-4\Omega_{\mathbb{C}})e^4+5610e^4\\ &-94080\cos 2\omega\sin^4 i\sin^4 i_{\mathbb{C}}\, e^2+67200\sin^4 i\sin^4 i_{\mathbb{C}}\, e^2+22400\cos 2\Delta\Omega\sin^2 i\sin^2 i_{\mathbb{C}}\, e^2\\ &+107520\cos 2\omega\sin^2 i\sin^2 i_{\mathbb{C}}\, e^2-80000\sin^2 i\sin^2 i_{\mathbb{C}}\, e^2-17600\cos 2\Delta\Omega e^2+8400\cos 4\Delta\Omega e^2\\ &-18480\cos 2\omega e^2-3360\cos(2(\omega-\Delta\Omega))e^2+5880\cos(2(\omega-2\Omega+2\Omega_{\mathbb{C}}))e^2\\ &+94080(3\cos 2\omega e^2+e^2+2)\cos^3 i_{\mathbb{C}}\,\sin i\sin^3(\Delta\Omega)\sin 2\omega\sin i_{\mathbb{C}}\, e^2+5880\cos(2(\omega+2\Omega)-4\Omega_{\mathbb{C}})e^2\\ &+3360\cos i_{\mathbb{C}}\,\sin i\sin(\Delta\Omega)\sin 2\omega\sin i_{\mathbb{C}}\,(14\cos 2\Delta\Omega e^2+21\cos(2(-\Delta\Omega-\omega))e^2+42\cos 2\omega e^2\\ &+21\cos(2(\omega-\Delta\Omega))e^2-18e^2-28(3\cos 2\omega e^2-e^2-2)\sin^2 i\sin^2 i_{\mathbb{C}}\,+28\cos 2\Delta\Omega-36)e^2+14960e^2\\ &+28(e^2+2)\cos 2\omega e^2+40e^2+8)\cos^4 i_{\mathbb{C}}\,\sin^4(\Delta\Omega)+13440\sin^4 i\sin^4 i_{\mathbb{C}}\,+1680\cos^4 i(21\cos 4\omega e^4+15e^4\\ &+40e^2+8)(\cos^2(\Delta\Omega)\cos^2 i_{\mathbb{C}}\,+\sin^2(\Delta\Omega))^2+4480\cos 2\Delta\Omega\sin^2 i\sin^2 i_{\mathbb{C}}\,-16000\sin^2 i\sin^2 i_{\mathbb{C}}\\ &-3520\cos 2\Delta\Omega+1680\cos 4\Delta\Omega+3360\cos^3 i\cos(\Delta\Omega)(\cos^2(\Delta\Omega)\cos^2 i_{\mathbb{C}}\\ &+\sin^2(\Delta\Omega))(-28(3\cos 2\omega e^2-e^2-2)\cos^2 i_{\mathbb{C}}\,\sin(\Delta\Omega)\sin 2\omega e^2-28(-3\cos 2\omega e^2+e^2+2)\sin(\Delta\Omega)\sin 2\omega e^2\\ &+2(21\cos 4\omega e^4+15e^4-28(e^2+2)\cos 2\omega e^2+40e^2+8)\cos i_{\mathbb{C}}\,\sin i\sin i_{\mathbb{C}}\,)\\ &+40\cos^2 i_{\mathbb{C}}\,\sin^2(\Delta\Omega)(630\cos 2\Delta\Omega e^4+588\cos(2(-\Delta\Omega-\omega))e^4+882\cos 4\omega e^4+588\cos(2(\omega-\Delta\Omega))e^4\end{aligned} \tag{C.5}$$

$$
\begin{aligned}
&+ 441\cos(2(2\omega-\Delta\Omega))e^4 + 441\cos(2(-\Delta\Omega-2\omega))e^4 - 330e^4 + 1680\cos 2\Delta\Omega e^2 + 1176\cos(2(-\Delta\Omega-\omega))e^2\\
&- 168(e^2+2)\cos 2\omega e^2 - 28(e^2+2)\cos 2\omega e^2 + 40e^2 + 8)\sin^2 i\sin^2 i_{\mathbb{C}}\\
&+ 1176\cos(2(\omega-\Delta\Omega))e^2 - 880e^2 - 84(63\cos 4\omega e^4 - 15e^4 - 40e^2 - 8)\sin^2 i\sin^2 i_{\mathbb{C}} + 336\cos 2\Delta\Omega - 176)\\
&+ 120\cos i\cos(\Delta\Omega)(784e^2(3\cos 2\omega e^2 + e^2 + 2)\sin^3(\Delta\Omega)\sin 2\omega\cos^4 i_{\mathbb{C}}\\
&- 56(63\cos 4\omega e^4 - 15e^4 - 40e^2 - 8)\sin i\sin^2(\Delta\Omega)\sin i_{\mathbb{C}}\cos^3 i_{\mathbb{C}} + 56e^2\sin(\Delta\Omega)\sin 2\omega(21\cos(2(-\Delta\Omega-\omega))e^2\\
&+ 21\cos(2(\omega-\Delta\Omega))e^2 - 16e^2 - 42(3\cos 2\omega e^2 - e^2 - 2)\sin^2 i\sin^2 i_{\mathbb{C}} + 14(e^2+2)\cos 2\Delta\Omega - 32)\cos^2 i_{\mathbb{C}}\\
&+ 2\sin i\sin i_{\mathbb{C}}(210\cos 2\Delta\Omega e^4 + 294\cos 4\omega e^4 - 441\cos(2(2\omega-\Delta\Omega))e^4 - 441\cos(2(-\Delta\Omega-2\omega))e^4 - 390e^4\\
&+ 560\cos 2\Delta\Omega e^2 + 448(e^2+2)\cos 2\omega e^2 - 1040e^2 + 28(21\cos 4\omega e^4 + 15e^4\\
&+ 112\cos 2\Delta\Omega - 208)\cos i_{\mathbb{C}} - 28e^2\sin(\Delta\Omega)\sin 2\omega(14\cos 2\Delta\Omega e^2 + 21\cos(2(-\Delta\Omega-\omega))e^2 + 42\cos 2\omega e^2\\
&+ 21\cos(2(\omega-\Delta\Omega))e^2 - 18e^2 - 28(3\cos 2\omega e^2 - e^2 - 2)\sin^2 i\sin^2 i_{\mathbb{C}} + 28\cos 2\Delta\Omega - 36))\\
&- 10\cos^2 i(84(63\cos 4\omega e^4 - 15e^4 - 40e^2 - 8)\sin^2 2\Delta\Omega\cos^4 i_{\mathbb{C}} - 1344\cos(2(-\Delta\Omega-\omega))e^2\\
&+ 28224e^2\cos^2(\Delta\Omega)(3\cos 2\omega e^2 - e^2 - 2)\sin i\sin(\Delta\Omega)\sin 2\omega\sin i_{\mathbb{C}}\cos^3 i_{\mathbb{C}}\\
&+ 2(960\cos 2\Delta\Omega e^4 - 630\cos 4\Delta\Omega e^4 - 672\cos(2(-\Delta\Omega-\omega))e^4 + 1323\cos(4(-\Delta\Omega-\omega))e^4 + 882\cos 4\omega e^4\\
&- 672\cos(2(\omega-\Delta\Omega))e^4 + 1323\cos(4(\omega-\Delta\Omega))e^4 + 750e^4 + 2560\cos 2\Delta\Omega e^2 - 1680\cos 4\Delta\Omega e^2\\
&- 1344(e^2+2)\cos 2\omega e^2 - 1344\cos(2(\omega-\Delta\Omega))e^2 + 2000e^2 - 504\cos^2(\Delta\Omega)(21\cos 4\omega e^4 + 15e^4\\
&+ 40e^2 + 8)\sin^2 i\sin^2 i_{\mathbb{C}} + 512\cos 2\Delta\Omega - 336\cos 4\Delta\Omega + 400)\cos^2 i_{\mathbb{C}} - 28(e^2+2)\cos 2\omega e^2\\
&- 2352e^2(3\cos 2\omega e^2 - e^2 - 2)\sin i(3\sin(3\Delta\Omega) - \sin(\Delta\Omega))\sin 2\omega\sin i_{\mathbb{C}}\cos i_{\mathbb{C}}\\
&+ 4\sin^2(\Delta\Omega)(-630\cos 2\Delta\Omega e^4 + 2646\cos 4\omega e^4 + 1323\cos(2(2\omega-\Delta\Omega))e^4 + 1323\cos(2(-\Delta\Omega-2\omega))e^4 + 330e^4\\
&- 1680\cos 2\Delta\Omega e^2 - 1344(e^2+2)\cos 2\omega e^2 + 880e^2 - 84(21\cos 4\omega e^4\\
&+ 15e^4 - 28(e^2+2)\cos 2\omega e^2 + 40e^2 + 8)\sin^2 i\sin^2 i_{\mathbb{C}} - 336\cos 2\Delta\Omega + 176)) + 2992\Big)
\end{aligned}
$$

C.3 Double averaged Moon disturbing function: Elliptical case

$$
\begin{aligned}
\bar{\bar{\mathcal{R}}}_{\mathbb{C},2} = \frac{\mu_{\mathbb{C}}}{32\,a_{\mathbb{C}}^3\,(1-e_{\mathbb{C}}^2)^{3/2}}\Big(&30\,e^2\cos\ 2\omega\cos^2\Delta\Omega + (2+3\,e^2)(-5+3\cos 2\Delta\Omega)\\
&+ 6(2+3\,e^2+5e^2\cos 2\omega)\sin^2\Delta\Omega\cos^2 i_{\mathbb{C}}\\
&- 6(-2-3\,e^2+5e^2\cos 2\omega)\cos^2 i(\sin^2\Delta\Omega + \cos^2\Delta\Omega\cos^2 i_{\mathbb{C}})\\
&- 60\,e^2\sin 2\omega\sin\Delta\Omega\cos i_{\mathbb{C}}\ \sin i\sin i_{\mathbb{C}} + 6(2+3\,e^2-5\,e^2\cos 2\omega)\sin^2 i\sin^2 i_{\mathbb{C}} +\\
&+ 6\cos i(-5\,e^2\sin 2\omega\sin 2\Delta\Omega(1-\cos^2 i_{\mathbb{C}}) + 2(2+3\,e^2-5\,e^2\cos 2\omega)\cos\Delta\Omega\cos i_{\mathbb{C}}\ \sin i\cos i_{\mathbb{C}})\Big)
\end{aligned}
\tag{C.6}
$$

$$
\begin{aligned}
\bar{\bar{\mathcal{R}}}_{\mathbb{C},3} = &-\frac{15\mu_{\mathbb{C}}\ a^3\, e\, e_{\mathbb{C}}}{512 a_{\mathbb{C}}^4\,(1-e_{\mathbb{C}}^2\,)^{5/2}}\Big(35e^2\cos(2(-\Delta\Omega-\omega))+35e^2\cos(2(\omega-\Delta\Omega))\\
&+10(e^2+6)\cos 2\Delta\Omega+70e^2\cos 2\omega-86e^2-68)\cos\omega_{\mathbb{C}}\\
&-20\cos\Delta\Omega\sin^2 i\cos\omega(7e^2\cos 2\omega-5e^2-2)\sin^2 i_{\mathbb{C}}\ \cos\omega_{\mathbb{C}}\\
&+20\sin^3\Delta\Omega\cos\omega(7e^2\cos 2\omega+e^2+6)\cos^3 i_{\mathbb{C}}\ \sin\omega_{\mathbb{C}}\ +\sin i\sin\omega\sin i_{\mathbb{C}}\ \sin\omega_{\mathbb{C}}\ (35e^2\cos(2(-\Delta\Omega-\omega))\\
&+35e^2\cos(2(\omega-\Delta\Omega))+10(5e^2+2)\cos 2\Delta\Omega+70e^2\cos 2\omega-46e^2-108)\\
&-20\sin^3 i\sin\omega(7e^2\cos 2\omega-e^2-6)\sin^3 i_{\mathbb{C}}\ \sin\omega_{\mathbb{C}}\\
&-20\cos^3 i\sin\omega(7e^2\cos 2\omega-e^2-6)(\sin^2\Delta\Omega+\cos^2\Delta\Omega\cos^2 i_{\mathbb{C}}\,)(\cos\Delta\Omega\cos i_{\mathbb{C}}\ \sin\omega_{\mathbb{C}}\\
&-\sin\Delta\Omega\cos\omega_{\mathbb{C}}\,)+10\sin^2\Delta\Omega\cos^2 i_{\mathbb{C}}\ (6\sin i\sin\omega(7e^2\cos 2\omega+5e^2+2)\sin i_{\mathbb{C}}\ \sin\omega_{\mathbb{C}}\\
&+2\cos\Delta\Omega\cos\omega(7e^2\cos 2\omega+e^2+6)\cos\omega_{\mathbb{C}}\,)\\
&+\cos i_{\mathbb{C}}\ (-60\sin\Delta\Omega\sin^2 i\cos\omega(7e^2\cos 2\omega-5e^2-2)\sin^2 i_{\mathbb{C}}\ \sin\omega_{\mathbb{C}}\\
&+20\sin 2\Delta\Omega\sin i\sin\omega(7e^2\cos 2\omega+5e^2+2)\sin i_{\mathbb{C}}\ \cos\omega_{\mathbb{C}}\ +\sin\Delta\Omega\cos\omega\sin\omega_{\mathbb{C}}\ (35e^2\cos(2(-\Delta\Omega-\omega))\\
&+35e^2\cos(2(\omega-\Delta\Omega))+10(e^2+6)\cos 2\Delta\Omega+70e^2\cos 2\omega-86e^2-68))\\
&-5\cos^2 i(\cos^2 i_{\mathbb{C}}\ (12\cos^2\Delta\Omega\sin i\sin\omega(7e^2\cos 2\omega-e^2-6)\\
&\sin i_{\mathbb{C}}\ \sin\omega_{\mathbb{C}}\ +(\cos\Delta\Omega+3\cos 3\Delta\Omega)\cos\omega(7e^2\cos 2\omega-5e^2-2)\cos\omega_{\mathbb{C}}\,)\\
&+12\sin\Delta\Omega\cos^2\Delta\Omega\cos\omega(7e^2\cos 2\omega-5e^2-2)\cos^3 i_{\mathbb{C}}\ \sin\omega_{\mathbb{C}}\\
&+4\sin^2\Delta\Omega(\sin i\sin\omega(7e^2\cos 2\omega-e^2-6)\sin i_{\mathbb{C}}\ \sin\omega_{\mathbb{C}}\\
&+3\cos\Delta\Omega\cos\omega(7e^2\cos 2\omega-5e^2-2)\cos\omega_{\mathbb{C}}\,)+2\cos i_{\mathbb{C}}\ (-2\sin 2\Delta\Omega\sin i\sin\omega(7e^2\cos 2\omega-e^2-6)\sin i_{\mathbb{C}}\ \cos\omega_{\mathbb{C}}\\
&-\sin\Delta\Omega(3\cos 2\Delta\Omega+1)\cos\omega(7e^2\cos 2\omega-5e^2-2)\sin\omega_{\mathbb{C}}\,))\\
&+\cos i(60\sin^2\Delta\Omega\cos\Delta\Omega\sin\omega(7e^2\cos 2\omega+5e^2+2)\\
&\cos^3 i_{\mathbb{C}}\ \sin\omega_{\mathbb{C}}\ +5\cos^2 i_{\mathbb{C}}\ ((3\sin 3\Delta\Omega-\sin\Delta\Omega)\sin\omega(7e^2\cos 2\omega+5e^2+2)\cos\omega_{\mathbb{C}}\\
&-12\sin 2\Delta\Omega\sin i\cos\omega(7e^2\cos 2\omega-5e^2-2)\sin i_{\mathbb{C}}\ \sin\omega_{\mathbb{C}}\,)+\cos i_{\mathbb{C}}\ (-60\cos\Delta\Omega\sin^2 i\\
&\sin\omega(7e^2\cos 2\omega-e^2-6)\sin^2 i_{\mathbb{C}}\ \sin\omega_{\mathbb{C}}\ -40\cos 2\Delta\Omega\sin i\cos\omega(7e^2\cos 2\omega-5e^2-2)\sin i_{\mathbb{C}}\ \cos\omega_{\mathbb{C}}\\
&+\cos\Delta\Omega\sin\omega\sin\omega_{\mathbb{C}}\ (105e^2\cos(2(-\Delta\Omega-\omega))+105e^2\cos(2(\omega-\Delta\Omega))\\
&+30(5e^2+2)\cos 2\Delta\Omega-70e^2\cos 2\omega-146e^2-148))\\
&+20\sin\Delta\Omega\sin^2 i\sin\omega(7e^2\cos 2\omega-e^2-6)\sin^2 i_{\mathbb{C}}\ \cos\omega_{\mathbb{C}}\\
&+20\sin 2\Delta\Omega\sin i\cos\omega(7e^2\cos 2\omega-5e^2-2)\sin i_{\mathbb{C}}\ \sin\omega_{\mathbb{C}}\\
&+\sin\Delta\Omega\sin\omega\cos\omega_{\mathbb{C}}\ (-105e^2\cos(2(-\Delta\Omega-\omega))-105e^2\cos(2(\omega-\Delta\Omega))\\
&-30(5e^2+2)\cos 2\Delta\Omega-210e^2\cos 2\omega-54e^2+68))\Big)
\end{aligned}
\tag{C.7}
$$

$$
\begin{aligned}
\bar{\bar{\mathcal{R}}}_{\mathbb{C},4} = -\frac{15a^3 e e_{\mathbb{C}}\,\mu_{\mathbb{C}}}{512 a_{\mathbb{C}}^4\,(1-e_{\mathbb{C}}^2)^{5/2}}\Big(& -20(7\cos 2\omega e^2 - e^2 - 6)(\cos^2\Delta\Omega\cos^2 i_{\mathbb{C}} \\
& + \sin^2\Delta\Omega)\sin\omega(\cos\Delta\Omega\cos i_{\mathbb{C}}\ \sin\omega_{\mathbb{C}} \\
& - \cos\omega_{\mathbb{C}}\ \sin\Delta\Omega)\cos^3 i - 5(12\cos^2\Delta\Omega\cos\omega(7\cos 2\omega e^2 - 5e^2 - 2)\sin\Delta\Omega\sin\omega_{\mathbb{C}}\ \cos^3 i_{\mathbb{C}} \\
& + (12(7\cos 2\omega e^2 - e^2 - 6)\sin i\sin\omega\sin i_{\mathbb{C}}\ \sin\omega_{\mathbb{C}}\ \cos^2\Delta\Omega \\
& + (\cos\Delta\Omega + 3\cos 3\Delta\Omega)\cos\omega(7\cos 2\omega e^2 - 5e^2 - 2)\cos\omega_{\mathbb{C}}\,)\cos^2 i_{\mathbb{C}} \\
& + 2(-2(7\cos 2\omega e^2 - e^2 - 6)\cos\omega_{\mathbb{C}}\ \sin i\sin 2\Delta\Omega\sin\omega\sin i_{\mathbb{C}} \\
& - (3\cos 2\Delta\Omega + 1)\cos\omega(7\cos 2\omega e^2 - 5e^2 - 2)\sin\Delta\Omega\sin\omega_{\mathbb{C}}\,)\cos i_{\mathbb{C}} \\
& + 4\sin^2\Delta\Omega(3\cos\Delta\Omega\cos\omega(7\cos 2\omega e^2 - 5e^2 - 2)\cos\omega_{\mathbb{C}} \\
& + (7\cos 2\omega e^2 - e^2 - 6)\sin i\sin\omega\sin i_{\mathbb{C}}\ \sin\omega_{\mathbb{C}}\,))\cos^2 i \\
& + (60\cos\Delta\Omega(7\cos 2\omega e^2 + 5e^2 + 2)\sin^2\Delta\Omega\sin\omega\sin\omega_{\mathbb{C}}\ \cos^3 i_{\mathbb{C}} \\
& + 5((7\cos 2\omega e^2 + 5e^2 + 2)\cos\omega_{\mathbb{C}}\,(3\sin 3\Delta\Omega \\
& - \sin\Delta\Omega)\sin\omega - 12\cos\omega(7\cos 2\omega e^2 - 5e^2 - 2)\sin i\sin 2\Delta\Omega\sin i_{\mathbb{C}}\ \sin\omega_{\mathbb{C}}\,)\cos^2 i_{\mathbb{C}} \\
& + (-60\cos\Delta\Omega(7\cos 2\omega e^2 - e^2 - 6)\sin^2 i\sin\omega\sin\omega_{\mathbb{C}}\ \sin^2 i_{\mathbb{C}} \\
& - 40\cos 2\Delta\Omega\cos\omega(7\cos 2\omega e^2 - 5e^2 - 2)\cos\omega_{\mathbb{C}}\ \sin i\sin i_{\mathbb{C}} \\
& + \cos\Delta\Omega(105\cos(2(-\Delta\Omega-\omega))e^2 - 70\cos 2\omega e^2 + 105\cos(2(\omega-\Delta\Omega))e^2 \\
& - 146e^2 + 30(5e^2+2)\cos 2\Delta\Omega - 148)\sin\omega\sin\omega_{\mathbb{C}}\,)\cos i_{\mathbb{C}} \\
& + 20(7\cos 2\omega e^2 - e^2 - 6)\cos\omega_{\mathbb{C}}\ \sin^2 i\sin\Delta\Omega\sin\omega\sin^2 i_{\mathbb{C}} \\
& + (-105\cos(2(-\Delta\Omega-\omega))e^2 - 210\cos 2\omega e^2 - 105\cos(2(\omega-\Delta\Omega))e^2 - 54e^2 \\
& - 30(5e^2+2)\cos 2\Delta\Omega + 68)\cos\omega_{\mathbb{C}}\ \sin\Delta\Omega\sin\omega \\
& + 20\cos\omega(7\cos 2\omega e^2 - 5e^2 - 2)\sin i\sin 2\Delta\Omega\sin i_{\mathbb{C}}\ \sin\omega_{\mathbb{C}}\,)\cos i \\
& - 20\cos\Delta\Omega\cos\omega(7\cos 2\omega e^2 - 5e^2 - 2)\cos\omega_{\mathbb{C}}\ \sin^2 i\sin^2 i_{\mathbb{C}}\ + \cos\Delta\Omega\cos\omega(35\cos(2(-\Delta\Omega-\omega))e^2 \\
& + 70\cos 2\omega e^2 + 35\cos(2(\omega-\Delta\Omega))e^2 - 86e^2 + 10(e^2+6)\cos 2\Delta\Omega - 68)\cos\omega_{\mathbb{C}} \\
& + 20\cos\omega(7\cos 2\omega e^2 + e^2 + 6)\cos^3 i_{\mathbb{C}}\ \sin^3\Delta\Omega\sin\omega_{\mathbb{C}}\ - 20(7\cos 2\omega e^2 - e^2 - 6)\sin^3 i\sin\omega \\
& \sin^3 i_{\mathbb{C}}\ \sin\omega_{\mathbb{C}}\ + (35\cos(2(-\Delta\Omega-\omega))e^2 + 70\cos 2\omega e^2 + 35\cos(2(\omega-\Delta\Omega))e^2 - 46e^2 \\
& + 10(5e^2+2)\cos 2\Delta\Omega - 108)\sin i\sin\omega\sin i_{\mathbb{C}}\ \sin\omega_{\mathbb{C}} \\
& + 10\cos^2 i_{\mathbb{C}}\ \sin^2\Delta\Omega(2\cos\Delta\Omega\cos\omega(7\cos 2\omega e^2 + e^2 + 6)\cos\omega_{\mathbb{C}} \\
& + 6(7\cos 2\omega e^2 + 5e^2 + 2)\sin i\sin\omega\sin i_{\mathbb{C}}\ \sin\omega_{\mathbb{C}}\,) \\
& + \cos i_{\mathbb{C}}\,(-60\cos\omega(7\cos 2\omega e^2 - 5e^2 - 2)\sin^2 i\sin\Delta\Omega\sin\omega_{\mathbb{C}}\ \sin^2 i_{\mathbb{C}} \\
& + 20(7\cos 2\omega e^2 + 5e^2 + 2)\cos\omega_{\mathbb{C}}\ \sin i\sin 2\Delta\Omega\sin\omega\sin i_{\mathbb{C}}\ + \cos\omega(35\cos(2(-\Delta\Omega-\omega))e^2 \\
& + 70\cos 2\omega e^2 + 35\cos(2(\omega-\Delta\Omega))e^2 - 86e^2 + 10(e^2+6)\cos 2\Delta\Omega - 68)\sin\Delta\Omega\sin\omega_{\mathbb{C}}\,)\Big)
\end{aligned}
\tag{C.8}
$$

+ go to next page

$$+\frac{a^2\mu_{\leftmoon}}{32a_{\leftmoon}^3(1-e_{\leftmoon}^2)^{3/2}}\Big(30e^2\cos^2\Delta\Omega\cos 2\omega+(3e^2+2)(3\cos 2\Delta\Omega-5)+6\sin^2\Delta\Omega(5e^2\cos 2\omega+3e^2+2)\cos^2 i_{\leftmoon}$$
$$-6\cos^2 i(5e^2\cos 2\omega-3e^2-2)(\sin^2\Delta\Omega+\cos^2\Delta\Omega\cos^2 i_{\leftmoon})+6\cos i(5e^2\sin 2\Delta\Omega\sin 2\omega(\cos^2 i_{\leftmoon}-1)$$
$$+2\cos\Delta\Omega\sin i(-5e^2\cos 2\omega+3e^2+2)\sin i_{\leftmoon}\cos i_{\leftmoon})$$
$$+60e^2\sin\Delta\Omega\sin i\sin 2\omega\sin i_{\leftmoon}\cos i_{\leftmoon}+6\sin^2 i(-5e^2\cos 2\omega+3e^2+2)\sin^2 i_{\leftmoon}\Big)$$
$$+\frac{9a^4(e_{\leftmoon}^2+2)\mu_{\leftmoon}}{1024a_{\leftmoon}^5(1-e_{\leftmoon}^2)^{7/2}}\Big(35(e^2-1)^2(\sin(\Delta\Omega)\sin\omega(-\cos i_{\leftmoon})\cos\omega_{\leftmoon}$$
$$+\cos i\cos\omega(\cos\Delta\Omega\cos i_{\leftmoon}\cos\omega_{\leftmoon}+\sin\Delta\Omega\sin\omega_{\leftmoon})+\sin i\cos\omega\sin i_{\leftmoon}\cos\omega_{\leftmoon}+\cos\Delta\Omega\sin\omega\sin\omega_{\leftmoon})^4$$
$$-70(6e^4-5e^2-1)(\sin\Delta\Omega\cos\omega\cos i_{\leftmoon}\cos\omega_{\leftmoon}+\cos i\sin\omega(\cos\Delta\Omega\cos i_{\leftmoon}\cos\omega_{\leftmoon}$$
$$+\sin\Delta\Omega\sin\omega_{\leftmoon})+\sin i\sin\omega\sin i_{\leftmoon}\cos\omega_{\leftmoon}-\cos\Delta\Omega\cos\omega\sin\omega_{\leftmoon})^2(\sin\Delta\Omega\sin\omega(-\cos i_{\leftmoon})\cos\omega_{\leftmoon}$$
$$+\cos i\cos\omega(\cos\Delta\Omega\cos i_{\leftmoon}\cos\omega_{\leftmoon}+\sin\Delta\Omega\sin\omega_{\leftmoon})+\sin i\cos\omega\sin i_{\leftmoon}\cos\omega_{\leftmoon}+\cos\Delta\Omega\sin\omega\sin\omega_{\leftmoon})^2$$
$$+35(8e^4+12e^2+1)(\sin\Delta\Omega\cos\omega\cos i_{\leftmoon}\cos\omega_{\leftmoon}+\cos i\sin\omega(\cos\Delta\Omega\cos i_{\leftmoon}\cos\omega_{\leftmoon}$$
$$+\sin\Delta\Omega\sin\omega_{\leftmoon})+\sin i\sin\omega\sin i_{\leftmoon}\cos\omega_{\leftmoon}-\cos\Delta\Omega\cos\omega\sin\omega_{\leftmoon})^4\Big)$$
$$+\frac{3a^4(15e^4+40e^2+8)(3e_{\leftmoon}^2+2)\mu_{\leftmoon}}{128a_{\leftmoon}^5(1-e_{\leftmoon}^2)^{7/2}}$$
$$+\frac{3a^4(3e_{\leftmoon}^2+4)\mu_{\leftmoon}}{512a_{\leftmoon}^5(1-e_{\leftmoon}^2)^{7/2}}\Big(-180e^4(\sin\Delta\Omega\cos\omega\cos i_{\leftmoon}\cos\omega_{\leftmoon}$$
$$+\cos i\sin\omega(\cos\Delta\Omega\cos i_{\leftmoon}\cos\omega_{\leftmoon}+\sin\Delta\Omega\sin\omega_{\leftmoon})+\sin i\sin\omega\sin i_{\leftmoon}\cos\omega_{\leftmoon}-\cos\Delta\Omega\cos\omega\sin\omega_{\leftmoon})^2$$
$$-410e^2(\sin\Delta\Omega\cos\omega\cos i_{\leftmoon}\cos\omega_{\leftmoon}+\cos i\sin\omega(\cos\Delta\Omega\cos i_{\leftmoon}\cos\omega_{\leftmoon}$$
$$+\sin\Delta\Omega\sin\omega_{\leftmoon})+\sin i\sin\omega\sin i_{\leftmoon}\cos\omega_{\leftmoon}-\cos\Delta\Omega\cos\omega\sin\omega_{\leftmoon})^2$$
$$+10(3e^4+e^2-4)(\sin\Delta\Omega\sin\omega(-\cos i_{\leftmoon})\cos\omega_{\leftmoon}+\cos i\cos\omega(\cos\Delta\Omega\cos i_{\leftmoon}\cos\omega_{\leftmoon}$$
$$+\sin\Delta\Omega\sin\omega_{\leftmoon})+\sin i\cos\omega\sin i_{\leftmoon}\cos\omega_{\leftmoon}+\cos\Delta\Omega\sin\omega\sin\omega_{\leftmoon})^2$$
$$-40(\sin\Delta\Omega\cos\omega\cos i_{\leftmoon}\cos\omega_{\leftmoon}+\cos i\sin\omega(\cos\Delta\Omega\cos i_{\leftmoon}\cos\omega_{\leftmoon}$$
$$+\sin\Delta\Omega\sin\omega_{\leftmoon})+\sin i\sin\omega\sin i_{\leftmoon}\cos\omega_{\leftmoon}-\cos\Delta\Omega\cos\omega\sin\omega_{\leftmoon})^2\Big)$$
$$+\frac{3a^4(9e_{\leftmoon}^2+4)\mu_{\leftmoon}}{512a_{\leftmoon}^5(1-e_{\leftmoon}^2)^{7/2}}(-180e^4(\sin\Delta\Omega\cos\omega\cos i_{\leftmoon}\sin\omega_{\leftmoon}+\cos i\sin\omega(\cos\Delta\Omega\cos i_{\leftmoon}\sin\omega_{\leftmoon}$$
$$-\sin\Delta\Omega\cos\omega_{\leftmoon})+\sin i\sin\omega\sin i_{\leftmoon}\sin\omega_{\leftmoon}+\cos\Delta\Omega\cos\omega\cos\omega_{\leftmoon})^2$$
$$-410e^2(\sin\Delta\Omega\cos\omega\cos i_{\leftmoon}\sin\omega_{\leftmoon}+\cos i\sin\omega(\cos\Delta\Omega\cos i_{\leftmoon}\sin\omega_{\leftmoon}$$
$$-\sin\Delta\Omega\cos\omega_{\leftmoon})+\sin i\sin\omega\sin i_{\leftmoon}\sin\omega_{\leftmoon}+\cos\Delta\Omega\cos\omega\cos\omega_{\leftmoon})^2$$
$$+10(3e^4+e^2-4)(-\sin\Delta\Omega\sin\omega\cos i_{\leftmoon}\sin\omega_{\leftmoon}+\cos i\cos\omega(\cos\Delta\Omega\cos i_{\leftmoon}\sin\omega_{\leftmoon}$$
$$-\sin\Delta\Omega\cos\omega_{\leftmoon})+\sin i\cos\omega\sin i_{\leftmoon}\sin\omega_{\leftmoon}-\cos\Delta\Omega\sin\omega\cos\omega_{\leftmoon})^2$$
$$-40(\sin\Delta\Omega\cos\omega\cos i_{\leftmoon}\sin\omega_{\leftmoon}+\cos i\sin\omega(\cos\Delta\Omega\cos i_{\leftmoon}\sin\omega_{\leftmoon}$$
$$-\sin\Delta\Omega\cos\omega_{\leftmoon})+\sin i\sin\omega\sin i_{\leftmoon}\sin\omega_{\leftmoon}+\cos\Delta\Omega\cos\omega\cos\omega_{\leftmoon})^2)$$

go to next page

$$+\frac{3\mu_{☾}\,a^4(3e_{☾}^2+2)}{1024a_{☾}^5\,(1-e_{☾}^2)^{7/2}}\Big(210(e^2-1)^2(-\cos\Delta\Omega\cos\omega_{☾}\,\sin\omega-\cos i_{☾}\,\sin\Delta\Omega\sin\omega_{☾}\,\sin\omega$$
$$+\cos\omega\sin i\sin i_{☾}\,\sin\omega_{☾}+\cos i\cos\omega(\cos\Delta\Omega\cos i_{☾}\,\sin\omega_{☾}$$
$$-\cos\omega_{☾}\,\sin\Delta\Omega))^2(-\cos i_{☾}\,\cos\omega_{☾}\,\sin\Delta\Omega\sin\omega+\cos\Delta\Omega\sin\omega_{☾}\,\sin\omega$$
$$+\cos\omega\cos\omega_{☾}\,\sin i\sin i_{☾}+\cos i\cos\omega(\cos\Delta\Omega\cos i_{☾}\,\cos\omega_{☾}$$
$$+\sin\Delta\Omega\sin\omega_{☾}))^2-70(6e^4-5e^2-1)(\cos\Delta\Omega\cos\omega\cos\omega_{☾}+\cos\omega\cos i_{☾}\,\sin\Delta\Omega\sin\omega_{☾}$$
$$+\sin i\sin\omega\sin i_{☾}\,\sin\omega_{☾}+\cos i\sin\omega(\cos\Delta\Omega\cos i_{☾}\,\sin\omega_{☾}$$
$$-\cos\omega_{☾}\,\sin\Delta\Omega))^2(-\cos i_{☾}\,\cos\omega_{☾}\,\sin\Delta\Omega\sin\omega+\cos\Delta\Omega\sin\omega_{☾}\,\sin\omega$$
$$+\cos\omega\cos\omega_{☾}\,\sin i\sin i_{☾}+\cos i\cos\omega(\cos\Delta\Omega\cos i_{☾}\,\cos\omega_{☾}$$
$$+\sin\Delta\Omega\sin\omega_{☾}))^2-280(6e^4-5e^2-1)(-\cos\Delta\Omega\cos\omega_{☾}\,\sin\omega-\cos i_{☾}\,\sin\Delta\Omega\sin\omega_{☾}\,\sin\omega$$
$$+\cos\omega\sin i\sin i_{☾}\,\sin\omega_{☾}+\cos i\cos\omega(\cos\Delta\Omega\cos i_{☾}\,\sin\omega_{☾}-\cos\omega_{☾}\,\sin\Delta\Omega))(\cos\Delta\Omega\cos\omega\cos\omega_{☾}$$
$$+\cos\omega\cos i_{☾}\,\sin\Delta\Omega\sin\omega_{☾}+\sin i\sin\omega\sin i_{☾}\,\sin\omega_{☾}$$
$$+\cos i\sin\omega(\cos\Delta\Omega\cos i_{☾}\,\sin\omega_{☾}-\cos\omega_{☾}\,\sin\Delta\Omega))(\cos\omega\cos i_{☾}\,\cos\omega_{☾}\,\sin\Delta\Omega$$
$$+\cos\omega_{☾}\,\sin i\sin\omega\sin i_{☾}-\cos\Delta\Omega\cos\omega\sin\omega_{☾}$$
$$+\cos i\sin\omega(\cos\Delta\Omega\cos i_{☾}\,\cos\omega_{☾}+\sin\Delta\Omega\sin\omega_{☾}))(-\cos i_{☾}\,\cos\omega_{☾}\,\sin\Delta\Omega\sin\omega$$
$$+\cos\Delta\Omega\sin\omega_{☾}\,\sin\omega+\cos\omega\cos\omega_{☾}\,\sin i\sin i_{☾}+\cos i\cos\omega(\cos\Delta\Omega\cos i_{☾}\,\cos\omega_{☾}$$
$$+\sin\Delta\Omega\sin\omega_{☾}))-70(6e^4-5e^2-1)(-\cos\Delta\Omega\cos\omega_{☾}\,\sin\omega$$
$$-\cos i_{☾}\,\sin\Delta\Omega\sin\omega_{☾}\,\sin\omega+\cos\omega\sin i\sin i_{☾}\,\sin\omega_{☾}$$
$$+\cos i\cos\omega(\cos\Delta\Omega\cos i_{☾}\,\sin\omega_{☾}-\cos\omega_{☾}\,\sin\Delta\Omega))^2(\cos\omega\cos i_{☾}\,\cos\omega_{☾}\,\sin\Delta\Omega$$
$$+\cos\omega_{☾}\,\sin i\sin\omega\sin i_{☾}-\cos\Delta\Omega\cos\omega\sin\omega_{☾}+\cos i\sin\omega(\cos\Delta\Omega\cos i_{☾}\,\cos\omega_{☾}+\sin\Delta\Omega\sin\omega_{☾}))^2$$
$$+210(8e^4+12e^2+1)(\cos\Delta\Omega\cos\omega\cos\omega_{☾}+\cos\omega\cos i_{☾}\,\sin\Delta\Omega\sin\omega_{☾}$$
$$+\sin i\sin\omega\sin i_{☾}\,\sin\omega_{☾}+\cos i\sin\omega(\cos\Delta\Omega\cos i_{☾}\,\sin\omega_{☾}-\cos\omega_{☾}\,\sin\Delta\Omega))^2(\cos\omega\cos i_{☾}\,\cos\omega_{☾}\,\sin\Delta\Omega$$
$$+\cos\omega_{☾}\,\sin i\sin\omega\sin i_{☾}$$
$$-\cos\Delta\Omega\cos\omega\sin\omega_{☾}+\cos i\sin\omega(\cos\Delta\Omega\cos i_{☾}\,\cos\omega_{☾}+\sin\Delta\Omega\sin\omega_{☾}))^2\Big)$$
$$\frac{9a^4(5e_{☾}^2+2)\mu_{☾}}{1024a_{☾}^5\,(1-e_{☾}^2)^{7/2}}\Big(35(e^2-1)^2(-\sin\Delta\Omega\sin\omega\cos i_{☾}\,\sin\omega_{☾}+\cos i\cos\omega(\cos\Delta\Omega\cos i_{☾}\,\sin\omega_{☾}$$
$$-\sin\Delta\Omega\cos\omega_{☾})+\sin i\cos\omega\sin i_{☾}\,\sin\omega_{☾}-\cos\Delta\Omega\sin\omega\cos\omega_{☾})^4-70(6e^4-5e^2-1)(\sin\Delta\Omega\cos\omega\cos i_{☾}\,\sin\omega_{☾}$$
$$+\cos i\sin\omega(\cos\Delta\Omega\cos i_{☾}\,\sin\omega_{☾}-\sin\Delta\Omega\cos\omega_{☾})+\sin i\sin\omega\sin i_{☾}\,\sin\omega_{☾}$$
$$+\cos\Delta\Omega\cos\omega\cos\omega_{☾})^2(-\sin\Delta\Omega\sin\omega\cos i_{☾}\,\sin\omega_{☾}+\cos i\cos\omega(\cos\Delta\Omega\cos i_{☾}\,\sin\omega_{☾}-\sin\Delta\Omega\cos\omega_{☾})$$
$$+\sin i\cos\omega\sin i_{☾}\,\sin\omega_{☾}$$
$$-\cos\Delta\Omega\sin\omega\cos\omega_{☾})^2+35(8e^4+12e^2+1)(\sin\Delta\Omega\cos\omega\cos i_{☾}\,\sin\omega_{☾}$$
$$+\cos i\sin\omega(\cos\Delta\Omega\cos i_{☾}\,\sin\omega_{☾}-\sin\Delta\Omega\cos\omega_{☾})+\sin i\sin\omega\sin i_{☾}\,\sin\omega_{☾}+\cos\Delta\Omega\cos\omega\cos\omega_{☾})^4\Big)$$

Appendix D

Third body disturbing potential: Sun

D.1 A and B coefficient

A coefficient

$$\begin{aligned} A_{\odot} = &\cos\lambda_{ecl}(\cos\omega\cos\Omega - \sin\omega\sin\Omega\cos i) + \\ &\sin\lambda_{ecl}(\cos\epsilon\cos\omega\sin\Omega + \cos\epsilon\cos\Omega\sin\omega\cos i + \sin\epsilon\sin\omega\sin i) \end{aligned} \tag{D.1}$$

B coefficient

$$\begin{aligned} B_{\odot} = &\cos\lambda_{ecl}(-\cos\Omega\sin\omega - \cos\omega\sin\Omega\cos i) + \\ &\sin\lambda_{ecl}(\cos\epsilon\sin\omega\sin\Omega + \cos\epsilon\cos\omega\cos\Omega\cos i + \sin\epsilon\cos\omega\sin i) \end{aligned} \tag{D.2}$$

D.2 Double averaged Sun disturbing function

$$\begin{aligned} \bar{\bar{\mathcal{R}}}_{\odot,2} = &\frac{\mu_{\odot}\, a^2}{16\, r_{\odot}^3}\Big[-8 - 12\, e^2 + 3(2 + 3\, e^2 + 5\, e^2\cos 2\omega)\cos^2\Omega - 15\, e^2\sin 2\omega\sin 2\Omega\cos i \\ &- 3(-2 - 3\, e^2 + 5\, e^2\cos 2\omega)\sin^2\Omega\cos^2 i - \Big(-3(\cos\epsilon\sin\omega\sin\Omega \\ &+ \cos\epsilon\cos\omega\cos\Omega\cos i + \cos\omega\sin\epsilon\sin i)^2 + 3\, e^2(-\cos\epsilon\sin\omega\sin\Omega + \\ &\cos\epsilon\cos\omega\cos\Omega\cos i + + \cos\epsilon\cos\omega\sin i) - 3(\cos\epsilon\cos\omega\sin\Omega + \\ &\cos\epsilon\cos\Omega\sin\omega\cos i\sin\epsilon\sin\omega\sin i)^2 - 12\, e^2(\cos\epsilon\cos\omega\sin\Omega + \\ &\cos\epsilon\cos\Omega\sin\omega\cos i + \sin\epsilon\sin\omega\sin i)^2\Big)\Big] \end{aligned} \tag{D.3}$$

$$\bar{\bar{\mathcal{R}}}_{\odot,3} = 0 \tag{D.4}$$

$$\bar{\bar{\mathcal{R}}}_{\odot,4} = \frac{3a^4\mu_\odot}{131072a_\odot^5}\Big(215040\cos^4\omega\cos^4\Omega e^4 + 26880\cos^4\Omega\sin^4\omega e^4 + 215040\cos^4\omega\cos^4\epsilon_\oplus\sin^4\Omega e^4$$
$$+ 26880\cos^4\epsilon_\oplus\sin^4\omega\sin^4\Omega e^4 - 322560\cos^2\omega\cos^4\epsilon_\oplus\sin^2\omega\sin^4\Omega e^4 - 322560\cos^2\omega\cos^4\Omega\sin^2\omega e^4$$
$$- 184320\cos^2\omega\cos^2\epsilon_\oplus\sin^2\Omega e^4 + 30720\cos^2\epsilon_\oplus\sin^2\omega\sin^2\Omega e^4 - 42000\cos 2\omega e^4 + 8820\cos 4\omega e^4 -$$
$$26880\cos(2(\omega-\Omega))e^4 - 4410\cos(4(\omega-\Omega))e^4 - 38400\cos 2\Omega e^4 - 6300\cos 4\Omega e^4 - 26880\cos(2(\omega+\Omega))e^4$$
$$- 4410\cos(4(\omega+\Omega))e^4 - 5880\cos(2(\omega+2\Omega))e^4$$
$$- 5880\cos(2(\omega-2\Omega))e^4 + 6300\cos(2\epsilon_\oplus)e^4 + 4410\cos(2(\epsilon_\oplus-2\omega))e^4$$
$$+ 5880\cos(2(\epsilon_\oplus-\omega))e^4 + 5880\cos(2(\omega+\epsilon_\oplus))e^4$$
$$+ 4410\cos(2(2\omega+\epsilon_\oplus))e^4 - 3150\cos(2(\epsilon_\oplus-2\Omega))e^4 - 3150\cos(2(2\Omega+\epsilon_\oplus))e^4$$
$$- 2205\cos(2(-2\omega+2\Omega+\epsilon_\oplus))e^4$$
$$- 2940\cos(2(-\omega+2\Omega+\epsilon_\oplus))e^4$$
$$- 2940\cos(2(\omega+2\Omega+\epsilon_\oplus))e^4 - 2940\cos(2(-\omega-2\Omega+\epsilon_\oplus))e^4 - 2940\cos(2(\omega-2\Omega+\epsilon_\oplus))e^4$$
$$- 2205\cos(2(2\omega-2\Omega+\epsilon_\oplus))e^4 - 2205\cos(2(\epsilon_\oplus-2(\omega+\Omega)))e^4$$
$$- 2205\cos(2(2(\omega+\Omega)+\epsilon_\oplus))e^4 - 1380e^4 + 322560\cos^4\omega\cos^4\Omega e^2$$
$$- 53760\cos^4\Omega\sin^4\omega e^2 + 322560\cos^4\omega\cos^4\epsilon_\oplus\sin^4\Omega e^2 - 53760\cos^4\epsilon_\oplus\sin^4\omega\sin^4\Omega e^2$$
$$+ 268800\cos^2\omega\cos^4\epsilon_\oplus\sin^2\omega\sin^4\Omega e^2 - 188160(3\cos 2\omega e^2 - e^2 - 2)\cos\epsilon_\oplus\sin^3 i\sin 2\omega\sin\Omega\sin^3\epsilon_\oplus e^2$$
$$+ 268800\cos^2\omega\cos^4\Omega\sin^2\omega e^2$$
$$- 419840\cos^2\omega\cos^2\epsilon_\oplus\sin^2\Omega e^2 + 10240\cos^2\epsilon_\oplus\sin^2\omega\sin^2\Omega e^2$$
$$- 84000\cos 2\omega e^2 - 53760\cos(2(\omega-\Omega))e^2 - 102400\cos(2\Omega)e^2 - 16800\cos(4\Omega)e^2$$
$$- 53760\cos(2(\omega+\Omega))e^2 - 11760\cos(2(\omega+2\Omega))e^2 - 11760\cos(2(\omega-2\Omega))e^2$$
$$+ 16800\cos(2\epsilon_\oplus)e^2 + 11760\cos(2(\epsilon_\oplus-\omega))e^2 + 11760\cos(2(\omega+\epsilon_\oplus))e^2 - 8400\cos(2(\epsilon_\oplus-2\Omega))e^2$$
$$- 8400\cos(2(2\Omega+\epsilon_\oplus))e^2 - 5880\cos(2(-\omega+2\Omega+\epsilon_\oplus))e^2$$
$$- 5880\cos(2(\omega+2\Omega+\epsilon_\oplus))e^2 - 5880\cos(2(-\omega-2\Omega+\epsilon_\oplus))e^2$$
$$- 5880\cos(2(\omega-2\Omega+\epsilon_\oplus))e^2 + 840(252\cos 2\omega e^2 + 42\cos(2(\omega-\Omega))e^2 + 28\cos(2\Omega)e^2$$
$$+ 42\cos(2(\omega+\Omega))e^2 + 42\cos(2(\epsilon_\oplus-\omega))e^2$$
$$+ 42\cos(2(\omega+\epsilon_\oplus))e^2 - 14\cos(2(\epsilon_\oplus-\Omega))e^2 - 21\cos(2(-\omega-\Omega+\epsilon_\oplus))e^2 - 21\cos(2(\omega-\Omega+\epsilon_\oplus))e^2$$
$$- 14\cos(2(\Omega+\epsilon_\oplus))e^2 - 21\cos(2(-\omega+\Omega+\epsilon_\oplus))e^2 - 21\cos(2(\omega+\Omega+\epsilon_\oplus))e^2 - 44e^2 + 56\cos(2\Omega)$$
$$+ 28(e^2+2)\cos(2\epsilon_\oplus) - 28\cos(2(\epsilon_\oplus-\Omega)) - 28\cos(2(\Omega+\epsilon_\oplus)) - 88)\sin i\sin 2\omega\sin\Omega\sin(2\epsilon_\oplus)e^2$$
$$- 3680e^2 + 26880\cos^4\omega\cos^4\Omega + 26880\cos^4\Omega\sin^4\omega$$
$$+ 26880\cos^4\omega\cos^4\epsilon_\oplus\sin^4\Omega + 26880\cos^4\epsilon_\oplus\sin^4\omega\sin^4\Omega$$
$$+ 53760\cos^2\omega\cos^4\epsilon_\oplus\sin^2\omega\sin^4\Omega + 3360(21\cos 4\omega e^4 + 15e^4 - 28(e^2+2)\cos 2\omega e^2$$

go to next page

(D.5)

$$+ 40e^2 + 8)\sin^4 i \sin^4 \epsilon_\oplus + \frac{105}{2}\cos^4 i(21\cos 4\omega e^4$$
$$+ 15e^4 - 28(e^2 + 2)\cos 2\omega e^2 + 40e^2 + 8)(-2\cos(2\Omega) + 2\cos(2\epsilon_\oplus) + \cos(2(\epsilon_\oplus - \Omega)) + \cos(2(\Omega + \epsilon_\oplus)) + 6)^2$$
$$+ 53760\cos^2\omega\cos^4\Omega\sin^2\omega - 40960\cos^2\omega\cos^2\epsilon_\oplus\sin^2\Omega - 40960\cos^2\epsilon_\oplus\sin^2\omega\sin^2\Omega$$
$$+ 20(5376\cos 2\omega e^4 - 8820\cos 4\omega e^4 - 420\cos(2\Omega)e^4 + 882\cos(2(2\omega + \Omega))e^4 + 882\cos(4\omega - 2\Omega)e^4$$
$$- 2646\cos(2(\epsilon_\oplus - 2\omega))e^4$$
$$- 2646\cos(2(2\omega + \epsilon_\oplus))e^4 - 630\cos(2(\epsilon_\oplus - \Omega))e^4 + 1323\cos(2(-2\omega - \Omega + \epsilon_\oplus))e^4$$
$$+ 1323\cos(2(2\omega - \Omega + \epsilon_\oplus))e^4 - 630\cos(2(\Omega + \epsilon_\oplus))e^4 + 1323\cos(2(-2\omega + \Omega + \epsilon_\oplus))e^4$$
$$+ 1323\cos(2(2\omega + \Omega + \epsilon_\oplus))e^4 - 1740e^4 + 10752\cos 2\omega e^2 - 1120\cos(2\Omega)e^2 - 1680\cos(2(\epsilon_\oplus - \Omega))e^2$$
$$- 1680\cos(2(\Omega + \epsilon_\oplus))e^2 - 4640e^2 - 224\cos(2\Omega) + 84(15e^4 + 40e^2 + 8)\cos(2\epsilon_\oplus) - 336\cos(2(\epsilon_\oplus - \Omega))$$
$$- 336\cos(2(\Omega + \epsilon_\oplus)) - 928)\sin^2 i\sin^2\epsilon_\oplus - 20480\cos(2\Omega) - 3360\cos(4\Omega) + 3360\cos(2\epsilon_\oplus) - 1680\cos(2(\epsilon_\oplus - 2\Omega))$$
$$- 1680\cos(2(2\Omega + \epsilon_\oplus)) + 1680\cos^3 i\cos\Omega(-2\cos(2\Omega) + 2\cos(2\epsilon_\oplus) + \cos(2(\epsilon_\oplus - \Omega))$$
$$+ \cos(2(\Omega + \epsilon_\oplus)) + 6)\sin\epsilon_\oplus(14(3\cos 2\omega e^2 - e^2 - 2)\sin 2\omega\sin\Omega\sin\epsilon_\oplus e^2 + (21\cos 4\omega e^4 + 15e^4$$
$$- 28(e^2 + 2)\cos 2\omega e^2 + 40e^2 + 8)\cos\epsilon_\oplus\sin i) - 10\cos^2 i(-3072\cos^2\omega\cos^2\Omega\cos^2\epsilon_\oplus e^4$$
$$+ 18432\cos^2\Omega\cos^2\epsilon_\oplus\sin^2\omega e^4 + 32256\cos^4\omega\cos^2\Omega\cos^4\epsilon_\oplus\sin^2\Omega e^4$$
$$+ 32256\cos^2\Omega\cos^4\epsilon_\oplus\sin^4\omega\sin^2\Omega e^4 + 32256\cos^4\omega\cos^2\Omega\sin^2\Omega e^4$$
$$- 274176\cos^2\omega\cos^2\Omega\cos^4\epsilon_\oplus\sin^2\omega\sin^2\Omega e^4 + 8064\sin^4\omega\sin^2(2\Omega)e^4 - 17136\sin^2 2\omega\sin^2(2\Omega)e^4$$
$$- 5376\cos 2\omega e^4 + 1764\cos 4\omega e^4 + 2688\cos(2(\omega - \Omega))e^4 + 2646\cos(4(\omega - \Omega))e^4 - 3840\cos(2\Omega)e^4 - 1260\cos(4\Omega)e^4$$
$$+ 2688\cos(2(\omega + \Omega))e^4 + 2646\cos(4(\omega + \Omega))e^4 + 882\cos(2(\epsilon_\oplus - 2\omega))e^4 + 882\cos(2(2\omega + \epsilon_\oplus))e^4$$
$$- 630\cos(2(\epsilon_\oplus - 2\Omega))e^4 - 630\cos(2(2\Omega + \epsilon_\oplus))e^4 + 1323\cos(2(-2\omega + 2\Omega + \epsilon_\oplus))e^4$$
$$+ 1323\cos(2(2\omega - 2\Omega + \epsilon_\oplus))e^4 + 1323\cos(2(\epsilon_\oplus - 2(\omega + \Omega)))e^4 + 1323\cos(2(2(\omega + \Omega) + \epsilon_\oplus))e^4$$
$$+ 3420e^4 - 1024\cos^2\omega\cos^2\Omega\cos^2\epsilon_\oplus e^2 + 41984\cos^2\Omega\cos^2\epsilon_\oplus\sin^2\omega e^2$$
$$- 26880\cos^4\omega\cos^2\Omega\cos^4\epsilon_\oplus\sin^2\Omega e^2 - 26880\cos^2\Omega\cos^4\epsilon_\oplus\sin^4\omega\sin^2\Omega e^2$$
$$- 26880\cos^4\omega\cos^2\Omega\sin^2\Omega e^2 - 53760\cos^2\omega\cos^2\omega\cos^4\epsilon_\oplus\sin^2\omega\sin^2\Omega e^2$$
$$- 6720\sin^4\omega\sin^2(2\Omega)e^2 - 3360\sin^2 2\omega\sin^2(2\Omega)e^2 - 10752\cos 2\omega e^2 + 5376\cos(2(\omega - \Omega))e^2 - 10240\cos(2\Omega)e^2$$
$$- 3360\cos(4\Omega)e^2 + 5376\cos(2(\omega + \Omega))e^2 - 1680\cos(2(\epsilon_\oplus - 2\Omega))e^2 - 1680\cos(2(2\Omega + \epsilon_\oplus))e^2$$
$$+ 1176(3\cos 2\omega e^2 - e^2 - 2)(-6\cos(2\Omega) + 6\cos(2\epsilon_\oplus) + 3\cos(2(\epsilon_\oplus - \Omega))$$
$$+ 3\cos(2(\Omega + \epsilon_\oplus)) + 2)\sin i\sin 2\omega\sin\Omega\sin(2\epsilon_\oplus)e^2 + 9120e^2 + 4096\cos^2\omega\cos^2\omega\cos^2\epsilon_\oplus$$
$$+ 4096\cos^2\Omega\cos^2\epsilon_\oplus\sin^2\omega - 5376\cos^4\omega\cos^2\omega\cos^4\epsilon_\oplus\sin^2\Omega$$
$$- 5376\cos^2\Omega\cos^4\epsilon_\oplus\sin^4\omega\sin^2\Omega - 5376\cos^4\omega\cos^2\Omega\sin^2\omega - 1344\sin^4\Omega\sin^2(2\Omega)$$
$$- 672\cos^4\epsilon_\oplus\sin^2 2\omega\sin^2(2\Omega) - 672\sin^2 2\omega\sin^2(2\Omega) - 84(21\cos 4\omega e^4 + 15e^4$$
$$- 28(e^2 + 2)\cos 2\omega e^2 + 40e^2 + 8)(2\cos(2\Omega) + 6\cos(2\epsilon_\oplus) + 3\cos(2(\epsilon_\oplus - \Omega))$$
$$+ 3\cos(2(\Omega + \epsilon_\oplus)) + 10)\sin^2 i\sin^2\epsilon_\oplus - 2048\cos 2\omega - 672\cos(4\Omega) - 28(15e^4 + 40e^2 + 8)\cos(2\epsilon_\oplus)$$

go to next page

$$
\begin{aligned}
&- 336\cos(2(\epsilon_\oplus - 2\Omega)) - 336\cos(2(2\Omega + \epsilon_\oplus)) + 1824) \\
&- 160\cos i\cos\Omega(-84(21\cos 4\omega e^4 + 15e^4 - 28(e^2+2)\cos 2\omega e^2 \\
&+ 40e^2 + 8)\cos\epsilon_\oplus \sin^3 i \sin^3\epsilon_\oplus + 588e^2(3\cos 2\omega e^2 - e^2 - 2)(3\cos(2\epsilon_\oplus) + 1) \\
&\sin^2 i \sin 2\omega \sin\Omega \sin^2\epsilon_\oplus - \frac{21}{2}e^2(-252\cos 2\omega e^2 - 42\cos(2(\omega - \Omega))e^2 - 28\cos(2\Omega)e^2 \\
&- 42\cos(2(\omega + \Omega))e^2 - 42\cos(2(\epsilon_\oplus - \omega))e^2 - 42\cos(2(\omega + \epsilon_\oplus))e^2 + 14\cos(2(\epsilon_\oplus - \Omega))e^2 \\
&+ 21\cos(2(-\omega - \Omega + \epsilon_\oplus))e^2 + 21\cos(2(\omega - \Omega + \epsilon_\oplus))e^2 + 14\cos(2(\Omega + \epsilon_\oplus))e^2 \\
&+ 21\cos(2(-\omega + \Omega + \epsilon_\oplus))e^2 \\
&+ 21\cos(2(\omega + \Omega + \epsilon_\oplus))e^2 + 44e^2 - 56\cos(2\Omega) - 28(e^2+2)\cos(2\epsilon_\oplus) + 28\cos(2(\epsilon_\oplus - \Omega)) \\
&+ 28\cos(2(\Omega + \epsilon_\oplus)) + 88)\sin 2\omega \sin\Omega \sin^2\epsilon_\oplus - \frac{3}{8}(1792\cos 2\omega e^4 - 588\cos 4\omega e^4 \\
&+ 420\cos(2\Omega)e^4 - 882\cos(2(2\omega + \Omega))e^4 \\
&- 882\cos(4\omega - 2\Omega)e^4 - 882\cos(2(\epsilon_\oplus - 2\omega))e^4 - 882\cos(2(2\omega + \epsilon_\oplus))e^4 \\
&- 210\cos(2(\epsilon_\oplus - \Omega))e^4 + 441\cos(2(-2\omega - \Omega + \epsilon_\oplus))e^4 + 441\cos(2(2\omega - \Omega + \epsilon_\oplus))e^4 \\
&- 210\cos(2(\Omega + \epsilon_\oplus))e^4 + 441\cos(2(-2\omega + \Omega + \epsilon_\oplus))e^4 + 441\cos(2(2\omega + \Omega + \epsilon_\oplus))e^4 \\
&- 1140e^4 + 3584\cos 2\omega e^2 + 1120\cos(2\Omega)e^2 - 560\cos(2(\epsilon_\oplus - \Omega))e^2 \\
&- 560\cos(2(\Omega + \epsilon_\oplus))e^2 - 3040e^2 + 224\cos(2\Omega) \\
&+ 28(15e^4 + 40e^2 + 8)\cos(2\epsilon_\oplus) - 112\cos(2(\epsilon_\oplus - \Omega)) \\
&- 112\cos(2(\Omega + \epsilon_\oplus)) - 608)\sin i \sin(2\epsilon_\oplus)) - 736)
\end{aligned}
$$

Acronyms

ADR	Active Debris Removal
COMPASS	Control for Orbital Manoeuvering through Perturbations for Application to Space System
ESA	European Space Agency
GEO	Geostationary Earth Orbit
HEO	Highly Elliptical Orbit
IADC	Inter-Agency Space Debris Coordination Committee
INTEGRAL	INTErnational Gamma-Ray Astrophysics Laboratory
LEO	Low Earth Orbit
MEO	Medium Earth Orbit
NASA	National Aeronautics and Space Administration
RAAN	Right Ascension of the Ascending Node
SRP	Solar Radiation Pressure
XMM-Newton	X-ray Multi-Mirror Mission-Newton

Bibliography

[1] Donald J Kessler and Burton G Cour-Palais. 'Collision frequency of artificial satellites: The creation of a debris belt'. In: *Journal of Geophysical Research: Space Physics* 83.A6 (1978), pp. 2637–2646.

[2] Donald J Kessler, Nicholas L Johnson, JC Liou and Mark Matney. 'The kessler syndrome: implications to future space operations'. In: *Advances in the Astronautical Sciences* 137.8 (2010), p. 2010.

[3] IADC Space Debris Mitigation Guidelines. *IADC Document no. IADC-02-01*. 15 October 2002, Revision 1 September 2007.

[4] Camilla Colombo, Elisa Maria Alessi and Markus Landgraf. 'End-of-life Disposal of spacecraft in Highly elliptical Orbits by Means of Luni-Solar Perturbations and Moon Resonances'. In: *6th European Conference on Space Debris. Darmstadt, Germany.* Vol. 723. 22 - 25 April 2013.

[5] M.L. Lidov. 'Evolution of the orbits of artificial satellites of planets as affected by gravitational perturbation from external bodies'. In: *AIAA Journal* 1.8 (1963), pp. 1985–2002.

[6] Yoshihide Kozai. 'Secular perturbations of asteroids with high inclination and eccentricity'. In: *The Astronomical Journal* 67 (1962), p. 591.

[7] Ivan I Shevchenko. *The Lidov-Kozai effect-applications in exoplanet research and dynamical astronomy*. Vol. 441. Springer, 2016.

[8] Bernard Kaufman. 'Variation of parameters and the long-term behavior of planetary orbiters'. In: *Astrodynamics Conference. Santa Barbara, California, U.S.A.* 19-21 August 1970, p. 1055.

[9] Bernard Kaufman and Robert Dasenbrock. *Higher Order Theory for Long-Term Behavior of Earth and Lunar Orbiters*. Tech. rep. NAVAL RESEARCH LAB WASHINGTON DC OPERATIONS RESEARCH BRANCH, 1972.

[10] Yoshihide Kozai. 'The motion of a close earth satellite'. In: *The Astronomical Journal* 64 (1959), p. 367.

[11] William M Kaula. 'Development of the lunar and solar disturbing functions for a close satellite'. In: *The Astronomical Journal* 67 (1962), p. 300.

[12] David Folta and David Quinn. 'Lunar frozen orbits'. In: *AIAA/AAS Astrodynamics Specialist Conference and Exhibit. Keystone, Colorado, U.S.A.* 23-24 August 2006, p. 6749.

[13] Alberto Abad, Antonio Elipe and Eva Tresaco. 'Analytical model to find frozen orbits for a lunar orbiter'. In: *Journal of Guidance, Control, and Dynamics* 32.3 (2009), pp. 888–898.

[14] Nicolas Delsate, Philippe Robutel, Anne Lemaitre and Timoteo Carletti. 'Frozen orbits at high eccentricity and inclination: application to Mercury orbiter'. In: *Celestial Mechanics and Dynamical Astronomy* 108.3 (2010), pp. 275–300.

[15] Martin Lara and Juan Felix San Juan. 'Dynamic behavior of an orbiter around Europa'. In: *Journal of Guidance, Control, and Dynamics* 28.2 (2005), pp. 291–297.

[16] J Carvalho, D.C. Mourão, Antonio Elipe, Rodolpho Vilhena de Moraes and A.F.B.A. Prado. 'Frozen orbits around Europa'. In: *International Journal of Bifurcation and Chaos in Applied Sciences and Engineering* 22 (2012).

[17] Scott Tremaine, Jihad Touma and Fathi Namouni. 'Satellite dynamics on the Laplace surface'. In: *The astronomical journal* 137.3 (2009), p. 3706.

[18] Camilla Colombo, Charlotte Lücking and Colin R McInnes. 'Orbital dynamics of high area-to-mass ratio spacecraft with J2 and solar radiation pressure for novel Earth observation and communication services'. In: *Acta Astronautica* 81.1 (2012), pp. 137–150.

[19] Eva Tresaco, Antonio Elipe and Jean Paulo S Carvalho. 'Frozen orbits for a solar sail around Mercury'. In: *Journal of Guidance, Control, and Dynamics* 39.7 (2016), pp. 1659–1666.

[20] Eva Tresaco, Jean Paulo S Carvalho, Antonio FBA Prado, Antonio Elipe and Rodolpho Vilhena de Moraes. 'Averaged model to study long-term dynamics of a probe about Mercury'. In: *Celestial Mechanics and Dynamical Astronomy* 130.2 (2018), p. 9.

[21] Smadar Naoz. 'The eccentric Kozai-Lidov effect and its applications'. In: *Annual Review of Astronomy and Astrophysics* 54 (2016), pp. 441–489.

[22] Sławomir Breiter. 'Lunisolar resonances revisited'. In: *Celestial Mechanics and Dynamical Astronomy* 81.1-2 (2001), pp. 81–91.

[23] Aaron J Rosengren, Elisa Maria Alessi, Alessandro Rossi and Giovanni B Valsecchi. 'Chaos in navigation satellite orbits caused by the perturbed motion of the Moon'. In: *Monthly Notices of the Royal Astronomical Society* 449.4 (2015), pp. 3522–3526.

[24] Camilla Colombo, Francesca Letizia, Elisa Maria Alessi, Markus Landgraf et al. 'End-of-life Earth re-entry for highly elliptical orbits: the INTEGRAL mission'. In: *The 24th AAS/AIAA space flight mechanics meeting. Santa Fe, New Mexico, U.S.A.* 26-30 January 2014, pp. 26–30.

[25] Camilla Colombo. 'Long-term evolution of highly-elliptical orbits: luni-solar perturbation effects for stability and re-entry'. In: *25th AAS/AIAA Space Flight Mechanics Meeting. Williamsburg, Virginia, U.S.A.* 11-15 January 2015.

[26] Camilla Colombo, Elisa Maria Alessi, Willem van der Weg, Stefania Soldini, Francesca Letizia, Massimo Vetrisano, Massimiliano Vasile, Alessandro Rossi and Markus Landgraf. 'End-of-life disposal concepts for Libration Point Orbit and Highly Elliptical Orbit missions'. In: *Acta Astronautica* 110 (2015), pp. 298–312.

[27] Camilla Colombo. 'Optimal trajectory design for interception and deflection of Near Earth Objects, Ph.D. Thesis'. PhD thesis. University of Glasgow, 2010.

[28] Joseph-Louis Lagrange. *Mécanique analytique, nouvelle édition, orig. 1788 (Paris: Courcier)*. 1811.

[29] William Rowan Hamilton. 'VII. Second essay on a general method in dynamics'. In: *Philosophical Transactions of the Royal Society of London* 125 (1835), pp. 95–144.

[30] Mauri Valtonen and Hannu Karttunen. *The three-body problem*. Cambridge University Press, 2006.

[31] William Ailor. 'Spacecraft End-of-Life Disposal'. In: *Encyclopedia of Aerospace Engineering* (2010).

[32] Minghe Shan, Jian Guo and Eberhard Gill. 'Review and comparison of active space debris capturing and removal methods'. In: *Progress in Aerospace Sciences* 80 (2016), pp. 18–32.

[33] Riccardo Benvenuto, Michèle Lavagna and Samuele Salvi. 'Multibody dynamics driving GNC and system design in tethered nets for active debris removal'. In: *Advances in Space Research* 58.1 (2016), pp. 45–63.

[34] DS Airbus. *Edeorbit Final Report Phase B1*. 2016.

[35] Jason Forshaw, Guglielmo Aglietti, Thierry Salmon, Ingo Retat, Christopher Burgess, Thomas Chabot, Aurélien Pisseloup, Andy Phipps, Cesar Bernal, Alexandre Pollini et al. 'The RemoveDebris ADR mission: preparing for an international space station launch'. In: *7th European Conference on Space Debris. Darmstadt, Germany.* 18-21 April 2017.

[36] Charlotte Lücking, Camilla Colombo and Colin R McInnes. 'A passive satellite deorbiting strategy for medium earth orbit using solar radiation pressure and the J2 effect'. In: *Acta Astronautica* 77 (2012), pp. 197–206.

[37] Charlotte Lücking, Camilla Colombo and Colin R McInnes. 'Solar radiation pressure-augmented deorbiting: passive end-of-life disposal from high-altitude orbits'. In: *Journal of Spacecraft and Rockets* 50.6 (2013), pp. 1256–1267.

[38] Camilla Colombo, Charlotte Lücking and Colin R McInnes. 'Orbit evolution, maintenance and disposal of SpaceChip swarms through electro-chromic control'. In: *Acta Astronautica* 82.1 (2013), pp. 25–37.

[39] David A Vallado. *Fundamentals of astrodynamics and applications*. Vol. 12. Springer Science & Business Media, 2001.

[40] Tomohiro Narumi and Toshiya Hanada. 'New Orbit Propagator to Be Used in Orbital Debris Evolutionary Models'. In: *Memoirs of the Faculty of Engineering, Kyushu University* 67 (December 2007), pp. 235–254.

[41] Howard Curtis. *Orbital Mechanics: for Engineering Students*. Second Edition. Aerospace Engineering. Butterworth-Heinemann, 2010.

[42] Chia-Chun George Chao. *Applied orbit perturbation and maintenance*. American Institute of Aeronautics and Astronautics, Inc., 2005.

[43] Pavel Efemovich El'iasberg. *Introduction to the Theory of Flight of Artificial Earth Satellites (Vvedenie Y Teoriu Poleta Iskusstvennykh Sputnikov Zemli)*. Israel Program for Scientific Translations, 1967.

[44] Leon Blitzer. 'Handbook of orbital perturbations'. In: *University of Arizona* (1970).

[45] National Geospatial-Intelligence Agency (NGA). *EGM2008 - WGS 84 Version*. URL: http://earth-info.nga.mil/GandG/wgs84/gravitymod/egm2008/egm08_wgs84.html.

[46] NA Mottinger, WL Sjogren and BG Bills. 'Venus gravity: A harmonic analysis and geophysical implications'. In: *Journal of Geophysical Research: Solid Earth* 90.S02 (1985).

[47] Carl D Murray and Stanley F Dermott. *Solar system dynamics*. Cambridge university press, 1999.

[48] Camilla Colombo. 'Planetary Orbital Dynamics (PlanODyn) suite for long term propagation in perturbed environment'. In: *6th International Conference on Astrodynamics Tools and Techniques (ICATT). Darmstadt, Germany.* 14-17 March 2016, pp. 14–17.

[49] Moqbil S Alenazi and Paolo Gondolo. 'Phase-space distribution of unbound dark matter near the Sun'. In: *Physical Review D* 74.8 (2006), p. 083518.

[50] Richard H Battin. *An Introduction to the Mathematics and Methods of Astrodynamics, revised edition*. American Institute of Aeronautics and Astronautics, 1999.

[51] Ioannis Gkolias, Martin Lara and Camilla Colombo. 'An Ecliptic Perspective for Analytical Satellite Theories'. In: *AAS/AIAA Astrodynamics Specialist Conference. San Diego, California, U.S.A.* 19-23 August 2018, pp. 1–15.

[52] Tommaso Sgobba. 'Space debris re-entries and aviation safety'. In: *International Association for the Advancement of Space Safety's 2013 conference* (2013).

[53] Carl G Justus and Robert D Braun. 'Atmospheric Environments for Entry, Descent and Landing (EDL)'. In: (2007).

[54] Angélique Gaudel, Catherine Hourtolle, Jean-François Goester, N Fuentes and M Ottaviani. 'De-orbit strategies with low-thrust propulsion'. In: *Space Safety is No Accident*. Springer, 2015, pp. 59–68.

[55] Anthea Evelina Comellini, Brice Dellandrea, Gautier Durand and Pierluigi Di Lizia. 'The semi-controlled reentry: development of a simulator and feasibility study'. In: (2017).

[56] ESA. *Basics about controlled and semi-controlled re-entry*. URL: http://blogs.esa.int/cleanspace/2018/11/16/basics-about-controlled-and-semi-controlled-reentry/.

[57] Blair Thompson, Thomas Kelecy, Thomas Kubancik, Tim Flora, Michael Chylla and Debra Rose. *Geosynchronous Patrol Orbit for Space Situational Awareness*. 2017.

[58] Hakan Svedhem, Dima Titov, F Taylor and O Witasse. 'Venus express mission'. In: *Journal of Geophysical Research: Planets* 114.E5 (2009).

[59] Abolfazl Shirazi. 'Multi-objective optimization of orbit transfer trajectory using imperialist competitive algorithm'. In: *Aerospace Conference, 2017 IEEE. Big Sky, Montana, U.S.A.* IEEE. 2017, pp. 1–14.

[60] Bernard J Bienstock. 'Pioneer Venus and Galileo entry probe heritage'. In: *Planetary Probe Atmospheric Entry and Descent Trajectory Analysis and Science*. Vol. 544. 2004, pp. 37–45.

[61] DV Titov, KH Baines, AT Basilevsky, E Chassefiere, G Chin, D Crisp, LW Esposito, J-P Lebreton, E Lellouch, VI Moroz et al. *Missions to Venus*. 2002.

[62] Christoph Winkler, G Di Cocco, N Gehrels, A Giménez, S Grebenev, W Hermsen, JM Mas-Hesse, F Lebrun, N Lund, GGC Palumbo et al. 'The INTEGRAL mission'. In: *Astronomy & Astrophysics* 411.1 (2003), pp. L1–L6.

[63] Arvind N Parmar, Christoph Winkler, Paul Barr, Lars Hansson, Erik Kuulkers, Rudolph Much and Astrid Orr. 'INTEGRAL mission'. In: *X-Ray and Gamma-Ray Telescopes and Instruments for Astronomy*. Vol. 4851. International Society for Optics and Photonics. 2003, pp. 1104–1113.

[64] Cédric Pralet and Gérard Verfaillie. 'AIMS: A Tool for Long-term Planning of the ESA INTEGRAL Mission'. In: *Proceedings of the 6th International Workshop on Planning and Scheduling for Space, IWPSS09, Pasadena, California, U.S.A.* 19-21 July 2009.

[65] PL Jensen, K Clausen, C Cassi, F Ravera, G Janin, C Winkler and R Much. 'The INTEGRAL spacecraft–in-orbit performance'. In: *Astronomy & Astrophysics* 411.1 (2003), pp. L7–L17.

[66] ESA. *INTEGRAL satellite*. URL: `http://www.esa.int/spaceinimages/Images/2001/11/Integral`.

[67] Roberto Armellin, Juan F San-Juan and Martin Lara. 'End-of-life disposal of high elliptical orbit missions: The case of INTEGRAL'. In: *Advances in Space Research* 56.3 (2015), pp. 479–493.

[68] F Jansen, D Lumb, B Altieri, J Clavel, M Ehle, C Erd, C Gabriel, M Guainazzi, P Gondoin, R Much et al. 'XMM-Newton observatory-I. The spacecraft and operations'. In: *Astronomy & Astrophysics* 365.1 (2001), pp. L1–L6.

[69] ESA. *XMM-Newton satellite*. URL: http://www.esa.int/spaceinimages/Images/2001/11/Integral.

[70] John M. Anthony Danby. *Fundamentals of celestial mechanics*. 1988.

[71] Wei-Duo Hu and DJ Scheeres. 'Averaging analyses for spacecraft orbital motions around asteroids'. In: *Acta Mechanica Sinica* 30.3 (2014), pp. 294–300.